2005

Design, Fabrication and Performance Evaluation of an Impedimetric Urea Biosensor System

Vandana Gupta
Virginia Commonwealth University

DESIGN, FABRICATION AND PERFORMANCE EVALUATION OF AN IMPEDIMETRIC UREA BIOSENSOR SYSTEM

A Thesis submitted in partial fulfillment of the requirements for the degree of Master of Science in Engineering at Virginia Commonwealth University.

by

VANDANA GUPTA
Bachelor of Science in Biomedical Engineering, Virginia Commonwealth University, 2003

Director: DR. ANTHONY GUISEPPI-ELIE
PROFESSOR, DEPARTMENT OF CHEMICAL ENGINEERING
PROFESSOR, EMERGENCY MEDICINE
DIRECTOR, CENTER FOR BIOELECTRONICS, BIOSENSORS AND BIOCHIPS

Virginia Commonwealth University
Richmond, Virginia
August 2005

Acknowledgement

I sincerely express deepest gratitude to my advisor, Dr. Anthony Guiseppi-Elie, for his thorough and steadfast guidance and dissemination of knowledge and expertise during the course of this study, which were significant factors in increasing my enthusiasm to undertake this research.

The completion of this project was due in large part to assistance and contributions from Dr. Sean Brahim, Research Associate at the Center for Bioelectronics, Biosensors and Biochips (C3B), Dr. Arvind K. Srivastava, former Research Associate at the Center for Bioelectronics, Biosensors and Biochips (C3B) and the entire C3B Research Group. The substantive contributions provided by the above made this project feasible to undertake.

Special acknowledgement must be made to Dr. Anthony Guiseppi-Elie for provision of the Center for Bioelectronics, Biosensors and Biochips (C3B) Master's Degree Fellowship. In addition, I am grateful to the Department of Chemical Engineering at Virginia Commonwealth University for all assistance provided during the course of this work.

Lastly, by no means least, I wish to sincerely thank my father, mother and sister, whom provided much needed encouragement, support and enthusiasm and who really understood and experienced the sacrifices one must make for the completion of such as study.

Table of Contents

List of Tables

Page

List of Figures

Page

Abstract

DESIGN, FABRICATION AND PERFORMANCE EVALUATION OF AN

IMPEDIMETRIC UREA BIOSENSOR SYSTEM

By

Vandana Gupta, B.S. (Biomedical Engineering)

A Thesis submitted in partial fulfillment of the requirements for the degree of Master of Science in Engineering at Virginia Commonwealth University.

Virginia Commonwealth University, 2005

Major Director: Dr. Anthony Guiseppi-Elie
Professor, Department of Chemical Engineering, School of Engineering
Professor, Department of Emergency Medicine, School of Medicine
Director, Center for Bioelectronics, Biosensors and Biochips

An impedance bioanalyzer system comprising an in-vitro biotransducer, instrumentation and control software for the measurement of urea, potentially in blood dialysate, has been developed. The biotransducer comprises of a microlithographically fabricated interdigitated microsensor electrode (IME) onto which was cast a biorecognition layer conferred with the specificity of the enzyme urease. Urease hydrolysis of urea produces NH_4^+, HCO_3^- and OH^- ions that decrease the device's impedance. The temporal rate of change (kinetic) and the extent of change (equilibrium) of ion concentration were measured as the sensor's response. Five formats: [i) unPEGylated urease-containing

poly(hydroxyethylmethacrylate) [p(HEMA)] hydrogel, ii) PEGylated urease-containing p(HEMA) hydrogel, iii) via glutaraldehyde crosslinking in the presence of albumin, iv) the direct covalent immobilization of urease to the IME, and v) solution borne urease]. Michaelis-Menten parameters K_M, Z_{MAX} and k_{cat} revealed the following rank: PEGylated urease-Gel >> Free Urease > unPEGylated urease-Gel = BSA in Glutaraldehyde > covalently immobilized urease. The unPEGylated-urease sensor provided a higher enzyme-substrate binding rate and catalysis rate than PEGylated and thus provided a faster impedimetric response to various molar concentrations of urea. Long-term stability (one month) of the PEGylated-urease hydrogel was favorable.

A dedicated three-element array impedimetric instrument, the 3EIC BioAnalyzer was designed and produced. A pair of demodulating logarithmic amplifiers (AD8302) was used to calculate the change in phase and amplitude corresponding to the impedimetric response to a 4.0 kHz, 50 mV_{PP} sine wave from a function generator (MAX038). A graphic user interface (GUI), programmed in LabVIEW 7.0 established instrument control, data acquisition via a USB-48A-30A16 μDAQ and graphical data presentation of temporal impedimetric responses.

Chapter 1. Introduction

1.1. Rationale for Urea Measurements in Dialysis

Urea is a waste product of nitrogen metabolism in mammals. It is a metabolite produced by the liver and transported to the kidneys via blood for excretion. Whenever humans suffer from kidney failure, high levels of urea can accumulate in the blood. High levels of urea in the blood can be toxic and is potentially fatal to mammals; hence, the need for hemodialysis. In hemodialysis, the blood is allowed to flow through a machine with a special filter that removes toxic urea and extra fluids. The dialyzed blood is then returned to the body. Removing harmful wastes, extra salt, and fluids helps control blood pressure and keeps the proper balance of chemicals like potassium and sodium in the body. Most patients go to a dialysis center three times a week for 3 to 5 hours or more each visit (Noordwijk 2001).

Physicians and dialysis centers are trying to determine a method to optimize the amount of time a patient spends on the dialysis machine. Since each person has a unique metabolism, the amount of time on the dialysis machine should be individually set and individually monitored. The recent emphasis on materials science and chemistry has opened new approaches to analytical sensing, influencing the design of sensors, particularly those using electrochemical or spectroscopic transduction methods. Several *in-vitro* biosensors have been developed using different transduction approaches to measure the amount of urea in the blood and calculate the amount of time that a person should spend on the dialysis machine.

A bioanalyzer system has been developed integrating an in-vitro biosensor, electrical circuit and control software to measure the amount of urea in the blood and calculate the amount of time that a person should spend on the dialysis machine.

1.2. Non-biosensor Detection Strategies for Urea

Other strategies besides the use of a biosensor can be utilized for detecting urea. O'Neill et al. (2004), used flow-through calorimetric instruments to study enzymatic reactions. They were able to use an urea/urease enzymatic system and determine Michaelis-Menten parameters from flow calorimetric data. Data obtained from flow calorimetry experiments provided thermodynamic and kinetic information. However, obtaining accurate results was nearly impossible. Calorimetric data is dependent upon the volume of the reacting solution seen by the calorimeter. It cannot be easily measured before introducing a test and reference reaction into an isothermal calorimeter. As a result, it is believed that most of the data obtained thirty years ago using this technique are in error, because several assumptions for the value of the thermal volume were made (O'Neill 2004). O'Neill et al. (2004) had decided to repeat an identical protocol and calorimeter based on previous experiments conducted almost 30 years ago, but this time used a properly identified value for the thermal volume.

It was accurately concluded from O'Neill's experiment that the urea/urease system followed Michaelis-Menten kinetics, where the saturation of urease was observed with increasing urea concentration (2004). Knowledge of the thermal volume allowed for the

direct determination of Michaelis-Menten parameters, free from assumptions, from calorimetric data.

1.3. Biosensor Detection Strategies for Urea

In the past, most biological and chemical analytical techniques have involved reactions that take place in solutions upon addition of reagents and samples. However, over the past few years, 'biosensor measurement systems' have evolved where the reagents are already immobilized as part of a biotransducer. In these systems, chemical reactions take place at the surface or within the biorecognition layer of the biotransducer and are called biosensors.

Biosensors are usually composed of an analyte and a selective interface in close proximity or integrated with a transducer. The transducer responds to the interaction between that surface and analyte through a mediator (Chaubey 2002). The analyte selective surface is a bioactive substance (usually an enzyme, antibody, DNA, sub-cellular organelle, tissue or micro-organism), which is able to recognize their specific analytes and regulate the specificity and sensitivity of the device (Chaubey 2002). A transducer is then able to convert the biochemical signal into an electronic signal, which is then processed and results in an electrical output.

1.3.1. Conductimetric Urea Biosensors

Conductimetric sensors are based on the measurement of electrical ion transport (resistance or conductance) as a function of time of exposure to the analyte of interest. The measurement device usually consists of two closely spaced platinum or gold electrodes

between which the urease enzyme is immobilized. The urease enzyme confers its biological specificity to urea via the following enzymatic reaction:

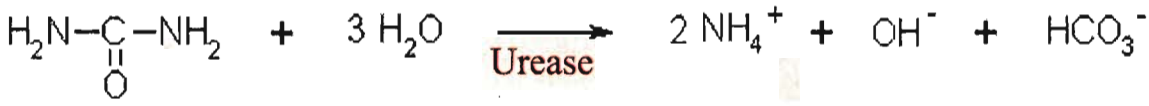

This sensor is based on the principle that the products of the enzymatic reaction (NH_4^+, OH^- and HCO_3^-) change the conductivity between the electrodes, yielding a signal. The performance of a conductimetric sensor is highly dependent on the concentration of the ionic environment and thus any fluctuation may generate unpredictable results.

Jdanova et al. (1996) decided to construct a conductimetric urea biosensor using additional membranes for the improvement of its analytical performance. His purpose was to determine if the analytical characteristics (dynamic characteristics, buffer concentration sensitivity) of conductimetric biosensor could be improved by adding polymeric membranes such as Nafion® and Polyvinylpyrrolidone (PVP). Jdanova fabricated two types of urea-sensitive biosensors: with/without Nafion® membrane and with/without PVP membrane. Through several conductimetric experiments, it was observed that Nafion® did not significantly change the sensor's response. However, when a PVP membrane was spin-coated on top of the electrode surface, it contributed an increase in sensor response. They concluded that the analytical characteristics of a conductimetric biosensor can be adjusted and improved.

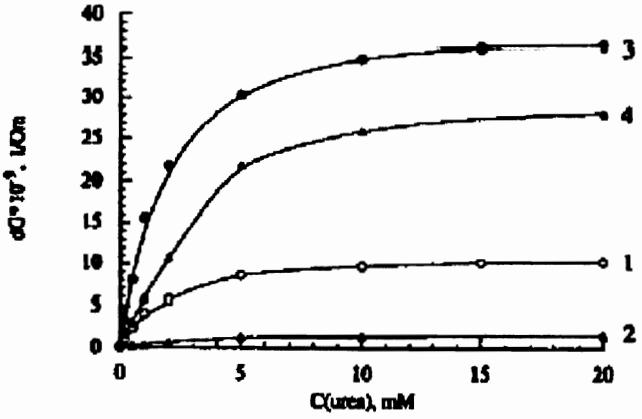

Figure 1: *Calibration graphs for the steady state response of the urea sensors without (1, 2) and with additional PVP membrane (3, 4) in Tris-HCl buffer, pH 7.4 (Jdanova 1996).*

1.3.2. Amperometric Urea Biosensors

Amperometric biosensors are based on the principle of monitoring the steady state current under a constant applied potential. The setup consists of three electrodes: a working, a reference and an auxiliary or counter electrode. A potentiostat controls the constancy of the potential of the working electrode. The working electrode contains an immobilized bioactive layer. The three-electrode configuration can be used in two types of hydrodynamic conditions: in quiescent or stirred batch, or in a flow injection system (Brett 1993).

The amperometric response of this biosensor is based on: diffusion of the analyte into the biorecognition layer, enzymatic reaction within the layer, diffusion of the product(s) out of the biorecognition layer, electrochemical detection of the product and diffusion of the product of the electrochemical reaction out of the biorecognition layer. The required operational condition for this type of biosensor is that the current be limited

by the mass transfer of the analyte rather than by enzyme kinetics or by electrode kinetics (Brett 1993).

There are various methods for using amperometry to detect urea. Yoneyama et al. (2001) were able to construct a sensing system that was based on combining the pH-Stat method and the flow injection analysis (FIA). Its purpose was to help solve the problem of potentiometry of dependency on buffer concentration of the response to urea and also to eliminate the response to interfering substances. The current sensing system has a small detection range and the potentiometric response is dependent on buffer concentration.

The pH-Stat FIA sensing system contains two flow paths for eliminating responses to interfering substances. The sample path allows the buffer solution and the sample to pass through. Enzymatic reactions occur within a urease tubing column when the sample solution is introduced via a rotary injection valve. The other path is the electrolysis path. Only the generated H^+ ions from the reaction and the buffer solution can run through this path. Both items are then mixed within a Field Effect Transistor (FET) cell and sent to the surface of an Ion-Sensitive Field Effect Transistor (ISFET). Yoneyama et al. (2001) describes that the ISFET detected a pH change at the outlet of the column and anodic water electrolysis proceeds at an Au electrode to maintain a constant pH with the ISFET detector using a feed back circuit. Since no new sample buffer solution is introduced into this path, no interfering substances are present and thus no response to these interfering substances take place. It was found by using the pH-stat FIA sensing system that the response to urea was independent of the buffer concentration and the relation between current response and urea concentration became linear (Yoneyama 2001).

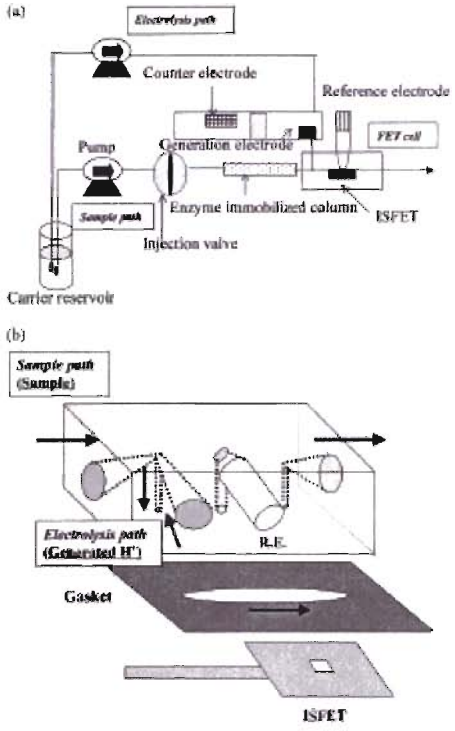

Figure 2: *Schematic drawing of the pH-stat FIA amperometric sensing system with the ISFET as a pH detector: (a) entire system; (b) details of the FET cell structure (Yoneyama 2001).*

Rajesh et al. (2005) developed an amperometric biosensor based on the covalent immobilization of urease onto an electrochemically prepared poly (N-3-aminopropyl pyrrole-co-pyrrole) film. It was developed for the quantitative determination of urea in an aqueous solution. The principle of operation for this biosensor was based on the use of pH-sensitive redox-active dissolved hematein molecule. Poly (N-3-aminopropyl pyrrole-co-pyrrole) is an electrochemically polymerized conducting polymer, which has received considerable attention over the last 2 decades. This copolymer, which has a remarkable switching capability between the conducting, oxidized (doped) and the insulating-reduced (undoped) state, has been the basis of many applications.

The urease enzyme was covalently immobilized on a conducting poly (N-3-aminopropyl pyrrole-co-pyrrole) film and then was electrochemically prepared onto an indium-tin-oxide (ITO)-coated glass plate. The covalent linkage of urease and the porous morphology of the polymer film lead to a high urease enzyme loading and increased lifetime stability of the urease electrode (Rajesh et al. 2005). The amperometric response was measured as a function of molar concentration of urea, at fixed bias voltage of 0.0V vs. Ag/AgCl in pH 7.0 phosphate buffer. It was observed that the electrode was able to provide a linear response range of 0.16 – 5.02 mM for urea in Tris-HCl buffer solution containing 0.1M NaCl. The response time was 40 seconds reaching to a 95% steady-state current value, and 80% of the enzyme activity is retained for about 2 months (Rajesh et al. 2005)

1.3.3. Optical Urea Biosensors

Optical transducers use fiber optic supports consisting of two optical leads, a source and a detector, and a reaction plate with an immobilized biorecognition layer. They can be classified into two groups: chemically mediated and non-mediated fiber optic biosensors. For chemically mediated fiber optic biosensors, both fibers lead to a reaction chamber containing some dye or indicator solution that is separated from the sample solution by a gas-permeable membrane. In non-mediated fiber optic biosensors, the biocatalyzed reaction is followed by direct monitoring of either the production or consumption of an optically measurable compound (Anonymous 1986).

Fiber optic biosensors can be used to build rapid-analyte-recognition systems based on multi fiber-optic sensor arrays. Fiber optic transducers have the advantage over other systems in so far that they have the ability to monitor multiple wavelengths with a single optical fiber. Also, a separate reference electrode is not required and intensity ratio measurements reduce the need for sensor recalibration (Anonymous 1986).

An example of an optical urease biosensor is fabricated by coating the surface of a glass waveguide slide with poly(vinylchloride) (PVC) matrix based thin ammonium optode membrane and with a reaction layer containing urease (Kovács 2003). This yielded a membrane thickness between 0.8μm – 1μm. When the ammonium ions are released in the enzymatic reaction, they are detected within the optode membrane containing nonactin as an ion selective ionophore and a chromoionophore in a 1μm plasticized PVC film (Kovács 2003). The ammonium optode membrane and urease reaction layer were spin coated onto the surface of the sensing microscope slide at 900 rpm. An attenuating HeNe laser light source propagating inside the glass wave-guide was used as the signal for urea measurements. A detection limit of 20μM was observed along with a dynamic range between 0.07mM – 8mM (Kovács 2003). These parameters, shown in **Figure 3**, are compared with results from earlier research studies. Kovács et al. showed a vast improvement for almost all parameters.

Results proved that with this particular arrangement of membranes, good sensitivity (0.05 absorption unit when going from 0.1 to 1mM urea) and a short response (16-20s) were accomplished. Flow injection urea measurements were also made within the

0.01-2mM concentration range since the response time had improved to an average of 18 seconds (Kovács 2003).

	This Work	Vaillo et al. (1995)[a]	Stamm et al. (1993)[b]
Forward Response Time[c] (s)	18 ± 2	210	420
Recovery Time[c] (s)	45 ± 3	-	-
Membrane[d] thickness (μM)	0.8 - 1	2 - 4	4
Detection limit (μM)	20	10	50
Dynamic range (mM)	0.07 - 8	0.05 - 10	-
[a] Micellar optode			
[b] Two layer optode			
[c] Measured in 10^{-4} M urea solution			
[d] Thickness of the ammonium ion sensitive layer			

Figure 3: *Comparison of optical urea sensors based on ammonium ion sensitive membrane.*

1.3.4. Enzymatic Field Effect Transistors

Also known as Ion-Sensitive Field-Effect Transistors (ISFET), these sensors have taken advantage of silicon micromachining technology and opened a door to the world of small-size and mass production of bioanalytical devices. The sensor contains a chip with two ISFETs and an inert electrode. The gate of one ISFET is covered by the biorecognition membrane layer containing active enzyme and the second gate is covered by a layer containing deactivated enzyme. The signal is then the difference in the output of the two ISFET devices (Cané 1997).

Urea sensitive Enzyme FETs (ENFETs) are based on the principles of the pH-sensitive field-effect transistors combined with the biospecific recognition of the urease enzyme. In one configuration, Gorchkov et al. (1997) were able to improve a sensor's sensitivity, detection limit, reproducibility and operational stability by adding permselective membranes (Nafion and poly 4-vinylpridine-co-styrene (PVP)) on top of a

layer of crosslinked urease in bovine serum albumin and glutaraldehyde. These permselective membranes were found to have different properties in terms of electrical charge. Sensor response was measured using both model buffer solutions and a diluted serum. Diluted serum was introduced for the purpose of learning about the possibilities of urea analysis in real biological samples.

Results showed that biosensors with Nafion or PVP eliminate the non-specific response of high concentration of proteins, thus increasing biosensor stability, sensitivity and accuracy. Also, in **Figure 4** below, it is shown that the sensor response (both with and without a Nafion membrane) were higher in model urea solutions than in diluted serum biological samples. Other characteristics such as the detection limit, linear dynamic range and reproducibility are greatly improved due the permselective membrane having different electrical charges. Detection limits of urea-senstive ENFETs without and with additional PVP and Nafion membranes were measured at 0.04 and 0.01mM respectively. The linear dynamic range for ENFETs with additional membranes was up to 0.5mM of urea (Gorchkov 1997).

Several advantages were noted by Gorchkov et al. (1997) when adding permselective membranes, such as measurements in steady-state or in kinetic modes, increased sensitivity, higher reproducibility and storage stability. Researchers also noted that they found no correlation between membrane properties and its influence on the sensor response.

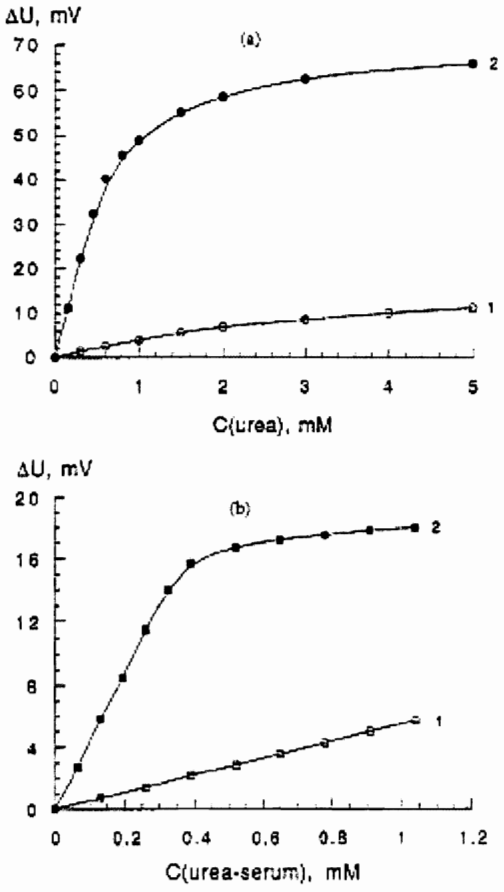

Figure 4: *Calibration graphs from steady-state response of the urea-sensitive ENFETs without (1) and with the additional Nafion (5.0%) (2) membranes. The measurements were conducted in model PBS buffer solution (a) and in diluted serum (b) (Gorchkov 1997).*

de Melo et al. (2003) constructed a urea biosensor based on urease-BSA membrane immobilized on the surface of an ISFET. The sensor was tested using various buffer solutions, such as potassium phosphate, Tris, citric acid and sodium tetraborate in order to determine which increased the sensor's sensitivity and dynamic range.

Bovine serum albumin has also been widely used for immobilization of the urease enzyme on the transducer surfaces via chemical cross-linking. A BSA membrane presents various advantages such as a simple preparation procedure, a satisfactory detection limit, a

high stability, and a rather high level of signal. Its main drawback was a narrow dynamic range and sensitivity. Due to this drawback, these types of sensors could not be used for direct urea measurement from human blood. The physiologic molar concentration of urea varies from 6 to 8 mM and can reach higher levels due to health complications (de Melo et al 2003).

The urease-BSA membrane deposited on the ISFET transducers had proven to be an excellent sensing element for urea determination at low concentrations. The ENFETs had shown remarkable properties such as high sensitivity, stability, and satisfactory reproducibility. Sodium tetraborate acted as a strong competitive inhibitor for the hydrolysis reaction of urea catalysed by urease, and to an extension of the dynamic range for the urea biosensor (de Melo et al. 2003).

Since the urea concentration in human blood serum and urine was within the analytical range of the developed biosensors, these results indicated that an ENFET based on urease-BSA membrane showed a strong potential for clinical routine analysis for urea assays (de Melo et al. 2003).

1.3.5. Electroconducting Polymer Urea Biosensors: PANi-Nafion and Polypyrrole

Electronically conducting polymers are a recent addition to the materials used for application in biosensors. Polyaniline (PANi) and polypyrrole (PPy) have been successfully used in biosensors for the determination of urea. This particular urea sensor was fabricated by electropolymerizing PANi using cyclic voltammetry (CV) on a Nafion/Au/ceramic plate electrode to form PANi-Nafion/Au/ceramic plate composite

electrode. Using this as a working electrode, the electrochemical response, characteristics and selectivity of ammonium ion in a buffer solution were investigated. The composite electrode was immobilized with urease and used as a sensing electrode to detect the concentration of urea in a batch system. Two immobilization methods were used: glutaraldehyde (GA) crosslinker and Nafion network (Luo 1997).

The urease/PANi-Nafion/Au/ceramic plate composite electrode showed a high sensitivity and selectivity of ammonium ion in a buffer solution due to the higher activity of urease on the composite electrode. The Nafion network was measured at a higher sensitivity (5.27 μA (mg $dl^{-1})^{-1}$ cm^{-2}) than the GA cross-linker (0.7 μA (mg $dl^{-1})^{-1}$ cm^{-2}). Also, the Nafion network had a higher detection limit of 6 mg dl^{-1} than 0.3 mg dl^{-1} for the GA crosslinker (Luo 1997).

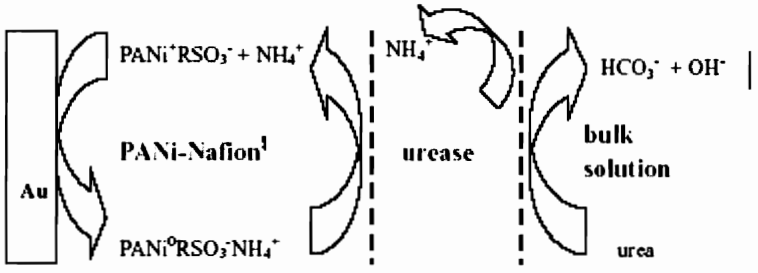

Figure 5: *Scheme of the sensing area on urease/PANi-Nafion®/Au/ceramic plate composite electrode (Luo 1997).*

Another electroconductive polymer is polypyrrole. Polypyrrole can be doped with various anions in an electrolyte solution with the great advantage of stability. In Japan, Osaka et al. (1996) designed and fabricated a high-sensitivity urea sensor consisting of electropolymerized electroinactive polypyrrole (PPy) with the polyion complex containing urease (Urs). This sensor exhibited potential response to urea within 20 seconds by

detection of pH change during enzymatic reaction with a pH-sensitive electroinactive PPy. It was concluded that the high sensitivity was due to the immobilization of the large number of urease by electropolymerization on the electrode pre-coated with polyion complex (Osaka 1996).

The fabrication of a biosensor by incorporation of urease into polypyrrole, enables the amplification of the non-Faradaic responses, such as adsorption, desorption or conductivity changes in analyte detection. This occurs through alteration of the resistance of the polypyrrole during the enzymatic reaction. However, the accomplished sensitivity and detection limit for these types of biosensors are often restricted when used in the dc-amperometric and potentiometric modes of detection (Adeloju 1997).

1.3.6. Evaluation of Urea Biosensors

Conductimetric biosensors have little light sensitivity and require no reference electrode. Due to the small driving voltage, it helps minimize the sensor's power consumption and reduces safety problems when used *in vivo*. One of the beneficial features of a conductimetric biosensors is that its enzymatic reactions involve charge production or consumption. An ionic composition modification of the membrane occurs as a result (Jdanova 1996).

Certain disadvantages of conductimetric biosensor are that they cannot function properly in a high ionic strength matrix since it is the membrane conductivity changes that are being measured. Also, the conductimetric response of the biosensor can be strongly influenced by the buffer capacity of the sample (Jdanova 1996).

Indirect/direct systems are the basis for amperometric biosensors. Indirect systems take advantage of conventional detectors to observe the metabolic product of a biological material. Direct systems involve a redox reaction which forms a close relationship between biology and electrochemistry. These direct systems involve the utilization of a modified electrode which is usually an electron acceptor in place of the natural electron donors. Amperometric biosensors are known to be reliable, cheaper and highly sensitive for the clinical, environmental and industrial purposes (Chaubey 2002).

Optical biosensors provide a low detection limit and fast analysis rate, which will be useful for many applications. Once its flow manifold is optimized and the measuring cell is redesigned, its analysis rate can be further increased.

Chemical field effect transistors have the following characteristics in mind: CMOS compatibility, mass fabrication, low cost, low power and ease of use. In turn, there are several drawbacks due to their interface with liquid solution such as the manufacturing of an integrated reference electrode, electrical insulation, packaging, temporal drift and CMOS compatibility of the different (bio)chemical sensitive materials (Sant 2003). These drawbacks must be overcome while developing collective technological processes for mass fabrication of ChemFETs.

These microsensors are usually fabricated on <100> oriented N-type silicon substrate. Its insulation between the electrical active zones and the electrolyte were performed using a standard P-well technology. The sensor applications were extended for urea detection by using "biocompatible, hydrophilic and photosensitive polyvinyl alcohol (PVA) layers" (Sant 2003). After diluting urease in an aqueous PVA solution, spin coating

and UV photolithography techniques have been developed and optimized in order to pattern urease PVA thin films. Thus, urease layers have been deposited on top of the SiO_2/Si_3N_4 pH-sensitive gate in order to form a SiO_2/Si_3N_4/PVA urea-sensitive gate. Enzymatic detection can be performed by diluting urea in citrate-phosphate buffered solutions or in dialysate (Sant 2003).

From experimentation results, it appears that urea-sensitive ChemFETs detection properties are saturated for urea concentrations higher than 25 mmol/l (Sant 2003). For high urea concentrations, it was found that detection properties are limited by enzymatic properties of the urease-based PVA layer: concentration, activity, etc.

The use of electroconductive polymers, such as polyaniline and polypyrrole, in urease biosensors is currently the largest area of analytical application for electropolymerized films. Its sudden wide interest is attributed to several essential advantages this procedure has concerning the immobilization of biocomponents. When electropolymerizing in the presence of urease in solution, it allows simple, one-step immobilization of urease in the polypyrrole layer formed.

Electroconductive polymers have several advantages. They have the ability to combine the role of the matrices or the immobilization with that of a signal transducer. Also, these procedures are recognized as spatially well controlled, which allow the fabrication of miniature biosensors. The main advantage of this immobilization technique is the electrochemical deposition is usually carried out under mild conditions and that the conducting polymer layer may act as an additional barrier for interfering species due to the sieve-effect and electrostatic interactions. Another advantage is that it allows for stable

immobilization of the electron transfer mediator in the polymer layer. Along with several advantages, come several disadvantages. The major challenges are the mechanisms of the electron transfer in configurations that usually run parallel to the charging of the double-layer at the electrode surface and the mass transport processes at the polymer interface. Electroconducting polymer biosensors are designed because of their "easy procedure, because the deposition process is simple to control, and because it is possible to use a polymer layer to discriminate interferences" (Trojanowicz 2003).

1.3.7. Conclusions

It has been found that biosensors have several major advantages over traditional analytical methods. This will lead to their more pronounced use in the biomedical field in the near future. Biosensors are disposed to miniaturization because biological molecules are available in small amounts. Tissue damage must be minimized in case of in-vivo monitoring. Biosensors are also characterized by short response times and their detection of the substrate is often made without prior separation. The most important advantage is that they are easy to use (Castillo 2004).

However, many urease biosensors still display a few drawbacks when compared to other analytical methods. One of the most difficult problems is that it has reduced stability. When enzymes are removed from their natural environment, they tend to rapidly loose their activity and thus limit the lifetime of the sensor. Another difficulty is the electrochemical interferences due to the complex sample matrices. Sample matrixes in the biomedical field are very complex. (Castillo 2004).

Urease enzyme biosensors have several detection strategies, which can meet most of the requirements of different applications. These different detection strategies allow researchers to utilize enzymatic sensors for different analytical purposes. It is the hope of the future to develop biosensors that can monitor bioavailable targets in remote places using portable devices. However, the step from research to product development and commercial availability is a large jump and will require collaboration and cooperation between research institutions, entrepreneurs, stakeholders and investors.

The current work aims to address some of the forgoing issues. Stability of the enzyme to temperature swings, pH shifts and time–dependent denaturation is to be achieved by immobilizing the enzyme within a 70% hydratable cross-linked hydrogel. This hydrogel, based on hydroxyethyl methacrylate (HEMA), provides a biorecognition matrix or milieu that supports enzyme stability (Abraham et al., 2005). Stability is to be further achieved by the PEGylation of the urease. PEGylation adds chains of polyethylene glycol (PEG) to the urease and thus surrounds the enzyme with a highly flexible and hydrophilic environment that prevents denaturation (Roberts 2002). Stability of the device from leaching of the urease is to be achieved by covalently immobilizing the PEGylated urease, using reactive functional groups on the distal end of the PEG chains, to the poly(HEMA) network. Finally, the chemistry of the poly(HEMA) network allows its covalent attachment to the microfabricated device surface as well as its molecular engineering to prevent protein fouling and confer interference shielding. The eventual goal is to combine the work of this thesis with electroactive polymers to make electroconductive hydrogels for enzyme biosensors.

Chapter 2. Background

2.1. Principles of Impedimetric Detection

Electrochemical impedance theory is a branch of alternating circuit (AC) theory that describes the response of an electrical circuit to an alternating voltage or current as a function of frequency. In direct current (DC) theory (where the frequency is equal to zero), resistance is defined by Ohm's Law: $V = I*R$. According to Ohm's law, a DC voltage can be applied to an electrical circuit, the resulting current can be measured and the resistance can be computed. However, in AC theory, where an alternating voltage is applied as a function of frequency, the analogous equation is: $V = I*|Z|$. In this equation, V is the AC voltage and I is the measured current. $|Z|$ is the magnitude impedance $((Z')^2 + (Z'')^2)^{1/2}$) or the AC equivalent of resistance, which is measured in ohms. Capacitors (C) and inductors (L) can also impede the flow of electrons in AC circuits just as resistors.

When performing electrochemical experiments, electrode kinetics, chemical reactions, adsorption and diffusion all contribute to impedance of electron/ion flow. These factors are considered to be analogous to resistors, capacitors and inductors, which impede electron flow in a circuit. Impedance is expressed as a complex number, the resistance is the real component and the combined capacitance and inductance is the imaginary component. The total impedance in a circuit is a combination of the opposition all the resistors, capacitors, and inductors to the flow of electrons. The opposition of capacitors and inductors is given the name reactance, symbolized by X and is measured in ohms (Ω).

The capacitance, C, contributes to the capacitive reactance, X_C. Also, inductance,L, contributes to the inductive reactance X_L.

When a sinusoidally varying voltage is applied across a given circuit and the resultant AC current waveform is measured, two AC waveforms can be observed on an oscilloscope: the applied potential and the resulting current. In the case of a purely resistive network, there is no change in time-dependent characteristics – phase, only the magnitude of the resulting current. Capacitors and inductors affect both the amplitude and phase of the current.

When most of the opposition of current flow comes from the capacitive reactance, a circuit becomes largely capacitive and the current leads the applied voltage in phase angle by 90 degrees. The more capacitive a circuit is, the closer the difference in phase angle approaches 90 degrees. However, when most of the opposition of current flow comes from the inductive reactance, a circuit becomes largely inductive and the current lags the applied voltage in phase angle by 90 degrees. The more inductive a circuit is, the closer the difference in phase angle approaches -90 degrees.

Figure 6a schematically illustrates an AC waveform for its applied potential and resulting current. The excitation voltage signal, expressed as a function of time, has the form: $V(t) = V_0 * \cos(\omega t)$, where V_0 = maximum peak-to-peak voltage, V(t) = voltage at any given instant, ω = frequency in radians per second = $2\pi f$ (where f = frequency in Hertz) and t = time. This signal is applied across the system of interest, which may consist of pure electrical components or of a biological or chemical sample between a pair of electrodes (Macdonald 1987).

The response signal, a current sine wave, can be described by the equation of the form: $I(t) = I_M * \sin(\omega t + \theta)$, where $I(t)$ = current at any given instant, I_M = maximum peak-to-peak current, ω = frequency in radians per second = $2\pi f$ (where f = frequency in Hertz), t = time and θ = phase shift in radians. Since the frequency and sinusoidal nature of the AC current response is unaffected by interaction with the system, the response signal can be characterized by both its amplitude and its phase shift with respect to the applied AC voltage. The ratio of the amplitudes of the applied and the response signal (V_0/I_M) and the phase shift between these signals (θ) can be used to determine the impedance, which can be represented as a complex number.

Impedance, which has both real and imaginary components, is defined as $Z(\omega) = R + jX$, where R is the resistance, $j = (-1)^{1/2}$, and the reactance $X = (-1/\omega C)$ for a capacitor or the reactance $X = (j\omega L)$ for an inductor. **Figure 6b** is a vector representation of impedance. Simple calculations show that $Z^2 = R^2+X^2$, and that $R = |Z|*\cos(\theta)$ and $X = -|Z|*\sin(\theta)$. Therefore, R and X, can be obtained from measurements of magnitude $|Z|$ and phase shift θ (Kell 1987, Suvarna et al. 2002). An impedance spectrum can be obtained when a frequency of the applied AC signal is varied within a specified frequency range and the impedance values are measured for each individual frequency.

(a)

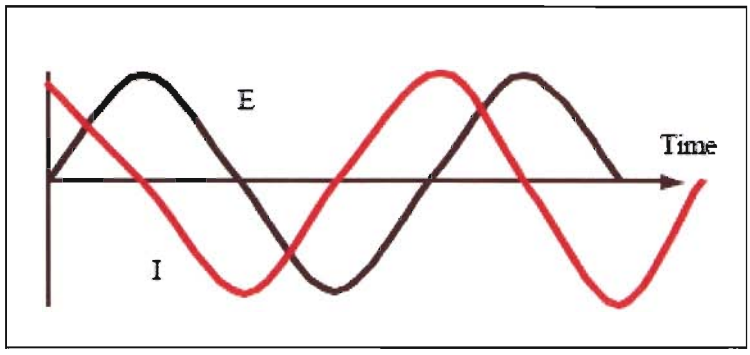

(b)

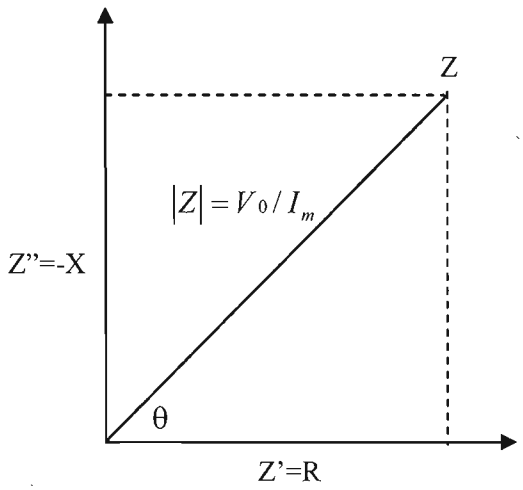

***Figure 6**: (a) AC waveforms for an applied potential and resulting current; (b) vector representation of impedance.*

Equivalent electrical circuits can be used to represent electrochemical reactions in the laboratory. These simple equivalent circuits provide impedance expressions. For example, the impedance of a resistor has no imaginary component. This means that the phase shift is zero degrees – or the current is in phase with the voltage. The current and impedance are frequency independent.

A capacitor has no real component, only an imaginary component that is a function of both capacitance and frequency. The current response is always leading the voltage

since the current through a capacitor is 90 degrees out of phase with the voltage drop across it. At high frequencies, a capacitor behaves like a short circuit since the impedance of a capacitor varies inversely with frequency. Also due to this inverse relationship between the capacitance and frequency, the impedance heads toward infinity at low frequencies.

In the case of an inductor, the current response is always lagging the voltage since the current through an inductor is 90 degrees out of phase (lags) with the voltage drop across it. At low frequencies, an inductor behaves like a short circuit since the impedance of an inductor varies proportionately with frequency. Also due to this inverse relationship between the inductor and frequency, the impedance heads toward infinity at high frequencies.

When determining the overall impedance of a combination of circuit elements, the impedance values of the individual components are combined according to some rules. For example, when two circuit elements are in series, the overall impedance is the vector sum of the individual impedance values, such as $Z_S = Z_1 + Z_2$. In a parallel circuit combination, the admittance values of the circuit components are added together (admittance is the inverse of impedance) in the form: $\frac{1}{Zp} = \frac{1}{Z_1} + \frac{1}{Z_2}$. In complex number representation, the real parts are added together to form the real component of the series combination, while the imaginary parts are added to form the imaginary component: $Z_S' + j\, Z_S'' = (Z_1' + Z_2') + j\,(Z_1'' + Z_2'')$ (Macdonald 1987).

At times, it is simpler to analyze the resulting plot of an impedance measurement on a circuit than deriving its impedance equation. The Randles circuit (**Figure 7**) represents the electrochemical impedance of an interface and matches with many simple electrochemical systems. R_Ω is the ohmic resistance of the solution between the working electrode (WE) and the reference electrode (RE). R_P is the charge-transfer resistance at the electrode/solution interface. C_{DL} is the double layer capacitance at this interface (Macdonald 1987).

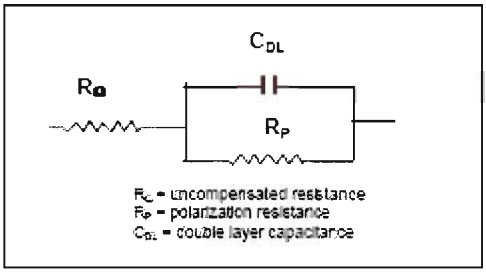

***Figure** 7: Equivalent electronic circuit for a simple electrochemical cell.*

For the Randles circuit, as the frequency increases, the impedance of a capacitor diminishes and the resistor remains constant. Above a certain frequency, the impedance of the capacitor, C_{DL}, becomes a value much smaller than the resistor, R_P. C_{DL} acts as a short and removes the R_P from the circuit since C_{DL} is in parallel with R_P. At the highest frequencies, the impedance of the capacitor becomes a value much smaller than the resistor, R_Ω, which means that the high frequency behavior of the Randles circuit is controlled entirely by R_Ω. However, for the Randles circuit at the lowest frequencies, the capacitor behaves as an open circuit. This makes the impedance of the Randles circuit the combined resistance of two resistors in series, $R_\Omega + R_P$.

Overall, at high and low frequencies, the Randles circuit behaves like a resistor. This means that the imaginary component is small, the phase angle is close to 0 degrees and the impedance is not affected by the frequency. At intermediate frequencies, the capacitor's impedance takes effect making the circuit more capacitive. The imaginary component becomes a significant factor and the phase angle starts to approach 90 degrees, which makes the circuit frequency dependent.

At times, a Randles circuit can be used to represent an electrochemical reaction coupled to a chemical reaction. The rate of an electrochemical reaction can be influenced by the diffusion of a reactant towards or a product away from the electrode surface, especially when a solution species must diffuse through a film on the electrode surface. Whenever diffusion effects dominate the electrochemical reaction mechanism entirely, the resulting impedance contribution is called the Warburg Impedance. **Figure 8** shows an equivalent circuit for an electrochemical reaction coupled to a chemical reaction. R_{CR} and C_{CR} represent the resistive and capacitive effects of the chemical reaction. The sub-circuit, R_W and C_W, represent the resistive and capacitive effects of diffusion - or Warburg Impedance. A Randles plot can then determine if the Warburg Impedance is a significant component in the circuit. If a Warburg Impedance is present, then an accurate reaction mechanism can be described (Macdonald 1987).

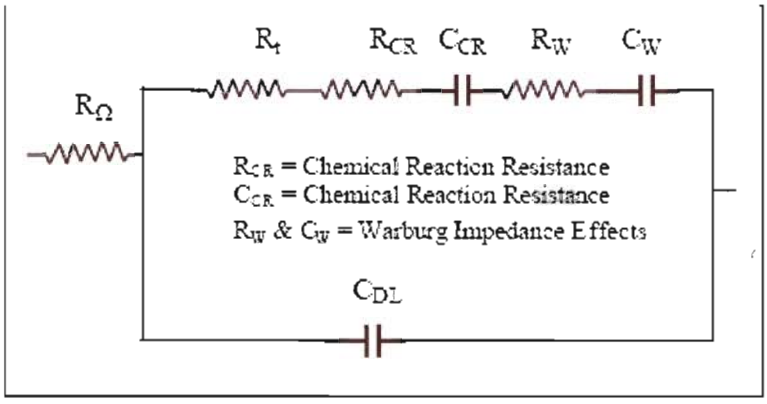

***Figure 8**: Equivalent circuit for an electrochemical reaction coupled to a chemical reaction.*

The standard procedure is to measure the impedance over a range of frequencies to determine which equivalent circuit appropriately describes the behavior of an electrochemical system. Usually an AC voltage is applied over a wide range of frequencies and the current response of the electrochemical system is measured. The system's impedance can then be calculated by analyzing the response signal at each frequency.

One of the most popular formats for evaluating electrochemical impedance data is called the Nyquist plot. In the Nyquist plot, the imaginary impedance component (Z") is plotted against the real impedance component (Z') at each excitation frequency. **Figure 9** illustrates the Nyquist plot of the Randles circuit in **Figure 7**. At high frequencies, the impedance of the circuit was mostly influenced by the ohmic resistance, R_Ω, which is located at the leftmost end of the semicircle (where the semicircle touches the x axis). At the low frequencies, the impedance of the Randles circuit becomes a pure resistance with

the value $R_\Omega + R_P$, which is located at the rightmost end of the semicircle (Macdonald 1987).

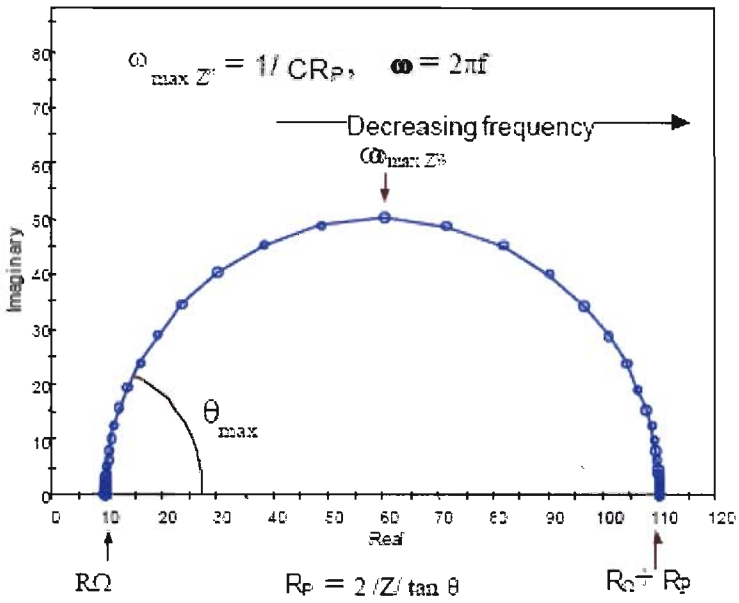

***Figure 9**: Nyquist Plot for a simple electrochemical system.*

There are several advantages when plotting impedance data using a Nyquist plot. The most advantageous one is being able to see the effects of the ohmic resistance on the Randles circuit. Also, if the ohmic resistance changes, it does not change the shape of the semicircle curve. Another advantage is that the Nyquist plot format emphasizes circuit components which are in series, like ohmic resistance.

However, in the Nyquist plot, the frequency does not appear explicitly. Also, the electrode capacitance can only be calculated when the frequency information is known, even though the ohmic resistance and polarization resistance can be read from the Nyquist plot. For example, as shown in **Figure 9**, the frequency which corresponds to the top of

the circle, $\omega_{(\theta=MAX)}$, can be used to determine the value of the capacitance, if R_P is known (Macdonald 1987).

Another popular format for plotting electrochemical impedance data is the Bode Plot. In the Bode Plot, the impedance magnitude, |Z|, and the phase shift, θ, can be examined as a function of frequency. Using a Bode Plot, it is easy to understand how the impedance depends on frequency since frequency appears explicitly on one of the axes. The logarithm of frequency on the x-axis allows for a wide frequency range to be plotted on one graph, and the logarithm of |Z| on the y axis allows for a wide impedance range to be plotted on the same graph. This is an advantageous feature, especially when the impedance depends strongly on the capacitance.

From the graph of log |Z| vs. log ω, the values of R_Ω and R_P can be taken. As shown in Figure 10, at the highest frequencies, log (R_Ω), can be read from the high frequency horizontal plateau. At the lowest frequencies, log ($R_\Omega + R_P$), can be read from the lowest horizontal plateau. At the intermediate frequencies on the log |Z| vs. log ω graph, the curve is a straight line with a slope equal to -1. When extrapolating this line to the y-axis, where log ω = 0, the value of C_{DL} can be calculated from the equation: $|Z| = (1/C_{DL})$, where $\omega = 2\pi f$. The phase angle, θ, is nearly zero at the high and low frequency. At the intermediate frequencies, since the imaginary component of the impedance increases, θ increases (Macdonald 1987).

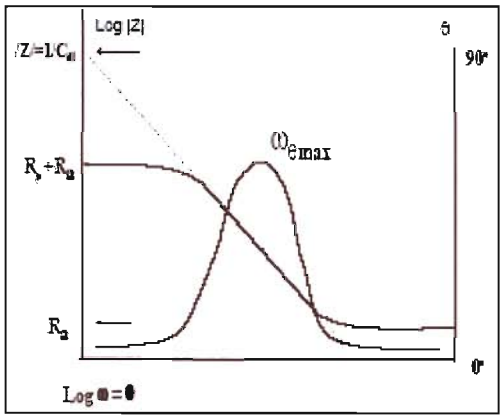

***Figure 10**: Bode Plot for a simple electrochemical system.*

The Bode plot is considered to be a more useful alternative than the Nyquist plot because the longer measurement times associated with low frequency R_P determinations can be avoided. Also, a more useful extrapolation of data from higher frequencies is possible. Overall, the Bode plot is able to provide a better interpretation of the electrical circuit's frequency dependent behavior than a Nyquist plot since its frequency values are implicit, rather than explicit.

However, a major disadvantage of a Bode Plot is that the shape of the curve changes if the circuit values change. **Figures 10** and **11** show the Bode plots for several circuits where the only difference is in the value of R_Ω. **Figure 11** shows how the slope of the central portion of the log |Z| plot is influenced by R_Ω. **Figure 12** shows that the location and height of the phase maximum (θ=MAX) are also dependent on the value of R_Ω (Macdonald 1987).

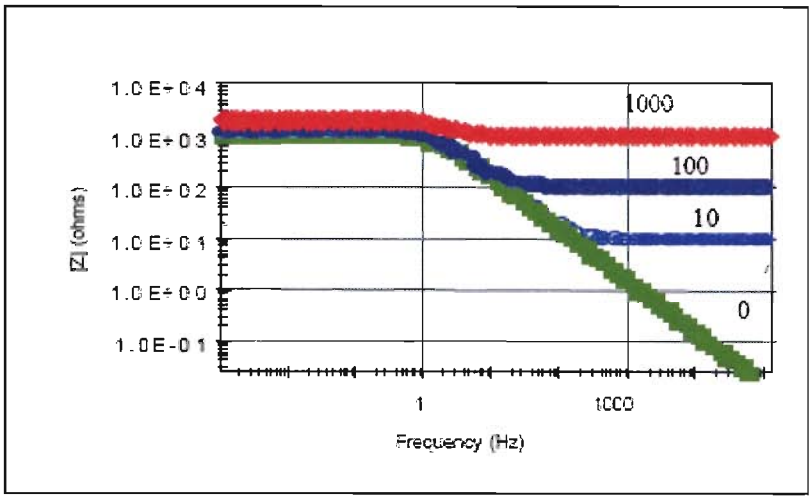

***Figure 11**: Bode Plots for selected values of R_Ω. (Impedance vs. Frequency).*

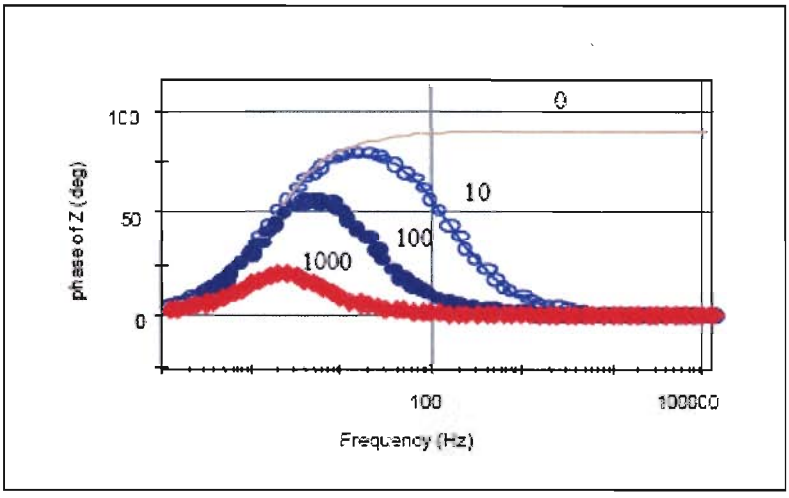

***Figure 12**: Bode Plots for selected values of R_Ω. (Phase Angle vs. Frequency).*

2.2. Impedimetry Applied to Urea Detection

The enzyme, urease, catalyzes the hydrolysis of urea into three ions: ammonium, bicarbonate and hydroxide. The production of these three ions increases the conductivity and pH of the environment where the enzyme is immobilized, thus reducing the impedance. The reaction of urease with urea involves the formation of an intermediate, which then reacts further with other substrates or decomposes to form ionic products.

These ionic products principally influence the value of R_Ω as they are not electroactive at the potentials normally used in impedimetry. However, these reaction products may also affect the value of R_p and C_{dl} through their influence on other electroactive species in the sample matrix and through their influence on the double layer. With thorough examination of the enzyme kinetics, it is possible to recognize several basic reaction steps involved in enzymatic catalysis, not a single reaction step. For all enzyme-catalyzed reactions, there is a hyperbolic dependence of reaction rate on substrate concentration. Initial rate data is where the rate of substrate consumption or product formation is determined over a short period of time following the initiation of the reaction. This is how all enzyme rate data is reported. The dependence of the initial rate on enzyme concentration is generally first order (Blanch and Clark 1997).

L. Michaelis and M. Menten strongly believed that there was a dependence of the initial rate of reaction on substrate and enzyme concentrations and set out to obtain a large amount of experimental data to support their contention (Blanch and Clark 1997). They proposed that when an enzyme-substrate complex is first formed, it is a reversible reaction since no chemical changes have occurred to the substrate. The enzyme and substrate are held together by physicochemical forces. Then a chemical change occurs, which results in the formation of product and the release of the product from the enzyme. This indicates that there is a first order dependence on the concentration of the enzyme-substrate complex:

$$E + S \left\langle K_S \right\rangle ES \left| k_2 \right\rangle E + P \qquad (1)$$

The equilibrium step is the first step in the Michaelis-Menten analysis. To determine the dissociation constant (K_S) of the enzyme substrate complex (ES), the equation can be:

$$K_S = \frac{[E][S]}{[ES]} \quad (2)$$

The rate of the product formation is given by:

$$\nu = k_2[ES] \quad (3)$$

A conservation equation is written for the total amount of enzyme in the system, where the enzyme serves as a catalyst:

$$[E_O] = [E] + [ES] \quad (4)$$

[E] can be substituted in terms of the known concentration of the total amount of enzyme initially in the reaction mixture, $[E_O]$, and also the enzyme-substrate complex into the equilibrium step equation:

$$[E] = [E_O] - [ES] \quad (5)$$

$$K_S = \frac{([E_O]-[ES])[S]}{[ES]} \quad (6)$$

With rearrangement and substitution, the rate of reaction is given by:

$$\nu = \frac{k_2[E_O][S]}{K_S + [S]} \quad (7)$$

Sometimes, the constants k_2 and E_O are multiplied together to give ν_{MAX}, the maximum rate of reaction. This is substituted into the eq. 7 to give:

$$\nu = \frac{\nu_{MAX}[S]}{K_M + [S]} \quad (8)$$

K_M is known as the Michaelis constant and is equal to K_S for simple reactions.

The initial rate of reaction is determined from the Michaelis-Menten expression above by assuming that the substrate concentration is sufficiently high so that it does not change significantly from its initial value over the period when the initial rate is determined experimentally ($[S] \sim [S_O]$).

$$\nu = \frac{k_2[E_O][S_O]}{K_S + [S_O]} = \frac{\nu_{MAX}[S_O]}{K_M + [S_O]} \qquad (9)$$

Equation 9 is referred to as the Michaelis-Menten equation and provides an explanation for the observed hyperbolic dependence of initial rate on substrate concentration and the linear dependence on enzyme concentration. This equation provides that the maximum rate per enzyme molecule is ν_{MAX}/E_O. For example, when urease has one active site, this will equal k_{CAT}. However, when the enzyme has *n* active sites per urease molecule, k_{CAT} will be $\nu_{MAX}/(n*[E_O])$ (Blanch and Clark 1997).

A Lineweaver-Burk plot is an established graphical method to arrive at these kinetic parameters. A Lineweaver-Burk plot allows the graphical determination of the values of ν_{MAX} and K_M by taking the double reciprocal of Equation 9 to form Equation 10. A plot of $1/\nu$ versus $1/[S]$ gives $1/\nu_{MAX}$ as intercept on the y-axis when $1/[S]$ approaches zero, and an intercept of $-1/K_M$ on the x-axis for ν approaching zero, as shown in **Figure 13**.

$$\frac{1}{\nu} = \frac{1}{\nu_{MAX}} + \frac{K_M}{\nu_{MAX}} \cdot \frac{1}{[S]} \qquad (10)$$

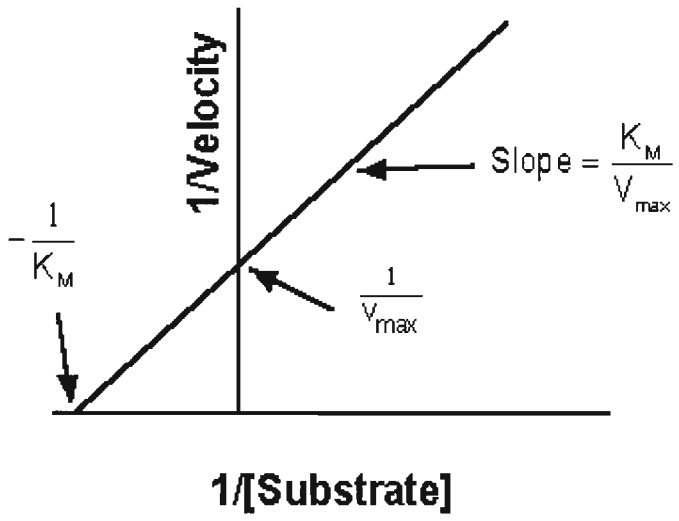

***Figure 13**: Lineweaver Burk Plot.*

All enzymes have optimum performance conditions, such as pH, temperature, molar concentration of substrate and buffer solution. Calibration tests are conducted first to determine the best molar concentration of urea to provide the best impedimetric response without under or over saturation of the enzyme. Temperature and pH profiles are then conducted in order to determine the optimum performance conditions of an enzyme without denaturation or deactivation of the enzyme. For a temperature profile experiment, a range from 10°C to 50°C, is typically used at an optimal urea concentration. It has been generally found that the temperature of the human body (37°C), provides the best temperature for urease to perform at its best. As far as pH profile experiments, a range from pH 4.0 to pH 8.0 is used at a particular urea concentration to also determine optimum ionic conditions without denaturation of urease. A neutral pH of 7.0 has been found to serve as the best condition for urease (Brahim 2001).

2.3. Biorecognition Membrane of Impedimetric Biotransducers

2.3.1. Hydrogels of HEMA

Polymeric materials, whether they are natural or synthetic, come in many different forms. However, they are usually categorized according to their macroscopic structure. Polymeric materials generally fall into the categories of linear or branched macromolecules and macromolecular networks. Polymeric hydrogels are polymeric networks that absorb water to cause macroscopic changes in their physical dimensions, but do not dissolve in water due to virtual, electrostatic or covalent cross-links that hold the structure intact. Hydrogels may be part branched and macroscopically cross-linked systems. They have a porous sponge-like structure which swell in water and become hydrated. The swelling has a defined limit depending on the degree of cross-linking (Peppas 1999, Abraham et al. 2005).

Hydrogels are extremely hydrophilic due to the presence of –OH, -COOH, $-CONH_2$, -CONHR, and $-SO_3H$ along the polymer chains. Due to the presence of crosslinks provided by crystalline regions, entanglements, covalent bonds, charge complexes, H-bonding, van der Waals or hydrophobic interactions, the insolubility and stability of hydrogels are quite strong (Byrne et al. 2002).

Due to their significant water content, hydrogels also possess a degree of flexibility very similar to natural tissue, which minimizes potential irritation to surrounding membranes and tissues. Hydrogels have been used as prime carriers for pharmaceutical applications, predominantly as carriers for delivery of drugs, peptides or proteins. They have also been used to regulate drug release in reservoir-based, controlled release systems

or as carriers in swellable and swelling-controlled release devices. Hydrogels are also used to engineer biocompatibility into biosensor materials (Byrne et al. 2002, Abraham et al. 2005).

Hydrogels can be classified as neutral, anionic or cationic. From a thermodynamic point of view, their swelling behavior is governed by a delicate balance between the polymer-water Gibbs free energy of mixing and the Gibbs free energy associated with the elastic nature of the polymer network. As equilibrium swelling is reached, the partial molar quantities of these free energies become equal. Hydrogels can be rendered sensitive to physiological conditions due to the presence of specific functional groups along their backbone polymer chains. The swelling behavior and associated release kinetics of these gels may be dependent on pH, temperature, ionic strength, or even drug concentration (Byrne et al. 2002, Abraham et al. 2005).

The measurement of the time dependent impedance of a hydrogel requires that a non-perturbating frequency to be chosen for the interrogation. The frequency is chosen to be larger that the heterogenous charge transfer rate of typical electrochemical reactions at the electrode-electrolyte interface. The voltage amplitudes are likewise chosen to negate the electrochemical reaction of any electroactive species within the hydrogel or that may diffuse into the hydrogel. A non-perturbating frequency such as 4kHz is sufficiently high to avoid interfacial charge transfer and 50 mV p-t-p is sufficiently small as to not induce electrochemical reactions.

Hydrogels come in one of two groups: conventional or environmentally sensitive. Conventional hydrogels do not exhibit much sensitivity to pH or temperature changes

(environmental sensitivity). However, the most commonly studied hydrogel having environmental sensitivity is poly (2-hydroxyethyl methacrylate) (p(HEMA). p(HEMA) is commonly used as a backbone for fabricating pH sensitive gels and is synthesized from the monomer hydroxyethyl methacrylate (HEMA). p(HEMA) is an appropriate biomaterial for *in-vivo* purposes due to its lack of toxicity since they have high water content, similarly to human body tissue, and degradation resistance (Cifova et al. 1988, Abraham et al. 2005).

2.3.2. Urease Immobilization within Hydrogels

Immobilization of urease via hydrogel cross-linking is also known as enzyme entrapment within a gel. This technique is based on the principle that the immobilization of an enzyme within the hydrogel matrix inhibits the release of the enzyme while allowing the penetration of substrate and release of product. Hydrogel entrapment involves entrapping urease within the interstitial spaces of cross-linked water-insoluble polymer gel. Gel formation is accomplished by polymerizing the monomer(s) in an aqueous solution of soluble urease and cross-linking agent. The formulation of this highly hydrophilic cross-linked hydrogel can be formed from p(HEMA) via UV cross-linking of HEMA and Triethylene glycol diacrylate (TEGDA). The cross-linking of the hydrogel is photoinitiated by 2,2-Dimethoxy-2- phenylacetophenone (DMPA). p(HEMA) is one of the most popular materials for hydrogel matrix composition (**Figure 14**) (Brahim et al. 2002).

Urease immobilization via hydrogel crosslinking is usually a mild procedure and can be used universally with almost any type of biomolecule. One major advantage of this immobilization technique is that the enzyme stays relatively untouched by the immobilization procedure itself. In turn, denaturation of urease as a result of free radical

formation is a possible disadvantage. Another disadvantage is the porosity of such a gel. With pore size distribution being so broad, the continuous leakage of the enzyme may occur.

Figure 14: *Picture illustrating concept of enzyme immobilization in p(HEMA) hydrogel layer.*

2.3.3. Consistent activity of the enzyme

When an enzyme is immobilized onto the surface of a sensor, its enzymatic behavior (activity and efficiency) is altered from its behavior in solution. Its altered behavior is greatly affected by its immobilization method. Placing an enzyme in a different environment and confining it to a microvolume has significant effects on enzyme characterizing variables (V_{max}, K_m, k_2 or k_{cat}/K_m).

According to Cunningham, an enzyme's efficiency "...may be the result of random orientation of the molecules, thus shielding the active site for some of the molecules, or it may involve a degree of denaturation during immobilization. It may also reflect effects of the environment that shift reaction conditions away from the solution optimum." Microenvironmental effects are usually related to the inner membrane's "...pH,

accessibility, ionic strength, polarity of the medium, and inhibitory action of accumulated products in the confined space" (Cunningham 1998).

The temperature, pH, presence of enzyme inhibitors and concentrations of substrates and enzymes in an enzyme-mediated reaction, are among the major factors affecting enzyme activity. The rate of biological reaction doubles with a 10°C increase in temperature. Also the maximum activity is usually observed between pH values of 5 and 9. Most enzymes denature at extremely low and high pH values. Small changes in pH have significant effects on the ionic state of the enzyme and substrate. The changes in pH alter the charge distribution on the binding site, causing a change in the efficiency of catalytic activity (Tozeren 2004).

2.3.4. Homogeneity of the layer

The purpose of a homogenous membrane layer with entrapped enzyme is to fabricate the thinnest layer possible but with the enzyme still retaining the highest possible specific activity. A homogenous membrane layer serves several important functions. First, it serves as a protective barrier to prevent large molecules such as other proteins (particularly proteases) from entering the enzyme layer. The membrane layer also prevents the leakage of enzyme into the sample solution. A properly chosen membrane "...exhibits permselective properties which are additionally beneficial to sensor function" (Cass 1990). The last property is that a membrane can function as a diffusional barrier for the substrate and interfering substances.

Enzymatic biosensors have linear dynamic ranges of "...several orders of magnitude because the response is controlled by diffusion through the membrane and not

by enzyme kinetics" (Cass 1990). For an enzyme with low activity, a thick and homogenous membrane will be needed to achieve a good, but slow, linear response. However, if the enzyme has high activity, then a thin and homogenous "...membrane is sufficient and a rapid response may be obtained" (Cass 1990).

2.3.5. Adhesion

Before enzyme immobilization can occur onto a substrate, surface modification of that substrate needs to be performed. Surface modification of a substrate has as its principal purpose the specific attachment of the enzyme or the bioactive polymer membrane to the electrode surface. Without it, enzyme attachment would not occur and the result may be delamination of the polymer membrane.

A common approach is the use of organosilanes such as 3-aminopropyl trimethyoxysilane (γ - APS) and alkane thiols such as cysteamine that possess ω–functional groups for the covalent attachment of the enzyme. These functional groups may also be used to immobilize hydrogels and other polymer membranes that carry the entrapped enzyme. Functionalization by derivatization of surface-confined, pendant primary amine functionalities of γ-APS with polyethylene glycol (PEG) chains using acrylol (polyethylene glycol) NHS ester (Acryl-PEG-NHS) was accomplished by and this served to immobilize a bioactive hydrogel (Sheppard 1995, Abraham et al. 2005).

After these essential steps, the substrate is ready to be utilized as an enzymatic chemical sensor. Immobilization techniques can be used to adhere the enzyme to the substrate and perform electrochemical impedance spectroscopy.

2.3.6. Other Immobilization Techniques

2.3.6.1. Covalent Crosslinking Via Glutaraldehyde

Glutaraldehyde is a common coupling agent used to create protein layers. According to a review by William Scouten (1995), polymers result from a process that begins with the abstraction of a proton from one monomer to form an α carbanion, which then condenses with a second monomer. The resulting dimer undergoes β elimination to form an α-β unsaturated ketone. This reactive species can undergo further polymerization or it can couple to a protein. These reactions are very complex and can never be overstated. Due to the low stability of glutaraldehyde activated sensor surfaces at high pH values, the usual pH to perform subsequent enzyme immobilization is around 7.0-8.5 (Lopez-Gallego et al 2005).

One of the major problems with using glutaraldehyde as a coupling agent is its reproducibility, the result of its arbitrary impact on the enzyme's active site. However, it is still a very convenient method for immobilizing enzymes. It has been noted in some cases with using glutaraldehyde that the immobilized protein is more active and/or more stable than the free protein. This is possible because of the multi-point attachment, which inhibits the unfolding of the protein. **Figure 15** illustrates the concept of using enzyme, BSA and glutaraldehyde as an enzyme immobilization technique (Scouten 1995, Lopez-Gallego et al. 2005).

When immobilizing urease via covalent glutaraldehyde crosslinking to the sensing area of the electrode, it is most commonly done through the functional groups of the enzyme. These functional groups originate from amino acid side chains, such as "∈-amino

groups of lysine, carboxyl groups from aspartate and glutamate, sulfhydryl groups from cysteine, and phenolic hydroxyl groups from tyrosine." To increase the amount of urease loading in the glutaraldehyde membrane, the enzyme is usually crosslinked with another benign protein such as bovine serum albumin (BSA). It is then able to form a thin layer on the support surface. Bovine serum albumin is a protein which dilutes the enzyme content in the polymer net to enhance its stability and the mechanical parameters of the biolayer (Cunningham 1998). The crosslinking agent, glutaraldehyde, is then able to react with the lysine amino groups of urease. The combination of the urease, bovine serum albumin and glutaraldehyde is placed on the electrode surface and left to dry either at room temperature or in the refrigerator.

This immobilization technique is simple and quick because it only requires direct contact between urease and the membrane. Certain advantages of this technique are that it is a stable biomolecule-support complex, leakage of the immobilized enzyme is unlikely and it is well suited for mass production and commercialization. The disadvantages are that it can be quite complicated, time consuming and there is the possibility of activity losses due to reaction involving groups essential for the biological activity (Cunningham 1998).

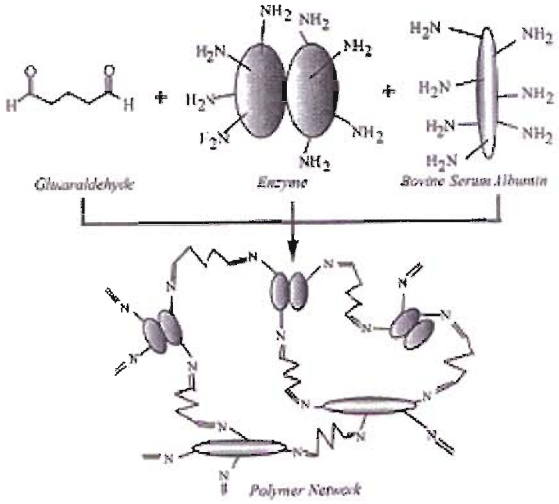

Figure 15: *Creation of a polymer net from glutaraldehyde, BSA, and the enzyme.*

2.3.6.2. Urease Immobilization Via Covalent Attachment

The covalent binding method is based on the covalent attachment of an enzyme to a water-insoluble support. It is the most widely used and most investigated enzyme immobilization technique. Only the functional groups not essential for catalytic action should be involved in covalent attachment to the support matrix. This can be used as a general application for immobilization due to the wide variety of binding reactions and of carriers with functional groups capable of covalent coupling.

This type of binding involves two steps: (i) activation of a solid matrix and (ii) binding of the enzyme (Katz 1994). Carbodiimide coupling is the most common method to covalently couple enzymes to an electrode surface (**Figure 16**) (Willner 1998). This reaction is provided by 1-ethyl-3- (3-dimethylaminopropyl)-carbodiimide (EDC) and promoted by N-hydroxysuccinimide (NHS). EDC is a water-soluble derivative of carbodiimide. Carbodiimide catalyzes the formation of amide bonds between carboxylic

acids and amines by activating carboxyl to form an O-urea derivative. NHS is often used to assist the carbodiimide coupling in the presence of EDC. The reaction includes formation of the intermediate active ester that further reacts with the amine function to yield the amide bond (Katz 1994).

In this reaction, EDC produces amide (-CONH-) bonds between the $-NH_2$ groups on the functionalized electrode surface with the available carboxylic acid (-COOH) groups of urease by activating the carboxyl. NHS is often used to assist in the coupling between the amine functionalities and carboxylic acid functionalities in the presence of EDC.

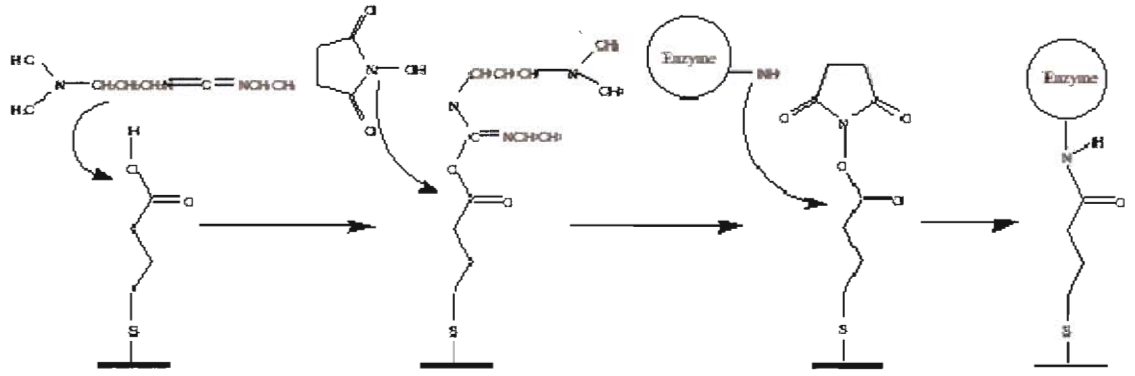

Figure 16: *Schematic diagram showing the covalent attachment of an enzyme to a self-assembled monolayer of thiol-carboxylic acid using EDC and NHS (Willner 1998).*

Covalent attachment holds several advantages such as a stable biomolecule-support complex and the unlikely chance of leakage of immobilized biomolecules. It is also well suited for mass production and commercialization. However, some of the drawbacks are that it is complicated and time consuming. There is also the possibility of activity losses due to reaction involving groups essential for the biological activity and the potential for time-dependent denaturation (Katz 1994).

2.3.6.3. Biosensor Limitations

Biosensors using enzyme immobilization have several issues, such as the relative lack of long-term stability of biological molecules, which are causing limitations in their commercialization. There is a belief that enzyme immobilization improves the stability of enzymes towards physical and chemical stress. However, under some situations, the immobilized enzyme shows decreased stability (Scouten 1995). These situations are brought on due to the enzyme being removed from their natural environment. A change in this environment causes loss of activity for the enzyme and thus limits the performance of the biosensor (Castillo 2004).

Another limitation is the specificity of the biological molecule used in biosensor construction. For example, glucose oxidase is a very specific enzyme, whereas amino acid oxidases will recognize a large spectrum of amino acids. As enzymes are further studied and become better defined, it will be possible to customize enzymes that can function in a specific way and with greater stability. These customized enzymes will be vital in cases where target analytes cannot be detected by available enzymes (Scouten 1995).

Chemical modification such as protein engineering, with site-directed mutagenesis is a possible approach to make enzymes more stable and specific. The pH optimum of the enzyme can also be shifted by mutating charged surface groups. This method is particularly useful in fabricating biosensors using two or three enzymes with different pH optima (Scouten 1995).

A third limitation of biosensors is retaining enzyme activity. It has been found that an adequate amount of enzyme can be immobilized so that only a relatively small percentage need be active for the sensor to be fully functional. There are certain cases where a large fraction of enzyme needs to be active. In some instances, it may be beneficial to immobilize the enzyme with the active site facing outwards from the electrode surface. This may be particularly applicable for large substrates, due to the fact that the matrix surface may be sterically inhibiting to the substrate from reaching active sites that are only partially blocked by poor orientation on the surface (Scouten 1995). The matrix surface itself is fairly complex and can cause electrochemical interferences. Being able to modify an electrode surface which favors exclusively one single electrochemical process is a fairly difficult task and is another source of biosensor limitations (Castillo 2004).

When a biosensor is used for in-vivo measurements, biocompatibility and biofouling are the two critical issues and sources of biosensor limitations (Castillo 2004). A small dynamic range, short enzyme lifetime, sensitivity to interferents and inhibitors and pH dependency are other specific enzymatic biosensor limitations (Chaubey 2002).

Chapter 3. Experimental

3.1. Materials

Urease (E.C. 3.5.1.5 from Jack Beans; 82.8 U/mg solid), photoinitiator (2, 2 – dimethoxy-2-phenyl acetophenone) (DMPA, 99%, MW ca. 256.30), urea (E.E.C. 200-315-5, MW ca. 60.06), bovine serum albumin (BSA) (96-99% lyophilized powder, E.C. 2329362, MW ca. 66kDa) and tris(hydroxymethyl)aminomethane (98.8%, E.C. 201-064-4, MW ca. 121.14) were obtained from Sigma Chemical Co (St. Louis, MO). The monomer, 2-hydroxyethyl methacrylate (HEMA) was obtained from Polysciences, Inc. (Warrington, PA). The crosslinker, tetraethyleneglycol diacrylate (TEGDA), γ-Aminopropyl trimethoxysilane (γ-APS, 97%), HEPES (sodium salt, 99%, E.C. 278-169-7), poly-(2-hydroxyethyl methacrylate) [p-(HEMA)], glutaric dialdehyde (50 wt% solution in water) and N,N,N',N'-tetramethylethylenediamine (redistilled, 99.5+%) were obtained from Aldrich Co. (Milwaukee, WI). Acryloyl (polyethylene glycol)$_{110}$ N-hydroxy succinamide ester (MW 3400) (Acryl-PEG-NHS) was obtained from Nektar Therapeutics, (Huntsville, AL). Microlithographically fabricated interdigitated microsensor electrodes (IMEs) (part number IME 1025.3-M-Pt-U) were purchased from ABTECH Scientific Inc. (Richmond, VA). Each borosilicate glass chip consisted of a pair of opposing electrodes comprising 10 μm wide platinum digits that were ca. 3 mm long and separated by 10 μm wide free spaces. There were 25 digits on each electrode bus that established a tortuous path of 14.75 cm of exposed glass surface between the digits.

3.2. Methods

3.2.1. Surface Cleaning/Activation

Surface modification of interdigitated microsensor electrodes (IMEs) have as its principal purpose the specific attachment of the bioactive hydrogel membrane to the electrode surface. The IMEs were cleaned in a Branson 1200 Ultrasonic Cleaner by sequential washing; first in acetone, followed by 2-propanol and finally in deionized water. For removal of residual organic/ionic contamination, the devices were immersed in a (5:1:1) solution of deionized water, ammonium hydroxide and hydrogen peroxide, respectively. The devices were then rinsed in deionized water for 5 min. Prior to silanization, the devices were cleaned in 15 min in UV/ozone cleaner, UV_Clean (Boekel Industries, PA), to remove adventitiously adsorbed organics. Then the devices were dried in an air-filtered convection oven at 80 °C for 45 min to remove traces of surface bound water.

Following cleaning, the devices were each made the working electrode in a three-electrode electrochemical cell in which a clean Pt mesh electrode served as the counter electrode and a Ag/AgCl, 3M Cl^- electrode served as reference. Platinum black was then potentiostatically deposited (PAR Model 273 Potentiostat/Glavanostat) from a solution of chloroplatinic acid (YSI 3140 Platinizing Solution). A current density of 59 mA /cm^2 was passed for 13 s to produce a deposit that was clearly visible under an optical microscope. The cleaned and platinized devices were further modified by immersion in a freshly prepared solution of γ-APS in anhydrous ethanol (0.1 vol %) at 40°C in a water bath for 30 minutes, rinsed profusely with ethanol (x3) and finally the adsorbed and hydrogen bonded

silanol layer was oven cured at 110°C for 30 min. Functionalization by derivatization of the surface confined, pendant primary amine functionalities of γ-APS of the device surface with PEG chains was accomplished by immersion of the device in a 0.5 mg/mL solution of Acryl-PEG-NHS prepared in HEPES buffer (0.01M, pH 8.5). The reaction was allowed to proceed for 2.5 hrs in the dark at room temperature (Sheppard 1995).

3.2.2. Preparation of Tris Buffer

A 10mM Tris buffer was prepared by dissolving 2.4g Tris into 2L DI H_20. An appropriate amount of stock HCl was added to adjust pH of Tris buffer to pH 7.0.

3.2.3. Preparation of Urea Stock Solutions

A 1M urea stock solution was prepared by dissolving 6.0g urea into 100mL of Tris buffer (10mM, pH 7.0). A 0.1M urea stock solution was prepared by serial dilution of 1M urea. Another urea stock solution of 0.01M was prepared by serial dilution of 0.1M urea. For impedance testing of all the urease biosensors, the urea molar concentrations were varied from 0μM to 5mM by injecting specified volumes of a particular stock solution. **Table 1** shows the volume and stock solution of urea.

Urea Solution Concentrations				
Final Concentration	Initial Molarity	Initial Volume	Final Molarity	Final Volume
10uM	0.01M	5.5uL	10uM	5.5
50uM	0.01M	27.5uL	50uM	5.5
100uM	0.01M	55uL	100uM	5.5
250uM	0.1M	13.75uL	250uM	5.5
500uM	0.1M	27.5uL	500uM	5.5
1mM	0.1M	55uL	1mM	5.5
2mM	1M	11uL	2mM	5.5
3mM	1M	16.5uL	3mM	5.5
4mM	1M	22uL	4mM	5.5
5mM	1M	27.5uL	5mM	5.5

Table 1: *Volume and stock solution of Urea.*

3.2.4. Synthesis of molecularly engineered p(HEMA) hydrogels

Prior to polymerization of the monomer cocktail, the neat monomer HEMA and cross-linker TEGDA were flowed over inhibitor removal columns (Aldrich Chemical Co.) to remove inhibitors. The cocktail consisted of 97 mol%:3 mol% (HEMA/TEDGA) formulation used to prepare a hydrogel for immobilization of urease. The formulation was placed in a vial and the photoinitiator (0.02 wt % monomer) was dissolved in the resulting monomer cocktail. The cocktail was then purged with argon for 10 min. The functionalized electrode surfaces (IMEs) were spin coated (3000 rpm) with the respective freshly purged monomer mixture (1-2 μL) to produce thin, even depositions. The electrodes were then

placed into a UV cross-linker (UVP CX-2000, CA) and immediately irradiated (λ = 365 nm) under an inert blanket of argon for 10 minutes.

3.2.5. Methods for Conferring Urea Specificity

3.2.5.1. Free Urease in Solution

After cleaning, platinization, silanization and activation, a blank IME 1025.3-M-Pt-U can be used for impedance calibration tests in free urease solution. A free urease solution was prepared by dissolving 110mg of urease into 55mL Tris buffer (pH 7.0, 10mM) (2mg/mL). The IME was placed in clamp and lowered in a water bath cell containing 5.5 mL of the urease stock solution. Fifteen minute experimental runs were set. At five minutes into the fifteen minute run, the appropriate concentration and volume of urea, from 0μM to 5mM, was injected into the water bath cell. Two trials for each molar concentration were performed. Between each experimental run, the IME was cleaned off with DI H_20 and dried before placing back in the clamp.

3.2.5.2. Urease Covalently Crosslinked via Glutaraldehyde

A 0.29 mol% solution of Bovine Serum Albumin (BSA, 66000 g/mol) was prepared by dissolving 10mg BSA into 100μ L Tris buffer (10mM, pH 7.0). The urease solution was prepared by dissolving 3.75mg of urease into the 100uL BSA solution (2mg/mL). This solution was then combined with 25μL of 5% glutaraldehyde (100.17 g/mol, 99.71mol%) and mixed thoroughly. A small volume (1-2 μL) was applied to the interdigit space of the IME that was previously surface functionalized with Acryl-PEG moieties and spin coated over the entire working area (ca. 3000 rpm, 5 s). The IME was placed in petri dish and stored in refrigerator for a minimum of 3 hours before use.

3.2.5.3. unPEGylated Urease Entrapped in p(HEMA) Hydrogel

This fabrication procedure first involved preparing a cocktail comprising 11.25 mg of urease in 100μL Tris buffer (10 mM, pH 7.0)) dissolved in a monomer mixture of HEMA and TEGDA (97:3 mol %) containing 0.02wt% dimethoxyphenyl acetophenone (DMPA). A small volume (1-2 μL) was applied to the interdigit space of the IME that was previously surface functionalized with Acryl-PEG moieties and spin coated over the entire working area (ca. 3000 rpm, 5 s). The enzyme-monomer coated electrode was then placed in a UV polymerization chamber (UVP Model CX-2000) and immediately irradiated with UV light (2.3 W/cm^2, 366 nm) for 10 min under an inert argon atmosphere to affect polymerization of the bioactive monomer mixture.

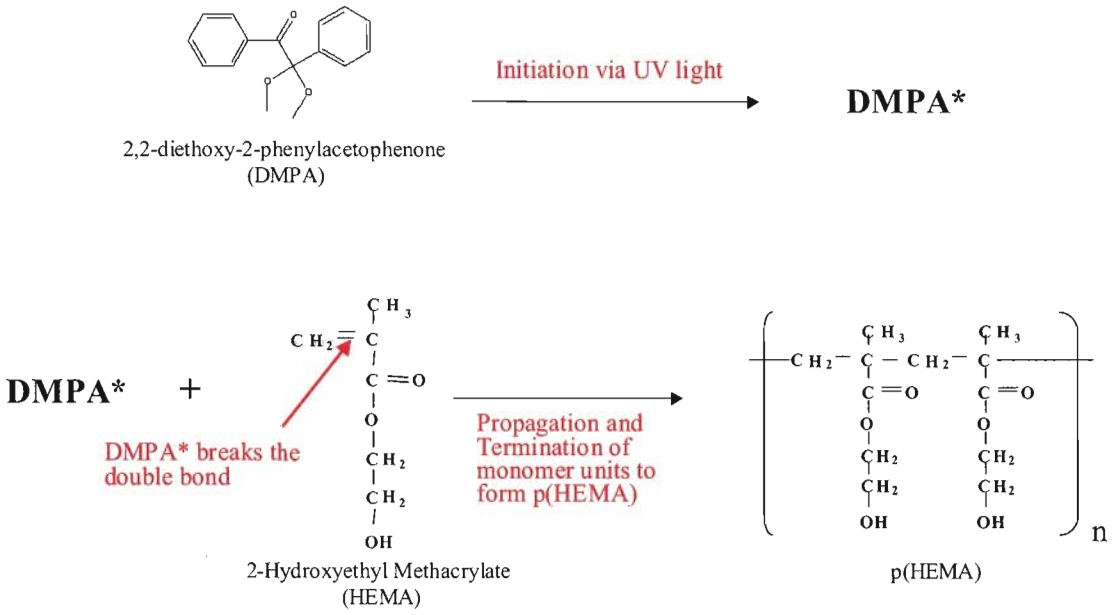

***Figure 17**: Free Radical Polymerization via DMPA; UV light creates the free radical of DMPA* to initiate the linking of HEMA monomer units.*

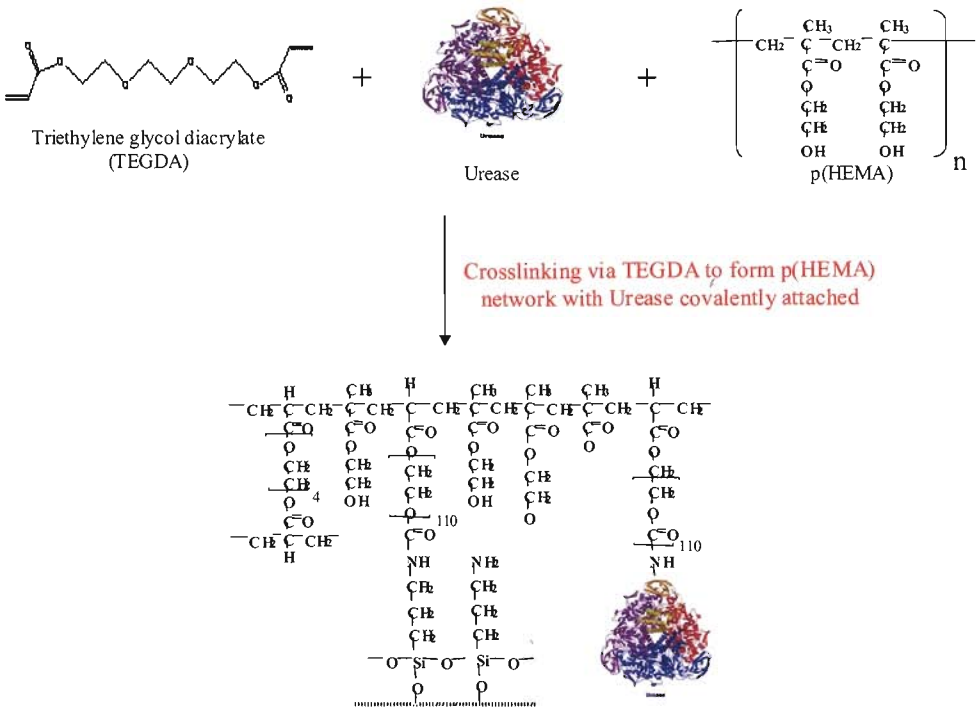

***Figure 18**: Crosslinking via TEGDA to form p(HEMA) hydrogel with Urease covalently attached.*

3.2.5.4. PEG (2:1)-Urease Entrapped in p(HEMA) Hydrogel

Urease was separately derivatized with the PEG moiety. This was achieved by coupling the activated ester functionality of the commercial Acryl-PEG-NHS ester to available amine groups of lysine residues on the enzyme. PEGylated-urease (2:1) was prepared by dissolving 7.5 mg urease and 0.10625 mg Acryl-PEG-NHS ester into 2000 μL of HEPES buffer solution (0.1 M, pH 8.5). The enzyme and PEG components were allowed to couple at room temperature in the dark for 2.5 hrs. Subsequently, 100 μL of this solution was pipetted into dialysis vials and dialyzed against Tris buffer (10 mM, pH 7.0) for at least 24 hours. During dialysis, excess water had diffused into the dialysis vials. Therefore, it was vital that after dialysis that the excess water was evaporated, using a

HyperVap system. The final volume of the PEGylated urease (2:1) was to be 200 μL after evaporation.

Following dialysis of the PEGylated-urease solution, 15 μL was introduced into 30 μL of a monomer mixture containing HEMA and TEGDA (97:3 mol %) with 0.02 wt% dimethoxyphenyl acetophenone (DMPA). The derivatized enzyme-monomer cocktail was then purged under an inert argon atmosphere for 2 min. A small volume (1-2 μL) was applied to the interdigit space of the IME that was previously surface functionalized with Acryl-PEG moieties and spin coated over the entire working area (ca. 3000 rpm, 5 s). The enzyme-monomer coated electrode was then placed in a UV polymerization chamber (UVP Model CX-2000) and immediately irradiated with UV light (2.3 W/cm^2, 366 nm) for 10 min under an inert argon atmosphere to affect polymerization of the bioactive monomer mixture. The resulting PEGylated-urease biosensor was stored in Tris buffer (10 mM, pH 7.0) at 4 °C when not in use.

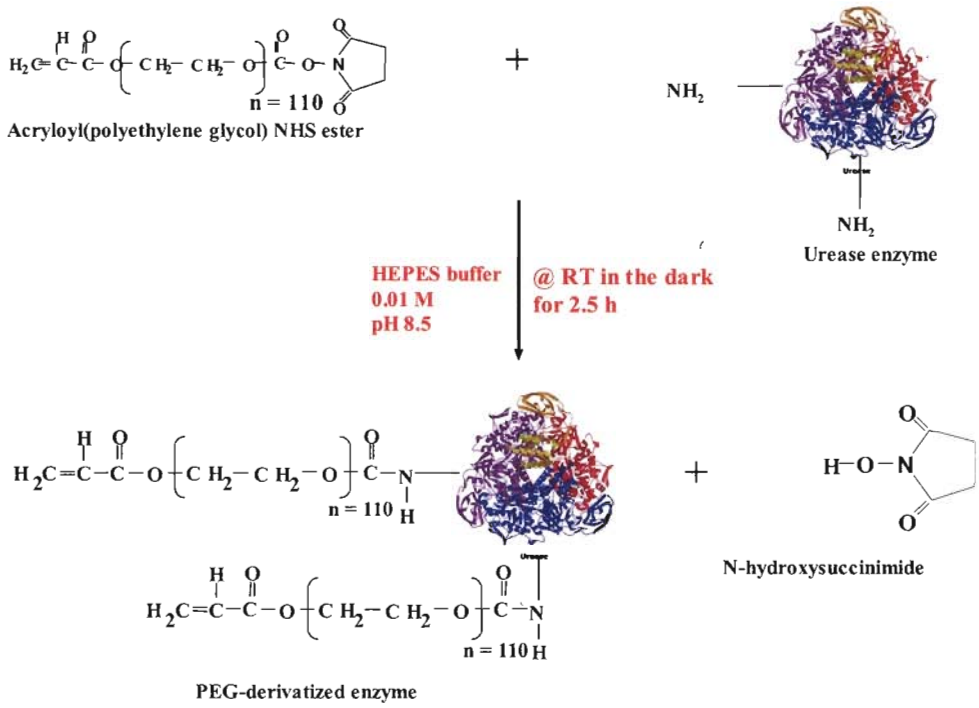

***Figure 19**: PEGylation of Urease.*

3.2.5.5. Covalently Attached Urease using EDC and NHS

After cleaning, platinization and silanization, a blank IME 1025.3-M-Pt-U was used for impedance calibration tests by covalently attaching urease enzyme to the IME. A 0.2M, pH 7.2 Sodium Phosphate (NaH_2PO_4, 120 g/mol) buffer was prepared by dissolving 2.4g in 0.1L DI H_2O. From the Sodium Phosphate buffer, 5mL was taken and a 50 mM equimolar solution of 1-ethyl-3- (3-dimethylaminopropyl)carbodiimide-HCl (EDC) and N-hydroxysulfosuccinimide (Sulfo-NHS) was made. For an urease enzyme concentration of 2mg/mL, 10 mg of urease was dissolved in the 5mL Sodium Phosphate buffer. The IME was then immersed into the solution and placed in the dark at room

temperature for 3 hours. After 3 hours, the IME was removed from solution and rinsed with 0.2M, pH 7.2 Sodium Phosphate buffer.

After covalent attachment of urease to the IME, the IME was cathodically cleaned to remove any enzyme adsorbed to the platinized electrode surface. A three-electrode cell arrangement was setup: electrode(s) to be cleaned as the working electrode, platinum counter electrode and an Ag/AgCl reference electrode. Phosphate buffered saline (0.15 M NaCl, 0.1 M NaH_2PO_4 at pH 7.2) (PBS) was used as the cleaning solution and the electrodes were cycled between –1.2V to –2.0V vs Ag/AgCl for 5-8 minutes. Afterwards the electrodes were rinsed with DI H_2O. When the IME was not being used in impedance testing, it was stored in 0.2M, pH 7.2 Sodium Phosphate buffer at 4°C.

The setup for impedance testing was different for this biosensor since DI H_2O was used. Evaluation of the sensor was carried out in a magnetically stirred, thermostatted cell at 37°C. Urea solutions of specified concentration were made by dilution of a 1 M stock solution of urea (Sigma, St. Louis, MO) dissolved in DI H_2O. Prior to tests, sensors were removed from storage in DI H_2O and placed in a SOIC-Clip (Ponoma, Model 5251). The pins of the clamp were connected to a potentiostat (Ametek, Princeton Applied Research Potentiostat/Galvanostat Model 283, Oak Ridge, TN) and impedance/gain-phase analyzer (Solatron Analytical Inc, Model 1260, Houston, TX). A 50 mV_{PP}, 4 kHz sine wave was applied to the enzyme electrode. Data were recorded for a period of up to 15 min. At 5 min within the 15 min run, aliquots of various molar concentrations of urea (0 μM – 5 mM) were injected into the thermostatted cell. The impedimetric response produced as a result of the enzymatic hydrolysis of urea was recorded. Following

completion of concentration-dependent urea responses, the individual sensors were returned to storage in DI H_2O at 4°C. Duplicate runs were performed and indicated no statistically significant variation in responses over the period of 24 h required to perform such experiments.

3.2.5.6. Fourier Transform Infrared Spectroscopy (FTIR) Analysis

Fourier Transform Infrared Spectroscopy (FTIR) results from the fact that organic compounds are able to absorb electromagnetic energy in the infrared region of the spectrum. The electromagnetic energy causes atoms and groups of atoms to vibrate faster about the covalent bonds that connect them. Thus, the organic compounds absorb infrared energy in particular regions of the spectrum. However, not all molecular vibrations result in the absorption of infrared energy. In order for a vibration to occur with the absorption of infrared energy, the dipole moment of the molecule must change as the vibration occurs (Solomans 1988).

FTIR is able to do everything accomplished by IR. A beam of infrared light is passed through a scanning Michelson interferometer. A sample compound is placed in the beam after the interferometer and absorbs particular frequencies so that their intensities are reduced in the interferogram. The Fourier Transform produced is the infrared absorption spectrum of the sample, which is a plot of intensity versus frequency. FTIR exceeds in performance for both speed and sensitivity than IR (Kemp 1991). Fourier Transform Infrared Spectroscopy (FTIR) is a powerful tool for identifying types of chemical bonds in a molecule by producing an infrared absorption spectrum that is like a molecular "fingerprint." FTIR is most useful for identifying chemicals that are either organic or

inorganic. It can be utilized to quantify some components of an unknown mixture. It can be applied to the analysis of solids, liquids, and gasses.

FTIR can be used to identify chemicals from spills, paints, polymers, coatings, drugs, and contaminants. FTIR is perhaps the most powerful tool for identifying types of chemical bonds (functional groups). The wavelength of light absorbed is characteristic of the chemical bond as can be seen in a spectrum. By interpreting the infrared absorption spectrum, the chemical bonds in a molecule can be determined. FTIR spectra of pure compounds are generally so unique that they are like a molecular "fingerprint". While organic compounds have very rich, detailed spectra, inorganic compounds are usually much simpler. For most common materials, the spectrum of an unknown compound can be identified by comparison to a library of known compounds. To identify less common materials, IR will need to be combined with nuclear magnetic resonance, mass spectrometry, emission spectroscopy, X-ray diffraction, and/or other techniques (Griffiths 1986).

Samples for FTIR can be prepared in a number of ways. For liquid samples, the easiest is to place one drop of a sample between two plates of sodium chloride (salt). Salt is transparent to infrared light. The drop forms a thin film between the plates. Solid samples can then be milled with potassium bromide (KBr) to form a very fine powder. This powder is then compressed into a thin pellet, which can be analyzed. KBr is also transparent in the IR (Griffiths 1986).

Alternatively, solid samples can be dissolved in a solvent such as methylene chloride, and the solution placed onto a single salt plate. The solvent is then evaporated

off, leaving a thin film of the original material on the plate. This is called a cast film, and is frequently used for polymer identification. Solutions can also be analyzed in a liquid cell. This is a small container made from NaCl (or other IR-transparent material), which can be filled with liquid. This creates a longer path length for the sample, which leads to increased sensitivity. Sampling methods include making a mull of a powder with a hydrocarbon oil (Nujol) or pyrolyzing insoluble polymers and using the distilled pyrolyzate to cast a film. Films can be placed in an Attenuated Total Reflectance (ATR) cell and gases in gas cells (Griffiths 1986). FTIR spectroscopy has been used as a characterizing tool to determine if the amino acid groups of urease enzyme have covalently attached to the carboxylic acid groups of the Acryl-PEG-NHS. Three samples were prepared, free urease, unPEGylated-urease and PEGylated (2:1)-urease in HEPES buffer (0.1M, pH 8.5).

3.2.6. Electrical Impedance Testing of Urea Biosensors

The urease biosensors were operated as impedimetric sensors for the detection of the ionic products formed from the enzymatic conversion of urea:

$$CH_4N_2O + 3\ H_2O \longrightarrow 2\ NH_4^+ + OH^- + HCO_3^-$$

Each urease enzyme electrode contained two contact pads. One contact pad was made to function as the working electrode with the other contact pad serving as the counter electrode. Evaluation of the sensors was carried out in a magnetically stirred, thermostatted cell at 37 °C. Urea solutions of specified concentration were made by dilution of a 1 M stock solution of urea (Sigma, St. Louis, MO) dissolved in Tris buffer (10 mM, pH 7.0, cell volume of 5.5 mL). Prior to tests, sensors were removed from storage in Tris buffer and placed in a SOIC-Clip (Ponoma, Model 5251). The pins of the clamp were

connected to a potentiostat (Ametek, Princeton Applied Research Potentiostat/Galvanostat Model 283, Oak Ridge, TN) and impedance/gain-phase analyzer (Solatron Analytical Inc, Model 1260, Houston, TX). A 50 mV_{PP}, 4 kHz sine wave was applied to the enzyme electrode. Data was recorded for a period of up to 15 min. At 5 min within the 15 min run, aliquots of various molar concentrations of urea (0 μM – 5 mM) were injected into the thermostatted cell. The impedimetric response produced as a result of the enzymatic hydrolysis of urea was recorded. Following completion of the concentration-dependent urea responses, the individual sensors were returned to storage in Tris buffer at 4 °C. Duplicate runs were performed and indicated no statistically significant variation in responses over the period of 24 h required to perform such experiments.

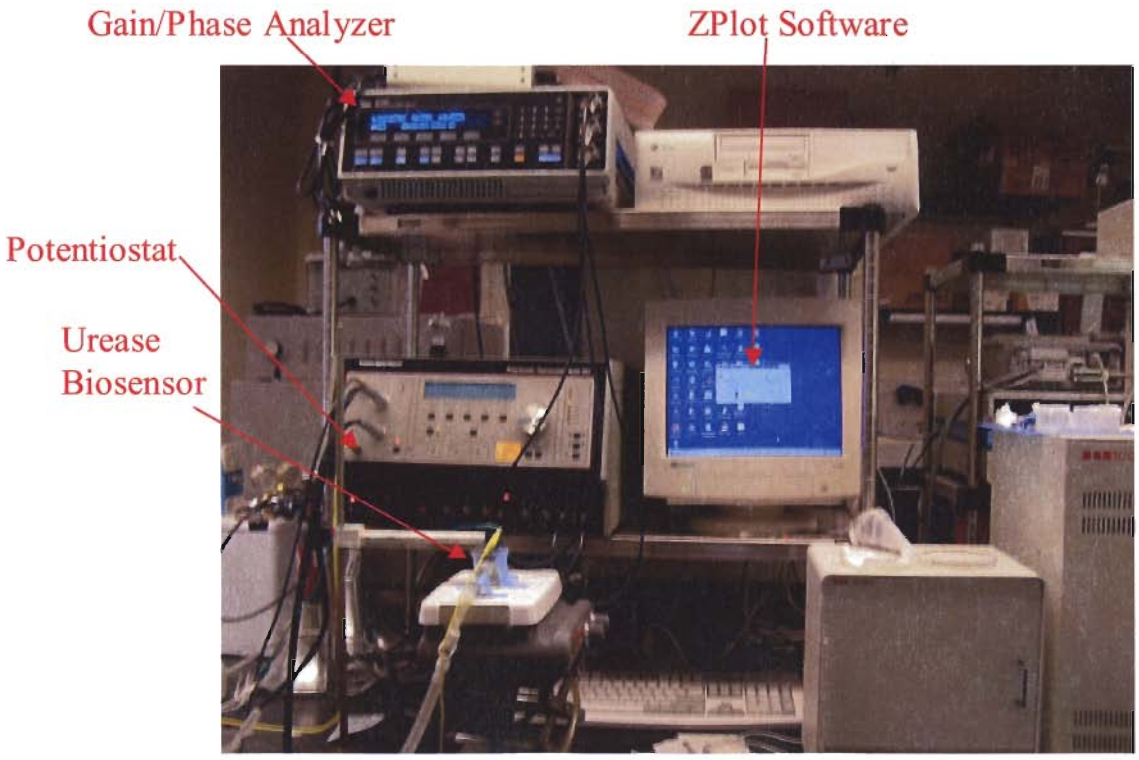

***Figure 20**: Urease Biosensor Testing setup.*

3.2.6.1. Temperature Profile Testing

From observing the results of the graph of Magnitude Impedance vs. Time, a urea concentration which showed the best impedimetric response to urease was picked. Using that particular urea concentration, Magnitude Impedance versus Temperature (°C) experimental runs were conducted. The temperature was varied from 10°C - 50°C at 10°C intervals at pH 7.0 for urea. Two trials at each 10°C interval were run. Between each trial, the sensor was allowed to equilibrate by keeping it submerged in 5.5mL Tris buffer (10mM, pH 7.0) at the specific temperature for at least 10 minutes. Temperature profile tests were only conducted for the unPEGylated and PEGyated-urease sensors.

3.2.6.2. pH Profile Testing

From observing the results of the graph of Magnitude Impedance vs. Time, a urea concentration which showed the best impedimetric response to urease was picked. Using that particular urea molar concentration with Tris buffer solutions at various pH values (pH 4.0, 5.0, 6.0, 7.0, 8.0), Magnitude Impedance versus pH experimental runs were conducted. Two trials at each pH were run at 37°C. Between each trial, the sensor was allowed to equilibrate by keeping it submerged in 5.5mL Tris buffer (10mM, 37°C) for at least 10 minutes. Temperature profile tests were only conducted for the unPEGylated and PEGylated-urease sensors.

3.2.6.3. Kinetic Parameter Calculations

Plots of the rate of catalysis (dZ/dt) of urease versus urea molar concentration of urea (moles/L) were made. Linearization of the calibration curves were obtained by plotting the reciprocal data from the (dZ/dt) versus (moles/L) graph. This linearization

graph was called the Lineweaver-Burk plot. From this plot, it could be concluded if Michaelis-Menten kinetics was the rate-limiting factor. The linearity of the Lineweaver-Burk plot would show if the impedimetric response was directly proportional to the substrate (urea) concentration or if the immobilized urease hydrogel provided any limitation to diffusion to the flux of urea.

Certain Michaelis-Menten kinetic parameters (i.e. Z_{MAX}, K_M, k_{cat} and E_o) were deduced from the Lineweaver-Burk plot. These parameters allowed proper understanding of the binding of enzyme to substrate and the rate of catalysis to form the product. Using BIOSOFT® Enzfitter software, a Lineweaver-Burk plot was graphed from the reciprocal data of (dZ/dt) versus Molar Concentration [moles/L].

Z_{MAX} was the catalytic velocity when all the enzyme's active sites were completely saturated with substrate. K_M, also known as the Michaelis constant, was the substrate concentration at which the catalytic reaction velocity was half maximal. The inverse of K_M, revealed the affinity of enzyme to substrate. From these parameters, k_{cat} and k_{cat}/K_M could be calculated to provide further kinetic analysis. k_{cat} was a rate constant for the conversion of the enzyme-substrate complex into enzyme and product. k_{cat}/K_M was a specificity constant for the encounter of free substrate with free enzyme, and thus provided an indication of the specificity of the enzyme for the substrate.

Chapter 4. Design and Construction of An Impedimetric Urea Biosensor System

4.1. Bioanalytical Biosensor 1025.3

A microlithographically fabricated IME had been designed containing three cells, also known as the three Electrochemical Impedance Cells (3EIC). Each cell contained one pair of opposing electrodes, one reference electrode (Ag/AgCl) and one counter electrode (Platinized/Pt). The pair of opposing electrodes are comprised of 10 μm wide platinum digits that were ca. 3 mm long and separated by 10 μm wide free spaces. There were 25 digits on each electrode bus that established a tortuous path of 14.75 cm of exposed glass surface between the digits.

All three cells contained a polymer film with entrapped urease on top of the electrodes. Each cell on the IME had a specific and separate purpose. The working cell sensed the various molar concentrations of urea and provided a corresponding voltage response. The control cell provided a constant voltage since its purpose was to serve as a comparison point with the working cell. The reference cell also provided a voltage response, which was the difference between the impedimetric response from the working and control cells. These signals from these cells were sent to the Impedance BioAnalyzer for signal processing into a corresponding impedimetric value.

4.2. Electrochemical Impedance Cells (3EIC) BioAnalyzer Hardware

The 3EIC BioAnalyzer consisted of signal processing and control software. It dealt with the design of an advanced and sophisticated instrument based on the impedimetric response of a chemical sensor for the real time monitoring of the hydrolysis of urea into

ammonium, bicarbonate and hydroxide ions via urease enzyme. For the measurement of impedimetric response of chemical sensor upon analyte injection, one pair of demodulating logarithmic amplifiers were used to calculate change in phase and amplitude. Amplitude and phase thus measured was then captured by a USB-48A-30A16 μDAQ at 20 Hz and converted to a digital signal in order to be interpreted by the computer. The development of a graphical user interface (GUI) program written in LabVIEW 7.0 was used to communicate between the computer and interface electronics via the USB-48A-30A16 μDAQ. This entire process was initiated, controlled and terminated through the GUI.

To study the behavior of the 3EIC BioAnalyzer in actual field-testing, a simulated experiment to determine the level of urea in blood stream and to estimate the time required for the patient to be on the dialysis unit could be performed by fabricating an immobilized urease sensor and injecting various molar concentrations of urea to provide corresponding impedimetric responses. A developed 3EIC BioAnalyzer promises applications in the area of medical diagnostics for kidney dialysis patients.

The principle of the 3EIC BioAnalyzer was to use one of the most straightforward methods of complex impedance measurement of the Device Under Test (DUT) in conjugation with an inverting amplifier as shown in **Figure 21**.

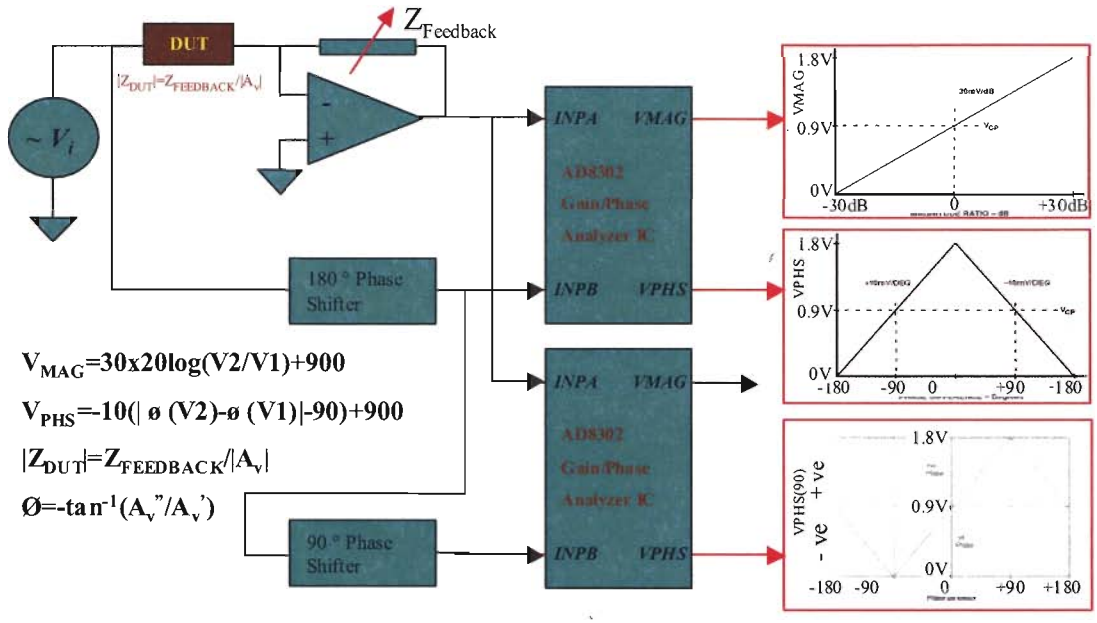

***Figure 21**: Conceptual schematic of 3EIC BioAnalyzer.*

The circuit shown in **Figure 21** operates on the principle that the current through the input impedance $\mathbf{Z_{DUT}}$ and feedback resistor $Z_{Feedback}$ would always be equal in order to maintain zero voltage difference at the inverting terminal. If $\mathbf{Z_{DUT}}$ was purely resistive, there would be a change in the amplitude. But if $\mathbf{Z_{DUT}}$ was capacitive/inductive then there would be always 90 degrees phase difference between output and input signals and also change in their amplitudes. Generally, if $\mathbf{Z_{DUT}}$ was complex impedance, which involved both resistive and capacitive/inductive reactances, output signal undergoes both amplitude and phase modulation. Thus if $\mathbf{V_i}=|V_i|\text{Sin}(\omega t)$ is the input (or excitation) signal and $\mathbf{V_o}=|V_o|\text{Sin}(\omega t+\phi)$ is the output signal, then according to the principle of the inverting amplifier equating the current in the inverting terminal and feedback path impedance of the device under test (DUT) as a complex vector could be given as

$$\mathbf{Z_{DUT}} = \mathbf{Z_{Feedback}}/(\mathbf{V_o}/\mathbf{V_i}) \qquad (10)$$

where $\mathbf{V_o/V_i}$ was the voltage gain $\mathbf{A_v}$. By substituting the absolute gain $|\mathbf{A_v}|$ in equation 10, magnitude of the impedance $|\mathbf{Z_{DUT}}|$ could be calculated while phase difference (ϕ) could be determined by comparing input and output sinusoids. Thus by using a large unity-gain bandwidth amplifier in the circuit, the frequency response of device under test could be generated over a wide range. Method of measuring $|\mathbf{A_v}|$ and ϕ will be described in section 4.2.3.

4.2.1. Power Supply Circuit

An Antec Minuet chassis was purchased from Page Computer, Inc. (PART NUMBER B1214291). This chassis contained a SmartPower 220Watt, ATX12V form factor power supply. It had a single 20 pin Main Power Connector and a 4-pin +12V Power Connector to connect to the motherboard. It also came with three 4-pin Peripheral Power Connectors and one 4-pin Floppy Drive Power Connector for the drives. It was backwards compatible to previous ATX form factor power supplies. If a motherboard did not support the +12V Power Connector, this power supply could still be used.

The ATX12V power supply provided several voltage pinouts: +3.3V, ±5.0V, ±12V, GND, PS-ON and PWR-OK. The ± 5V provided the input supply voltages for all the integrated circuits on the motherboard. The PS-ON was shorted with the GND by a non-latching switch to start the cooling fan and the ATX12V power supply. The non-latching switch only held the connection while the chassis switch was depressed. The non-latching switch could be converted into a latching switch in order to keep the connection between PS-ON and GND shorted together, until the switch on the outside of the computer chassis was depressed again.

Several integrated circuits had been used to design a latching circuit for the Urea Impedance BioAnalyzer. **Figure 22** shows a conceptual schematic of how this was accomplished. When the chassis switch was depressed, the clock (CLK) of the JK Flip-flop (74LS07) changed from "HIGH" to "LOW." The falling edge of the CLK held the Q output (74LS07) to "HIGH" (only if the previous state was "LOW"), which closed the switch between S1 and D1 (ADG 721, SPST). When the chassis switch was released, the CLK (74LS07) changed from "LOW" to "HIGH." Q output was held in the "HIGH" state. The switch between S1 and D1 (ADG 721, SPST) remained closed. The ADG 721 was called a Single Pole/Single Throw (SPST) switch since it contained one source and one drain for each logic input.

When the chassis swith was pressed again, the CLK (74LS07) changed from "HIGH" to "LOW." This held the Q output to "LOW" (only if the previous state was "HIGH"). The switch between S1 and D1 (ADG 721, SPST) opened. When the chassis switch was released, the CLK (74LS07) changed from "LOW" to "HIGH." Q output was held in the "LOW" state. The switch between S1 and D1 remains open. The Q output served as the input signal of the IN1 (ADG721, SPST). This input signal closed the switch, which shorted the PS-ON and GND (pins on the ATX12V power connector) and started the chassis fan and power supply.

With the JK Flip-flop and the SPST switch, there was a noticeable bouncing effect due to the mechanical switch. This resulted in multiple switchings in a second. A 555 Timer in the monostable mode was then used as a debouncing circuit to filter out spikes caused by the momentary latch before it is sent to the JK Flip-flop (74LS07).

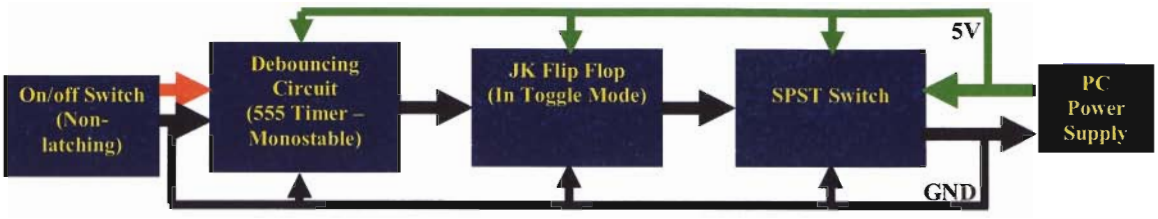

***Figure 22**: Latching circuit for non-latching computer chassis switch.*

4.2.2. Function Generator

The function generator (MAX038) provided a 2Vpp, 4kHz sine wave. The output of this function generator, was inputted into an inverting amplifier (MAX410, 38kΩ resistor and 1kΩ resistor in feedback) to be broken down into a 50mVpp, 4kHz sine wave, which would serve as the interrogation signal. This interrogation signal was only be used during the Interrogation phase of the experiment.

4.2.3. Cell Circuit

Operation of the 3EIC BioAnalyzer followed a sequence of three phases: a pre-initialization phase, initialization phase and an interrogation and data capture phase. These three phases, executed in sequence, represented a single complete cycle for the successful extraction and capture of raw sensor response data. The switching from one phase to the next was performed by electronic switches (ADG633). **Table 2** shows the DIO configuration for each phase, which was set by the USB-48A-30A16 μDAQ. The raw data extracted should be relatable to the desired measurement objective, i.e. the activities (chemical potential) of analytes to which the device was sensitive. Subsequent data reduction, analysis, and presentation followed these three phases.

In the Pre-Initialization Phase, the 3EIC performed a real-time measurement of

the open-circuit potential of shorted working electrodes versus an external reference electrode. In the Initialization Phase, a DC potential between ±1 V was applied to the counter electrode. The voltage was compared with the voltage of an external reference electrode using a differential amplifier. For the Interrogation Phase, a 50mVpp, 4kHz sine wave was applied to the working electrodes and compared that resulting voltage with the Reference electrode. The resulting output voltage was sent through a feedback resistor logic circuit and then a gain/phase analyzer. Shift in magnitude voltage and phase voltage due to the interaction between urease and urea was measured by gain/ phase analyzer circuit. The voltages were then sent to an USB-48A-30A16 μDAQ and converted to a digital signal to be interpreted by the computer. The final output was displayed on a computer screen indicating the impedance and phase angle values of the urea biosensor when various molar concentrations of urea were injected.

USB30 uDAQ DIO configuration						
	Pre-Initialization	Initialization	Interrogation W1,W2,Ref	Interrogation W1,W2	Interrogation W1+W2, Ref	Interrogation W1+W2
DIO 0	1	1	0	1	0	1
DIO 1	0	0	1	1	1	1
DIO 2	1	0	1	1	0	0
DIO 3	1	1	0	0	0	0
DIO 4	0	0	1	0	1	0
DIO 5	1	1	0	0	1	1
DIO 6	0	0	1	1	1	1
DIO 7	--	--	--	--	--	--
DIO 8	--	--	--	--	--	--
DIO 9	--	--	--	--	--	--
DIO 10	--	--	--	--	--	--
DIO 11	0	0	1	1	1	1
DIO 12	--	--	--	--	--	--
DIO 13	--	--	--	--	--	--
DIO 14	--	--	--	--	--	--
DIO 15	--	--	--	--	--	--
DIO 16	0	0	1	1	1	1
DIO 17	--	--	--	--	--	--
DIO 18	--	--	--	--	--	--
DIO 19	--	--	--	--	--	--
DIO 20	--	--	--	--	--	--
DIO 21	0	0	1	1	1	1
DAC 0	0	10	0	0	0	0

***Table 2**: USB-48A-30A16 uDAQ DIO configuration*

4.2.4. Feedback Resistor Logic Circuit

The Feedback Resistor Logic circuit came to play an important part during the Interrogation phase of impedimetric analysis. **Figure 23** illustrated a conceptual schematic of the Feedback Resistor Logic circuit. The output voltage from the cell circuit (ADG633, SPDT, C1_S3) was sent to the inverting input of an operational amplifier (MAX 410, U96). The feedback of this operational amplifier consisted of an array of SPST switches (ADG622, SPST) and resistors. The voltage was sent through the resistors and an appropriate resistor was chosen when its matching SPST switch was closed. The chosen resistor value represented the factor by which the voltage gain, A_V, can be

multiplied with in order to yield Z_{DUT} as close as possible to 0dB, with a ± 5dB error range. As a result, the output of the operational amplifier (MAX410, U96) provided an accurate voltage representing the voltage response of the DUT, which was then sent to the Gain/Phase Analyzer (AD8302, U73). In order to output an accurate V_{MAG} and V_{PHS} from the Gain/Phase Analyzer (AD8302, U73), V_{MAG} and V_{PHS} must be within ± 5dB range.

However, at times the Gain/Phase Analyzer did not provide an accurate V_{MAG} and V_{PHS} response to represent the DUT. This was when the V_{MAG} voltage was sent back into the comparator circuit of the feedback resistor logic. Depending on the output voltage of the comparator circuit, an output logic (High/Low) from an X-OR gate (74LS86) would be sent into a JK Flip-flop. The JK Flip-flop would continue to toggle between a high and low state, indicating that V_{MAG} and V_{PHS} are outside of the ± 5dB range.

Figure 23 illustrated how this was accomplished. A 555 Timer (ICM7555) sent a square wave signal to the clock input of both JK Flip Flops (74LS107). The comparators (MAX412) functioned between a voltage range of 0.75V to 1.05V (±5dB) to provide either LL, LH or HL voltage signal to the X-OR gate. When the comparators provided LL, the X-OR gate outputted L, the inverter (74LS04) outputted H and thus the JK Flip-flops became reset. This indicated that the V_{MAG} and V_{PHS} were within the ±5dB range. When this occurred, the Feedback Resistor Logic remained at the appropriate resistance. But, when the comparators provided LH or HL, the X-OR gate outputted H, the inverter outputted H and thus the JK Flip-flops toggled between high and low states on the negative edge of the 7555 timer. This indicated that the V_{MAG} and V_{PHS} had exceeded the ±5dB range.

When this occurred, the Feedback Resistor Logic reset itself to the appropriate resistance to bring V_{MAG} and V_{PHS} back within the ±5dB range. The outputs from the JK Flip-flop were sent to an Up/Down Binary Counter (74F193). The purpose of the counter was to provide a 4-bit combination corresponding to each of the resistors and switches in the feedback resistor logic array. The 4-bit combination (0000....1111) only changed state when the V_{MAG} and V_{PHS} exceeded the ±5dB range.

The 4-bit combination was sent to a 4:16 Line decoder (MM74HC154). Each output of the decoder was connected to an individual resistor and switch in the feedback resistor logic array. Depending on the 4-bit integer value (0-15), the appropriate SPST switch closed. This resistor corresponding with that closed switch became the feedback resistor to bring V_{MAG} and V_{PHS} between the ±5dB range.

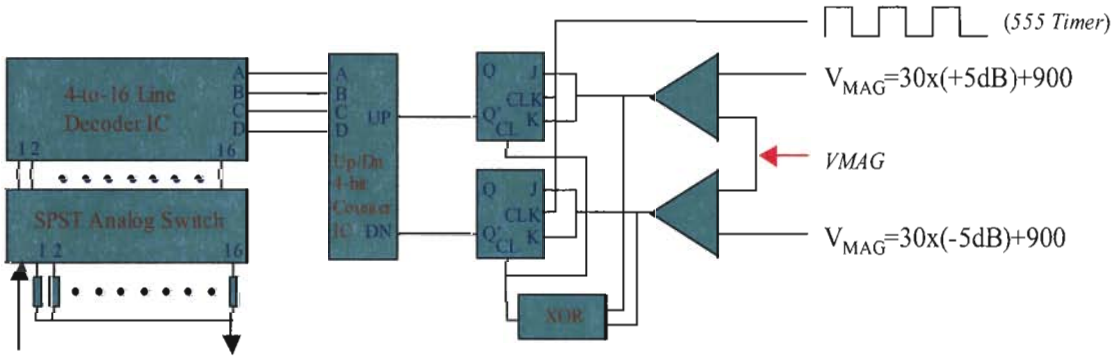

***Figure 23**: Conceptual schematic of Feedback Resistor Logic circuit.*

4.2.5. Gain/Phase Circuit

A pair of matched logarithmic amplifiers (log amps) as shown in **Figure 24** provided gain measurement in dB, and their well-defined upper voltage limit drove the phase detector. The AD8302 operates at a sensitivity of 29 mV/dB. The logarithmic

amplifier provided a logarithmic compression function that converted a large range of input signal levels to a compact decibel-scaled output. The general mathematical form was

$$V_{OUT}=V_{SPL} * \log(V_{IN}/V_Z) \quad (11)$$

where V_{IN} was the input voltage, V_Z was called intercept (voltage) and V_{SPL} was called slope (voltage). If log(x) represented $\log_{10}(x)$ function, V_{SLP} would be in the volts/decade, and since a decade of a voltage corresponded to 20dB, V_{SLP} was the volts/dB. While the slope was fundamentally a characteristic of the log amp, the intercept was a function of the input waveform.

By taking the difference of the output of the two identical log amps, each one driven by signals of similar waveforms but at the different levels, resulted in the ratio in the linear domain, given in terms of output voltage V_{MAG} as below:

$$V_{MAG}=V_{SLP} * \log(V_{INA}/V_{INB}) \quad (12)$$

where V_{INA} and V_{INB} were input voltages, which in the present case were $|V_o|$ and $|V_i|$ respectively. Note that the intercept, V_Z, had dropped out. This technique depended on two log amps being well matched in slope and intercept that ensured cancellation.

For the measurement of phase hard-limiting outputs, the log amps could be driven by an exclusive-OR style digital phase detector the output of which had general form:

$$V_{PHS}=V_\phi[\phi(V_{INA})-\phi(V_{INB})] \quad (13)$$

where V_ϕ was the phase slope in mV/degree and ϕ was each signal's relative phase. Since this type of phase detector had a phase range that ranges either 0 degree to +180 degree centered at +90 degree or 0 degree to -180 degree centered at -90 degree, therefore to determine the sign of phase shift, a pair of X-OR phase detectors could be employed. One

of the phase detectors would have had two signals, V_{INA} and V_{INB} (reference signal), connected directly to it, whereas the other would have had reference signal connected through a 90 degree phase shift circuit. The outputs from two phase detectors can be offset in a manner to unambiguously determine the relative phase by comparing the two phase detector outputs. It can also be determined in which quadrant the relative phase angle lies and the magnitude of the relative phase.

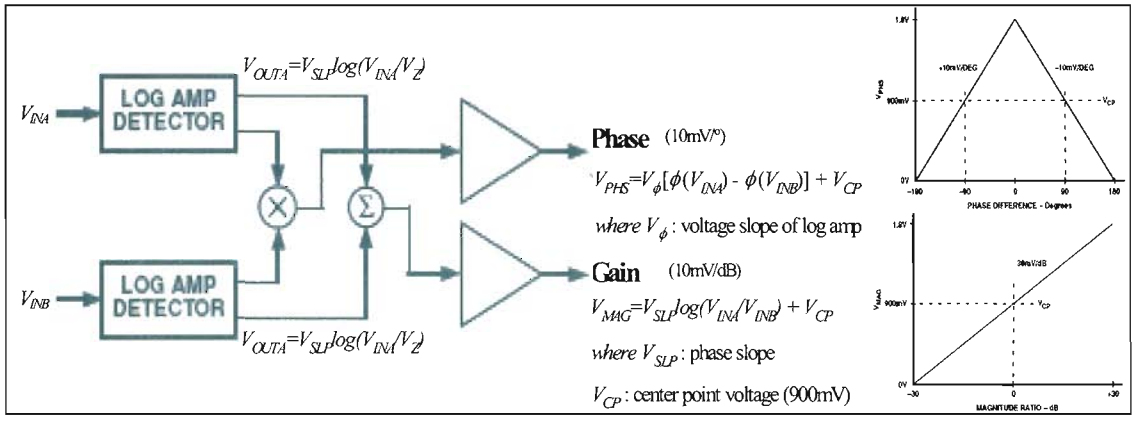

***Figure 24**: (a)Basic Connection; (b) Idealized transfer characteristics for gain and phase.*

4.2.6. 3EIC Chip Holder

A chip holder was made to serve as an interface between the Bioanalytical Biosensor 1025.3 and the 3EIC BioAnalyzer hardware. The glass biosensor would be adhered within the groove of the chip holder. The bonding pads on the chip holder were to match up with the bonding pads on the biosensor for a total area of 2mm by 2mm. Lead lines from the chip holder bonding pads were sent to the pin holes for the 15-pin D-sub connector (MF11). From the D-sub connector, a ribbon cable was connected and sent into another 15-pin D-sub connector in the 3EIC BioAnalyzer printed circuit board. Thus,

impedimetric responses from the Bioanalytical Biosensor 1025.3 were measured by the 3EIC Impedance BioAnalyzer.

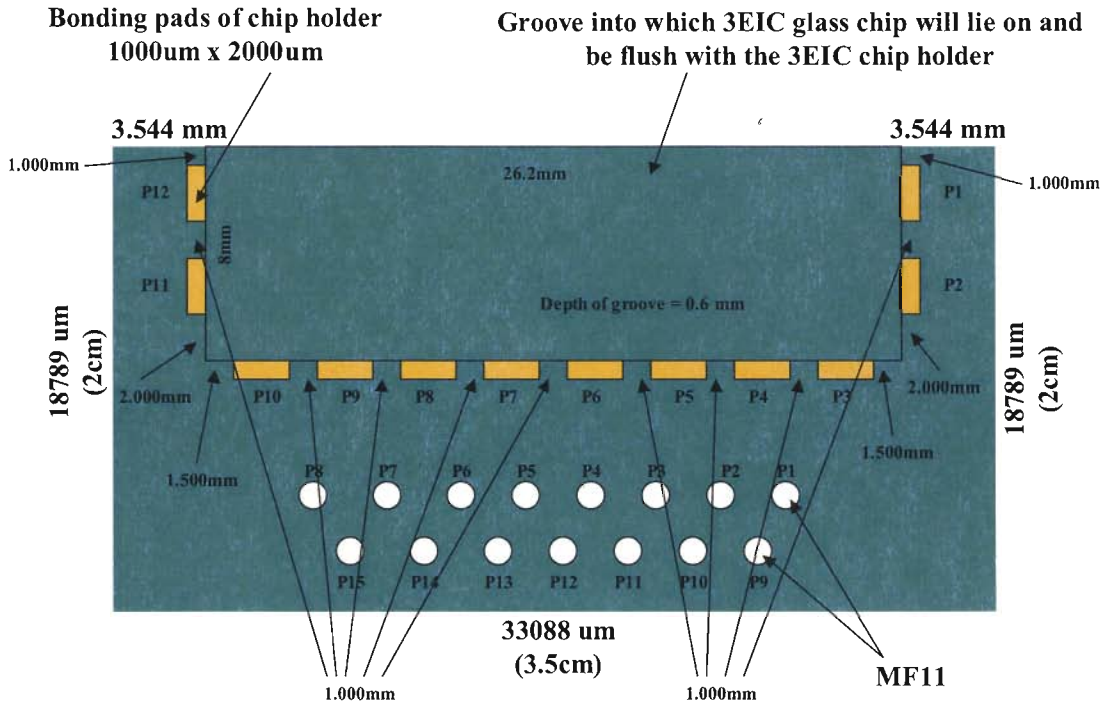

***Figure 25**: 3EIC Chip Holder with dimensions.*

4.2.7. Manufacture of Circuit Boards, Chip Holder and Assembly

Mass Design Incorporated was the chosen designer and fabricator of the printed circuit board and 3EIC chip holder for the Urea Impedance BioAnalyzer. The following is the contact information for Mass Design Incorporated: Mass Design Incorporated; 22 Tanquay Ave.Nashua, NH 03063; 603-886-6460; www.massdesign.com.

***Figure 26**: Printed circuit board for 3EIC Impedance BioAnalyzer.*

***Figure 27**: Printed circuit board for 3EIC Impedance BioAnalyzer inside Antec Minuet chassis.*

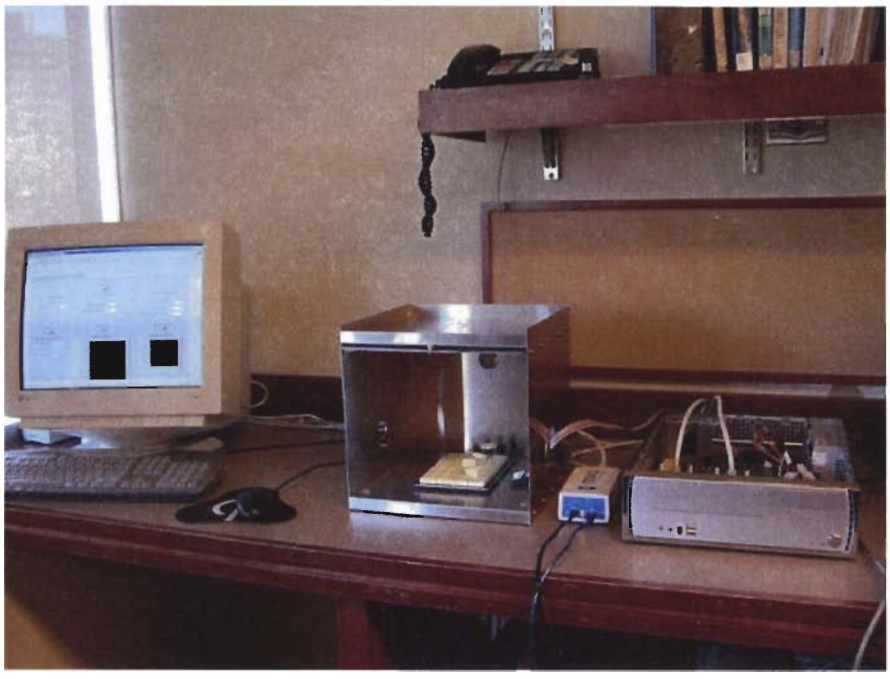

***Figure 28**: Urea Impedance BioAnalyzer System (left to right): LabVIEW software, DUT, 3EIC Impedance BioAnalyzer.*

4.3. Electrochemical Impedance Cells BioAnalyzer Data Acquisition and Instrumentation Control Software

As mentioned earlier, the voltages from each of the phases were sent to an USB-48A-30A16 μDAQ and converted to a digital signal to be interpreted by the computer. The data acquisition and control software had been written in LabVIEW 7.0 to compute the voltage from Pre-Initialization, the current from Initialization and the magnitude impedance and phase angle from Interrogation. For example, the magnitude impedance and phase angle were computed from the voltages of the Gain/Phase analyzer circuit. This final output was then displayed on a computer screen indicating the impedance and phase angle values of the urea biosensor when various molar concentrations of urea were injected. The user was provided the option of performing

each analysis phase independently or all three phases as one. The user was also given the option of applying each analysis phase to one, two or all three cells of the sensor. **Figure 29** provides the graphical user interface (GUI) of the Urea Impedance Biosensor System software. Details of the coding for the Instrumentation control software are provided in **Appendix E**.

The multi-function data acquisition device, USB-48A-30A16 μDAQ, was used as an interface block between the PC and the interface & control electronics. The USB-48A-30A16 μDAQ is a Universal Serial Bus architecture digital input/ output, counter-timer and analog I/O data acquisition device. Featuring 16 analog inputs, the unit was used to measure voltage signals from the sensors at the sampling rate of 250k/sec with 14 bits of resolution. It also featured four 14-bit analog outputs, which was used as reference voltages. The digital I/O is available in 6 sets of 8, which can be programmed as inputs or outputs. Since no data sheet for the USB-48A-30A16 μDAQ could be obtained, the data sheet for the USB-30 μDAQ has been shown in **Figure 30**. The only significant difference between the USB-48A-30A16 μDAQ and the USB-30 μDAQ was that there are 48 DIO TTL I/O lines, not 24 TTL I/O lines. The pin out specifications of theUSB -48A-30A16 μDAQ were given in **Figure 31**.

The USB-48A-30A16 μDAQ acted as an interface between the PC and the control electronics. Out of total 16 analog input, there were 14 inputs corresponding to the Feedback Resistor, Gain, Phase and Phase Sign. DIOs were used to control the experiments and program the hardware. The Enhanced Software Development kit supplied

with the unit provided an easy interface and the GUI developed in LabVIEW 7.0 enabled the user to interact with the system in user friendly way.

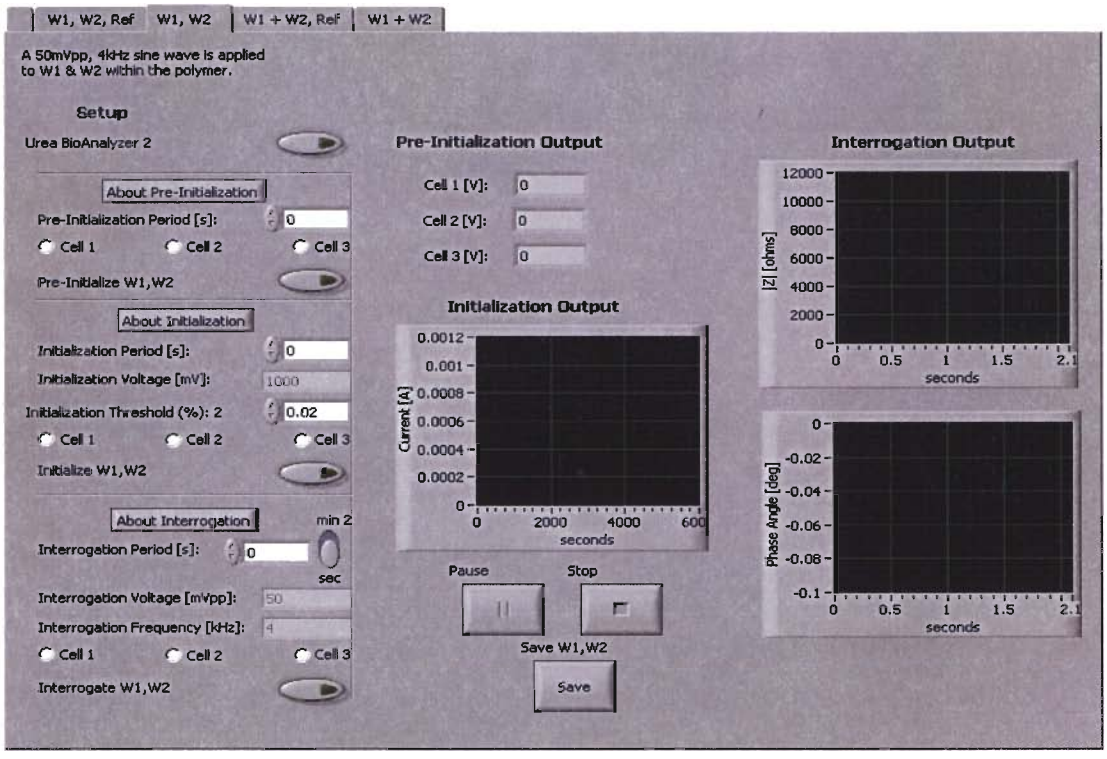

***Figure 29**: Graphical User Interface of Urea Impedance Biosensor system.*

Specifications

ANALOG INPUTS (A/D)	
Input Characteristics	
Input Channels:	16 Single-Ended or 8 Differential
Input Ranges:	±2.5, ±5V; ±10V; 0-5V; 0-10V
Gain:	1; 10; 100
Resolution:	14-bit (1 in 16384)
Input Coupling:	DC
A/D Conversion Characteristics	
Max sampling rate:	250 kHz
Relative Accuracy:	16K
Acquisition Modes:	Triggered Interrupt
Input Impedance:	1M Ohm
System Noise:	1 LSB
ANALOG OUTPUT (D/A)	
No of Channels:	4x 14-bit
Output Ranges:	±10V
Full Scale Error:	±2 LSB
Settling Time:	1mS to 0.1% of full scale 2mS to 0.015% of full scale
Output Drive:	±10V @ 5mA
Power On State:	0V
DIGITAL I/O (DIO)	
No of TTL I/O lines:	24
Logic Levels: Input Low Voltage:	-0.5V to 0.8V
Input High Voltage:	2.0V to 5.0V
Output High Voltage Min:	2.4V
Output Low Voltage Max:	0.45V
Maximum Output Current:	2mA
DIGITAL TRIGGER	
Trigger Source:	External Trigger
Compatibility:	TTL
Pulse Width:	100nS

Figure 30: USB-30 µDAQ specifications.

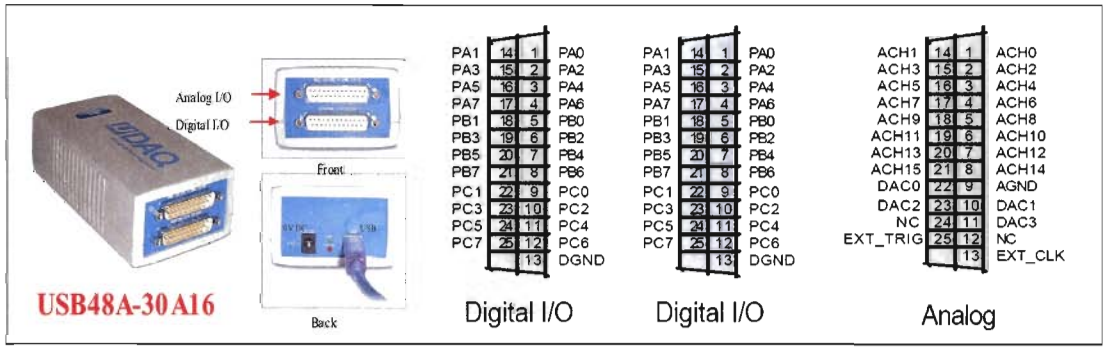

Figure 31 *USB-48A-30A16 Analog & Digital I/O unit.*

Chapter 5. Results and Discussion

5.1. Comparison of the performance of the five (5) different formats of conferring urea specificity

Calibration curves of the initial rate of change of impedance (d|Z|/dt) and the equilibrium change (Δ|Z|) versus urea concentration (moles/L) over the range from 0μM to 5mM were obtained for all five urea biosensor formats: [i) unPEGylated-urease containing p(HEMA) hydrogel, ii) PEGylated-urease containing p(HEMA) hydrogel iii) via glutaraldehyde crosslinking in the presence of albumin, iv) the direct covalent immobilization of urease to the IME, and v) solution borne urease]. From the (d|Z|/dt) calibration plot, a linearization via the Lineweaver-Burk method allowed calculation of the Michaelis-Menten kinetic parameters Z_{MAX}, K_M, k_{cat} and E_o. These parameters were obtained for each format investigated. From these parameters, k_{cat} and k_{cat}/K_M were calculated to provide further kinetic analysis. The rate constant for the conversion of the enzyme-substrate complex into enzyme and product is defined as k_{cat}. The specificity constant for the encounter of free substrate with free enzyme is defined as k_{cat}/K_M. These parameters thus provided an indication of the specificity of the enzyme for the substrate. Additionally, the pH dependence and temperature dependence of these parameters was investigated for the two formats corresponding to i) and ii) above, i.e urease containing poly(hydroxyethylmethacrylate) hydrogel [p(HEMA)] and PEGylated-urease containing p(HEMA) hydrogel.

5.1.1. Characterization of the unPEGylated-Urease-p(HEMA) format

Figure 32 shows the impedimetric dose response plots obtained for the urea biosensor formed from the unPEGylated urease immobilized within the p(HEMA) hydrogel. The response is typical of enzyme-based biosensors with a rapid initial fall followed by an approach to an asymptotic limit. **Figure 33** shows the calibration plots (a) d|Z| vs. [S] and (b) d|Z|/dt vs. [S] obtained from the equilibrium responses and the initial responses respectively. **Figure 34** shows the linearized Lineweaver-Burk plot of the initial rate of impedimetric response from which was extracted the enzyme kinetic parameters. The kinetic parameters obtained for this urea biosensor format are shown in **Table 3, row 1**.

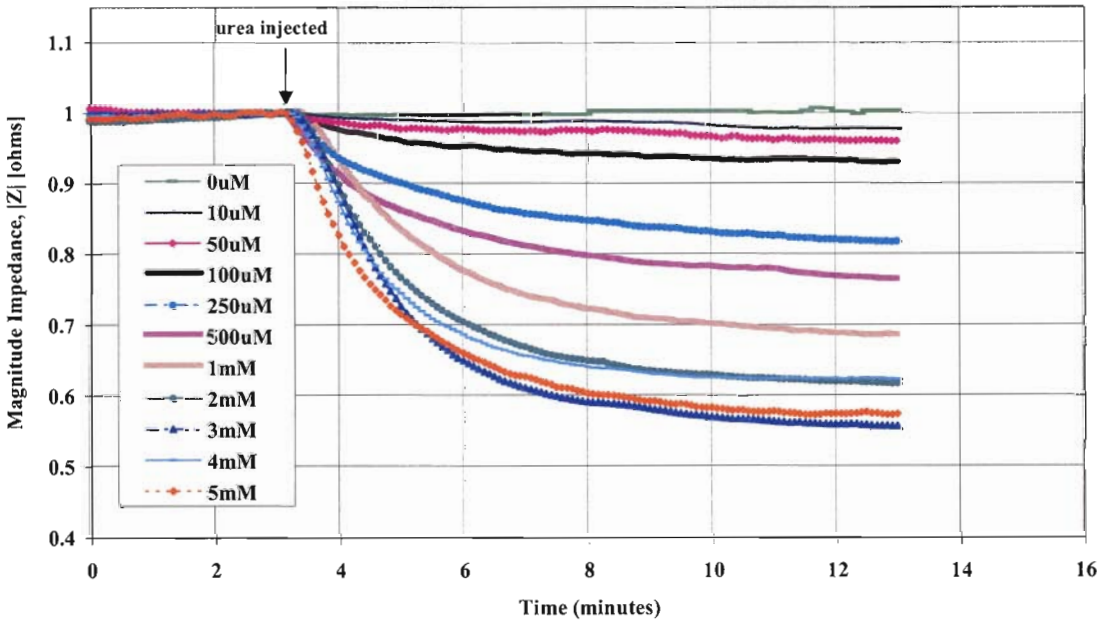

***Figure 32:** Impedimetric dose response curves for unPEGylated-urease – p(HEMA) hydrogel biosensor.*

For the unPEGylated urease in p(HEMA) hydrogel biosensor, the K_M value, reflecting the velocity of enzyme and substrate binding at active sites, was lower (0.8 mM) than that of free urease in solution (1.3 mM).

(a)

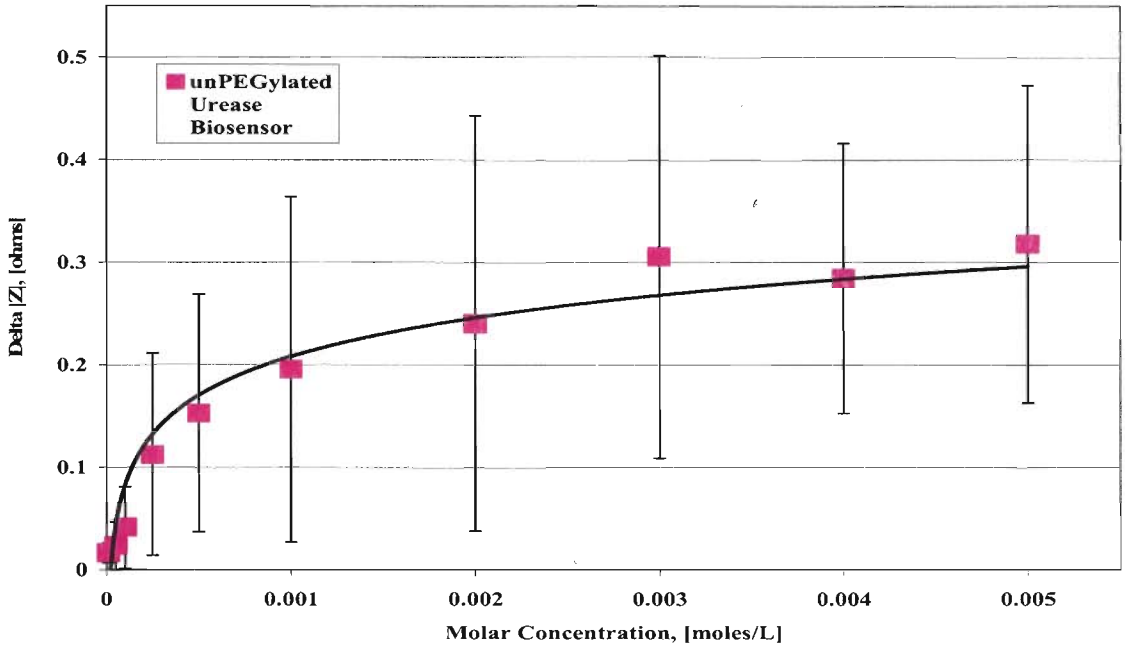

(b)

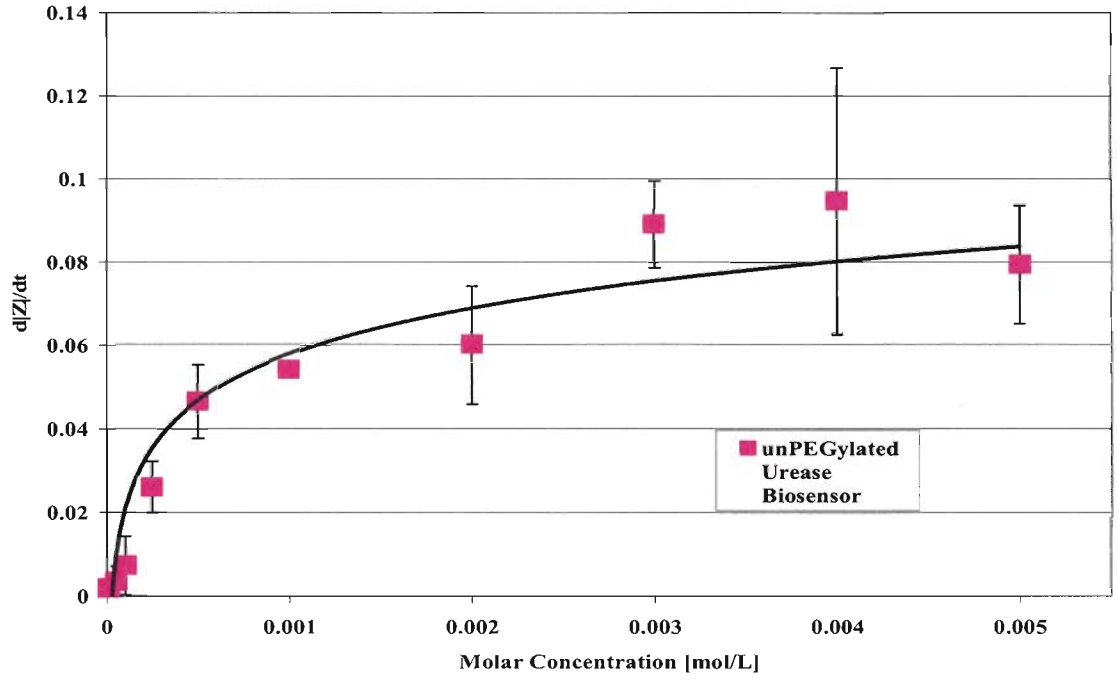

Figure 33: *Calibration plots of (a) Δ|Z| vs. [S] and (b) d|Z|/dt vs. [S] for unPEGylated urease –p(HEMA) hydrogel biosensor.*

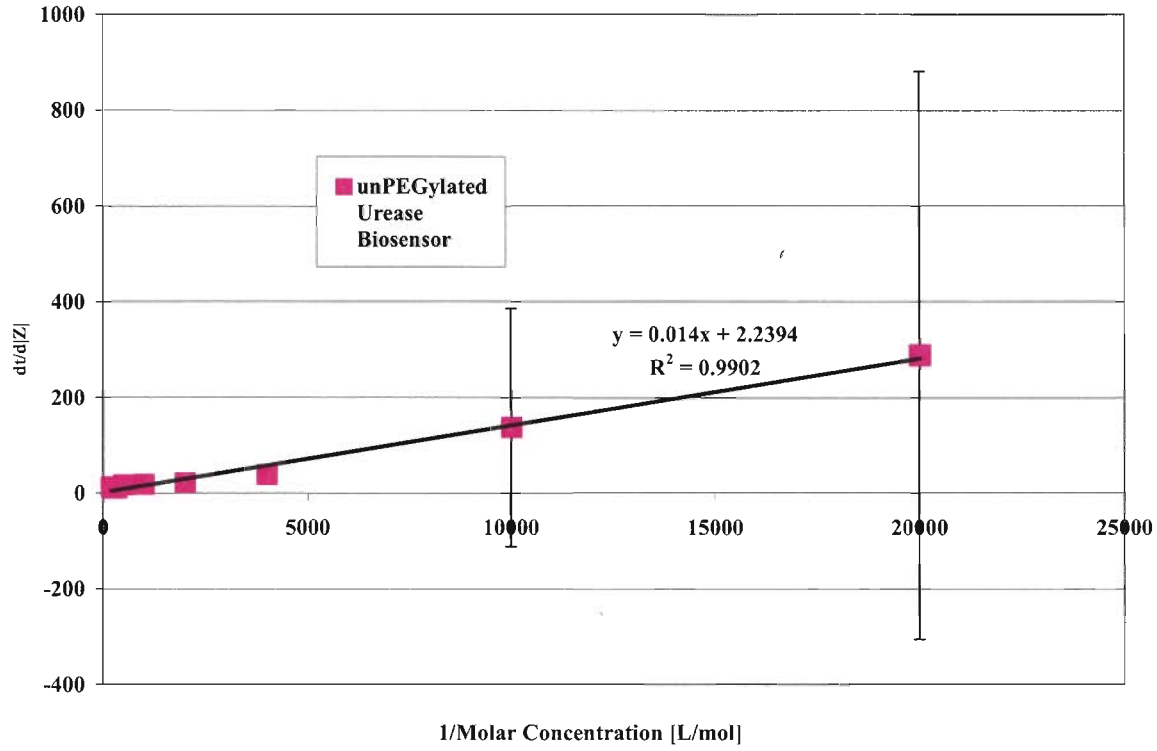

Figure 34: *Lineweaver-Burk plot of the impedimetric response for unPEGylated urease –p(HEMA) hydrogel biosensor.*

5.1.2. Characterization of the PEGylated-Urease-p(HEMA) format

Figure 35 shows the impedimetric dose response plots obtained for the urea biosensor formed from the PEGylated-urease immobilized within the p(HEMA) hydrogel. As before, the response is typical of enzyme-based biosensors possessing a rapid initial fall followed by an approach to an asymptotic limit. **Figure 36** shows the calibration plots (a) $\Delta|Z|$ vs. [S] and (b) $d|Z|/dt$ vs. [S] obtained from the equilibrium responses and the initial responses respectively. **Figure 36** shows the linearized Lineweaver-Burk plot of the initial rate of impedimetric response from which was extracted the enzyme kinetic parameters. The kinetic parameters obtained for this urea biosensor format are shown in **Table 3, row 2**.

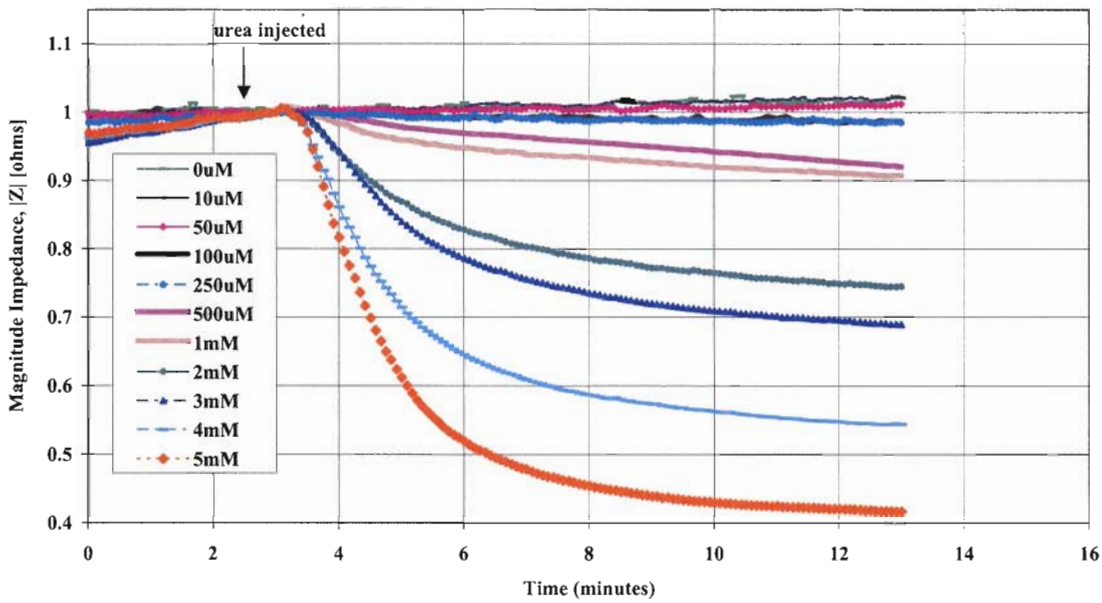

***Figure 35**: Impedimetric dose response curves for PEGylated(2:1) urease – p(HEMA) hydrogel biosensor.*

(a)

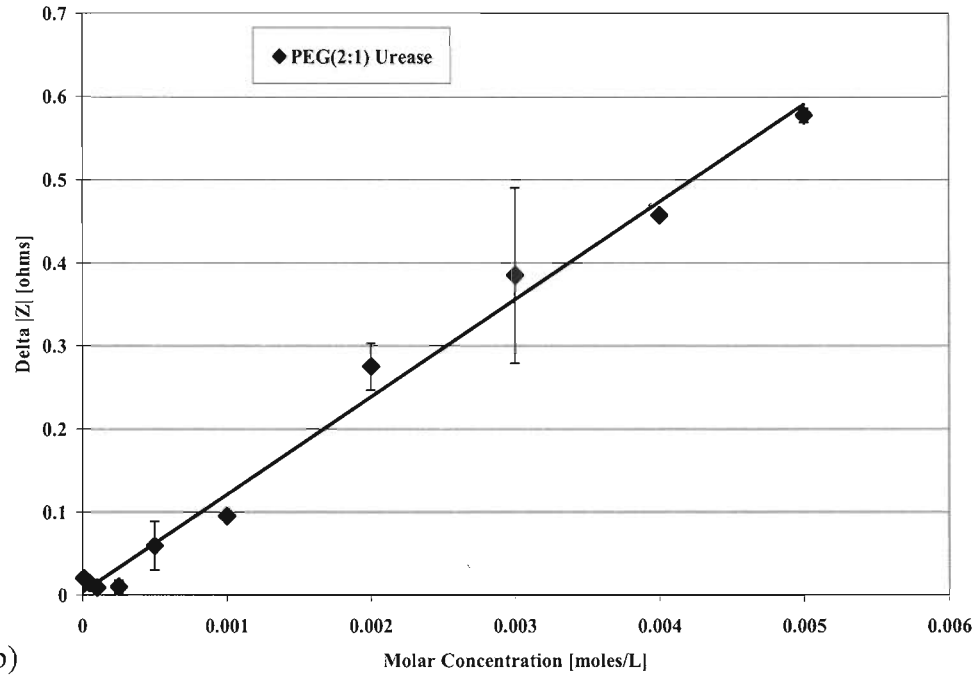

(b)

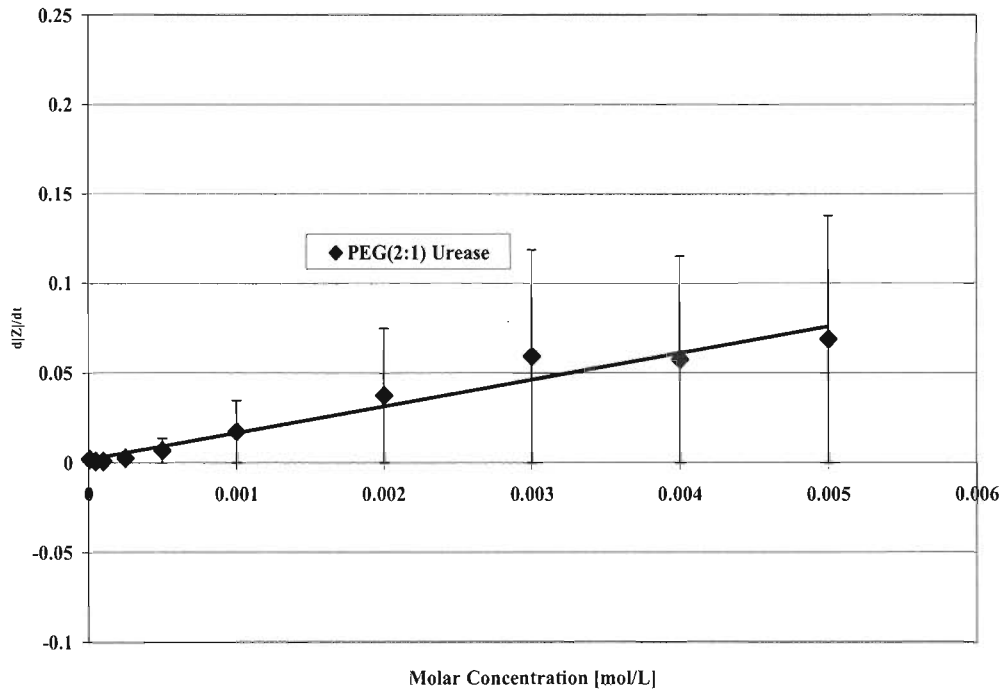

Figure 36: *Calibration plots of (a) Δ|Z| vs. [S] and (b) d|Z|/dt vs. [S] for PEGylated-urease –p(HEMA) hydrogel biosensor.*

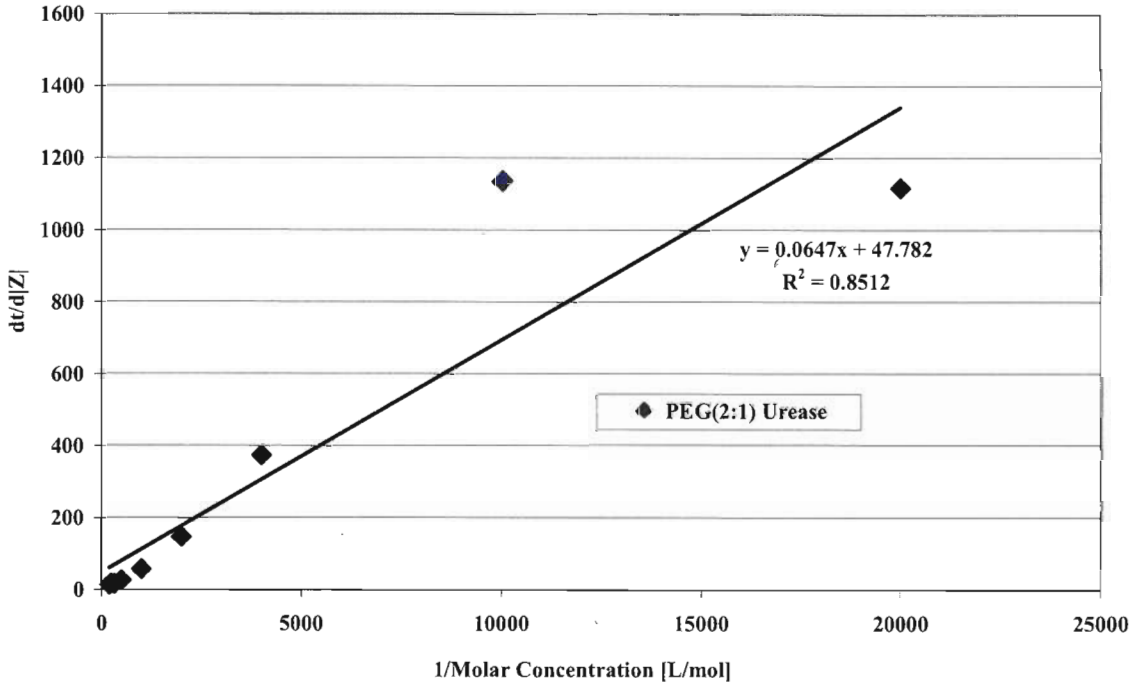

Figure 37: *Lineweaver-Burk plot of the impedimetric response for PEGylated (2:1)-urease–p(HEMA) hydrogel biosensor.*

For the PEGylated-urease in p(HEMA) hydrogel biosensor, the K_M value, reflecting the velocity of enzyme and substrate binding at active sites, was larger (34.2 mM) than that of free urease in solution (1.3 mM). This 26-fold increase in K_M may be explained by the fact that PEGylation may have altered or blocked the enzyme's active site.

In both cases, the biosensors show the expected increase in response with increase in molar concentration of urea. However, the change in impedance magnitude ($\Delta|Z|$) of the unPEGylated urease was larger than that of the PEGylated-urease. On the other hand, the dynamic range and detection limit for the unPEGylated-urease was higher than that of the PEGylated(2:1)-urease biosensor. The unPEGylated-urease biosensor reached saturation at

5mM, but the PEGylated(2:1)-urease did not respond at the low urea molar concentrations between 0μM to 250μM. Its saturation limit appears to be higher than 5mM.

5.1.3. Temperature effect on PEGylated and unPEGylated-urease-p(HEMA) format

Temperature dependence of the impedimetric response of the PEGylated-urease and unPEGylated-urease biosensors was determined at 10°C intervals over the range 10°C to 50°C. Tests were performed in 4mM and 2mM urea (10 mM Tris buffer, pH 7.0), respectively. The particular molar concentrations were picked based on observations from the impedimetric calibration curves for the optimum enzymatic response. **Figure 38** shows the temperature dependent response of unPEGylated and PEGylated-urease biosensors over the range of 10 – 50°C. The optimum responses were determined by normalizing all responses to the largest response, which was selected to be 100%.

For unPEGylated-urease the optimum was found to be at 40 °C. For PEGylated-urease the optimum was found to be at 30°C. For unPEGylated-urease the response decreased dramatically when the temperature exceeded 40°C (ca 60% drop). The decrease in activity may be due to enzyme denaturation arising from extensive conformational changes at the active site. For PEGylated urease, the response showed a modest decrease of less then 20%. The temperature stability is believed to arise from the PEGylation of the enzyme.

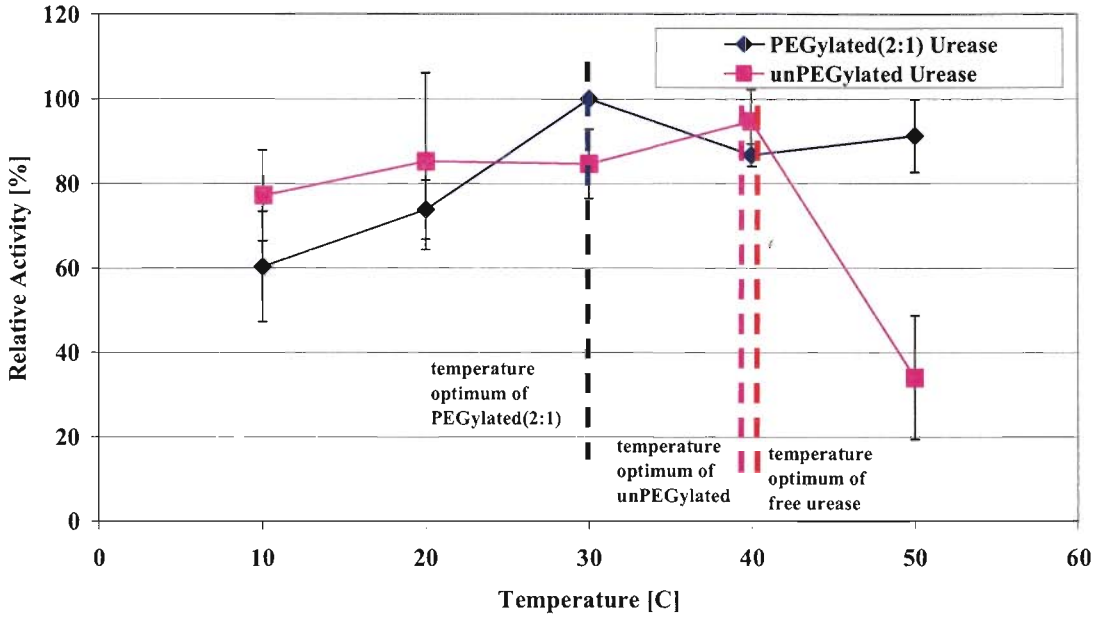

***Figure 38**: Temperature dependent responses of unPEGylated and PEGylated (2:1)-urease biosensors.*

5.1.4. pH effect on PEGylated and unPEGylated-urease-p(HEMA) format

pH dependence of the impedimetric response of the PEGylated-urease and unPEGylated-urease biosensors was determined at pH 1.0 intervals over the range 4.0 – 8.0 at 37°C. Tests were performed in 1mM and 4mM urea (10 mM Tris buffer, pH 4.0 – 8.0), respectively. The particular molar concentrations were picked based on observations from the impedimetric calibration curves for the optimum enzymatic response. **Figure 39** shows the pH dependent response of unPEGylated and PEGylated-urease biosensors over the range of pH 4.0 – 8.0. The pH optimum was found to be at pH 7.0 for both formats. This is consistent with literature values and favors in clinical chemistry without the need to adjust the pH of samples prior to analysis (Brahim et al. 2002). Deviations from the optimum pH of 7.0 had a very dramatic deleterious effect (-60%) on the response of the unPEGylated-

urease biosensor. While decreases were observed for the PEGylated-urease, such decreases were modest, being around –30%.

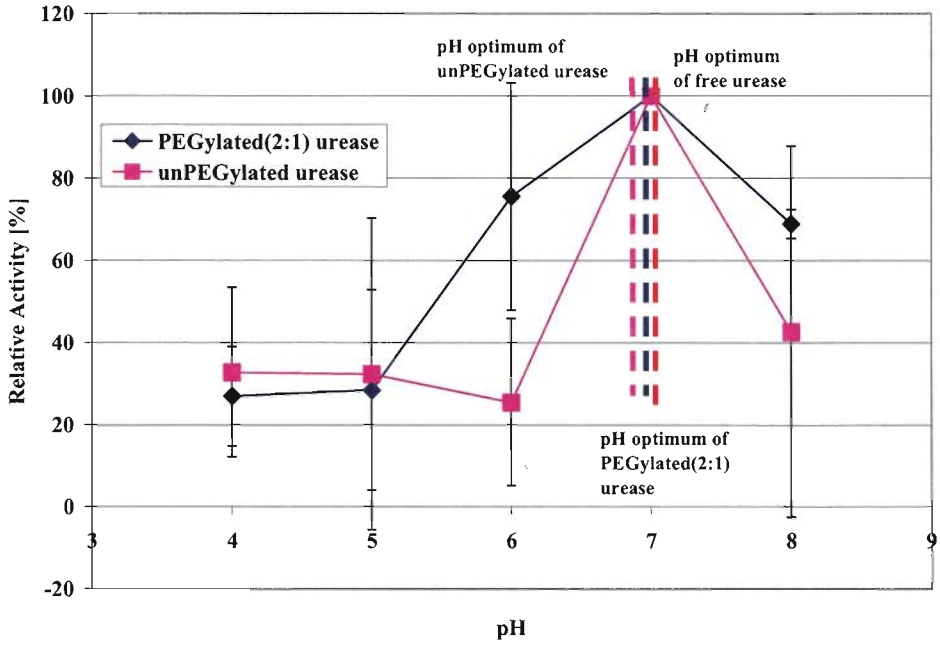

***Figure 39**: pH dependent responses of unPEGylated and PEGylated-urease biosensors.*

5.1.5. Characterization of urease immobilized in bovine serum albumin using glutaraldehyde format

Dose response tests were performed on this particular sensor for characterizing an immobilized enzyme outside of a hydrogel matrix. These dose response tests consisted of measuring the impedimetric response to various molar concentrations of urea, just as described in the above sections. It was observed that as the molar concentration of urea increased, the magnitude impedance change ($\Delta |Z|$) also increased, respectively, from its equilibrium state. **Figure 40** shows the calibration plots (a) $\Delta|Z|$ vs. [S] and (b) $d|Z|/dt$ vs. [S] obtained from the equilibrium responses and the initial responses respectively. **Figure**

41 shows the linearized Lineweaver-Burk plot of the initial rate of impedimetric response from which was extracted the enzyme kinetic parameters. The kinetic parameters obtained for this urea biosensor format are shown in **Table 3, row 3**.

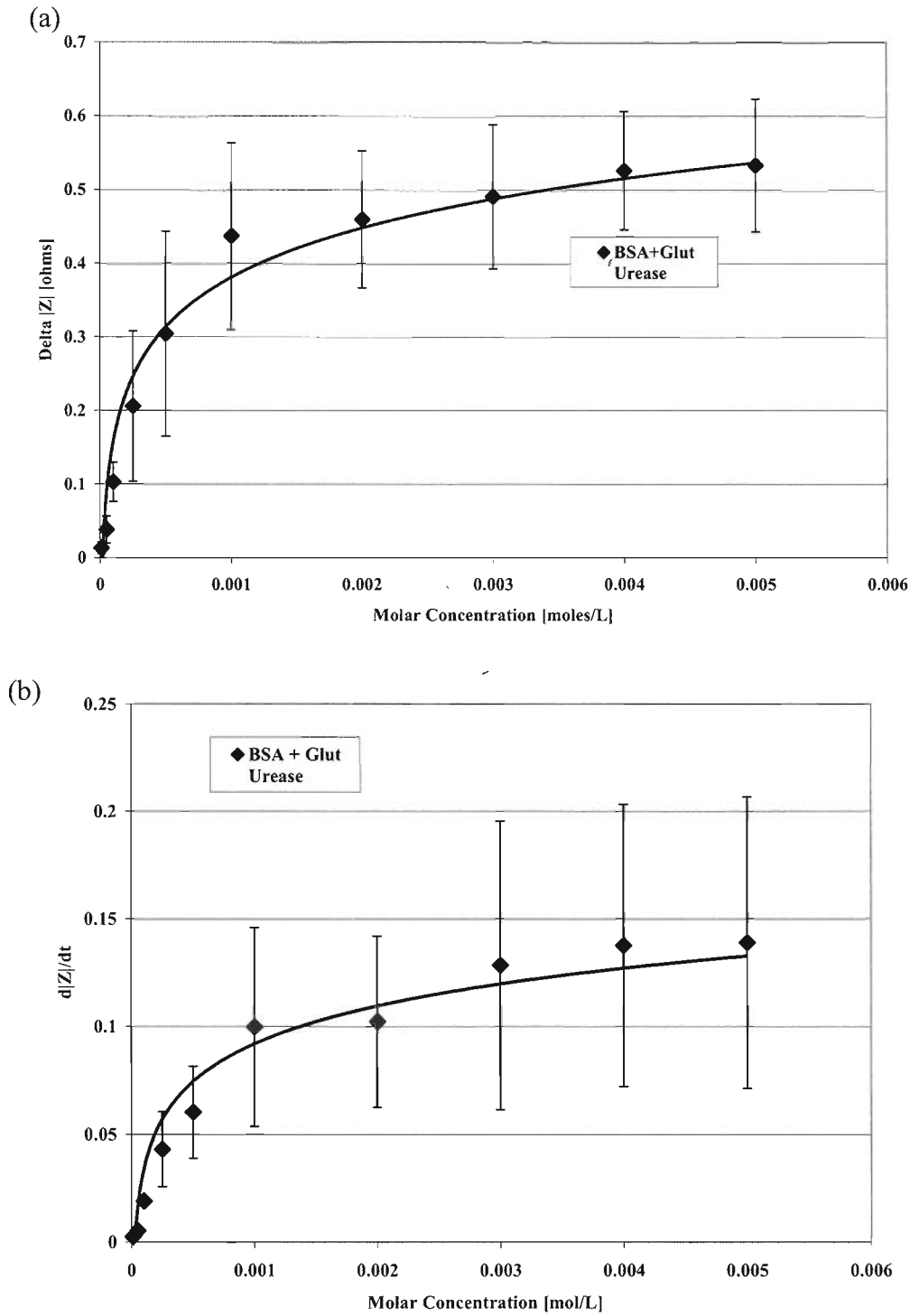

Figure 40: *Calibration plots of (a) $\Delta|Z|$ vs. [S] and (b) $d|Z|/dt$ vs. [S] for Urease immobilized in BSA and Glutaraldehyde biosensor.*

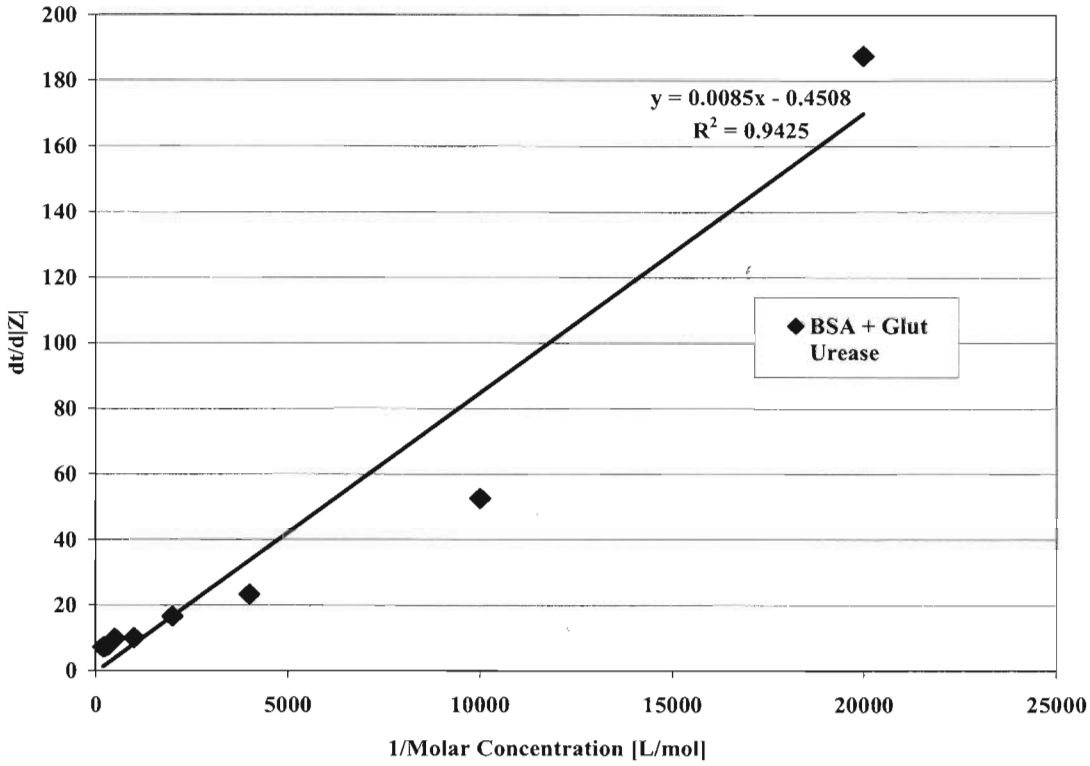

Figure 41: *Lineweaver-Burk plot of the impedimetric response for Urease immobilized in BSA and Glutaraldehyde biosensor.*

5.1.6. Characterization of free urease format

Dose response tests were performed on this particular sensor for the purpose of determining its kinetic parameters (i.e. Z_{MAX}, K_M, k_{cat} and E_o) for comparison with urease immobilized in BSA, unPEGylated-urease in hydrogel, PEGylated urease in hydrogel sensors. These dose response tests consisted of measuring the impedimetric response to various molar concentrations of urea, just as described in the above sections. It was observed that as the molar concentration of urea increased, the magnitude impedance change (Δ |Z|) also increased, respectively, from its equilibrium state. **Figure 42** shows the calibration plots (a) $\Delta|Z|$ vs. [S] and (b) $d|Z|/dt$ vs. [S] obtained from the equilibrium

responses and the initial responses respectively. **Figure 43** shows the linearized Lineweaver-Burk plot of the initial rate of impedimetric response from which was extracted the enzyme kinetic parameters. The kinetic parameters obtained for this urea biosensor format are shown in **Table 3, row 5**.

(a)

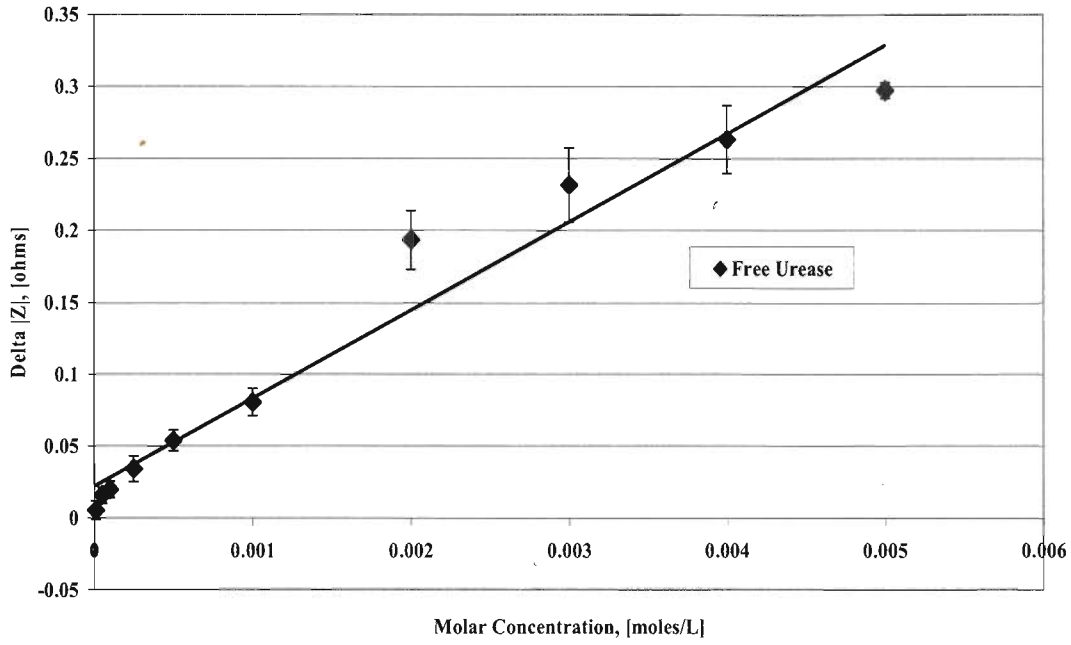

(b)

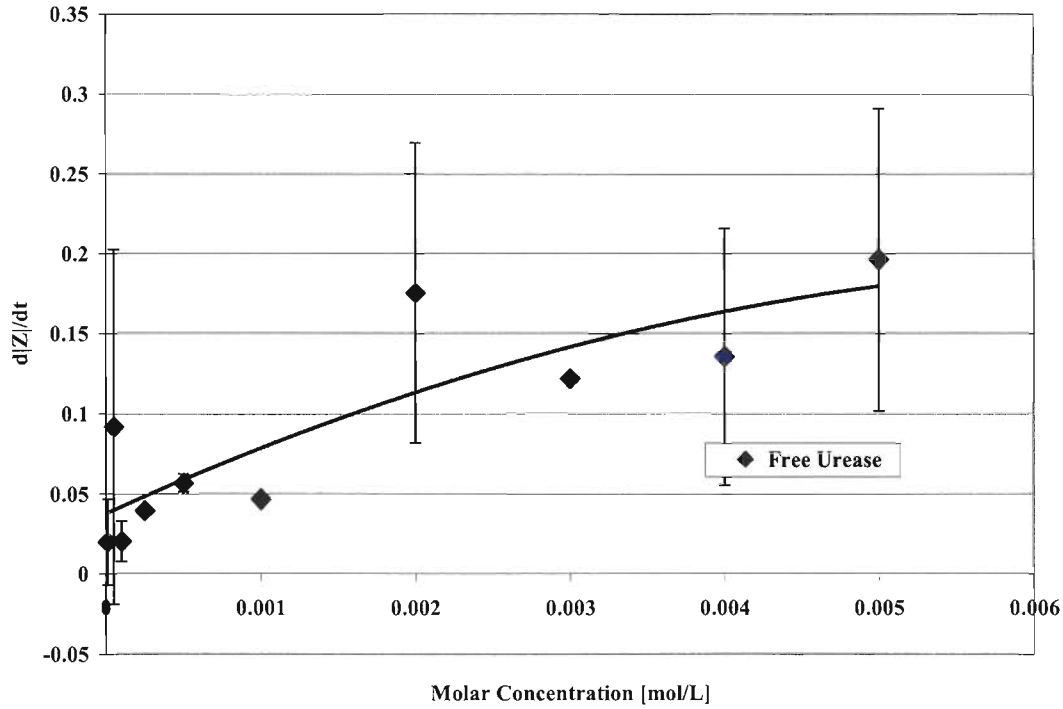

Figure 42: *Calibration plots of (a) Δ|Z| vs. [S] and (b) d|Z|/dt vs. [S] for Free Urease.*

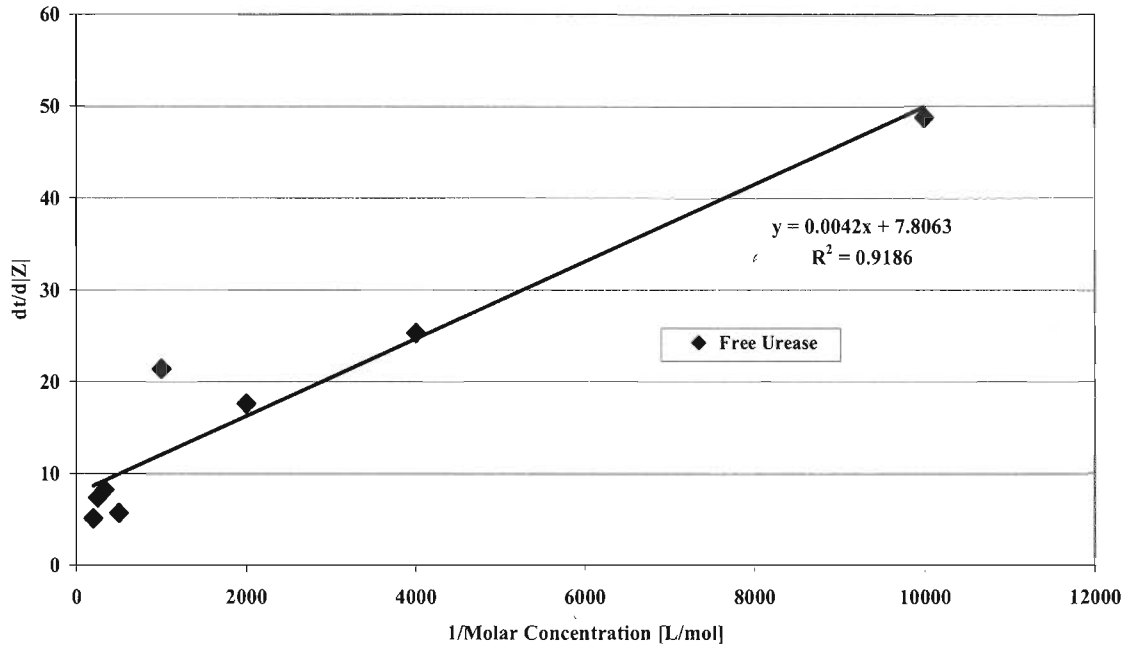

Figure 43: *Lineweaver-Burk plot of the impedimetric response for Free Urease.*

5.1.7. Characterization of Covalently Attached Urease format

These dose response tests consisted of measuring the impedimetric response to various molar concentrations of urea, just as described in the above sections. It was observed that as the molar concentration of urea increased, the magnitude impedance change (Δ |Z|) also increased, respectively, from its equilibrium state. **Figure 44** shows the calibration plots (a) $\Delta|Z|$ vs. [S] and (b) $d|Z|/dt$ vs. [S] obtained from the equilibrium responses and the initial responses respectively. **Figure 45** shows the linearized Lineweaver-Burk plot of the initial rate of impedimetric response from which was extracted the enzyme kinetic parameters. The kinetic parameters obtained for this urea biosensor format are shown in **Table 3, row 4.**

(a)

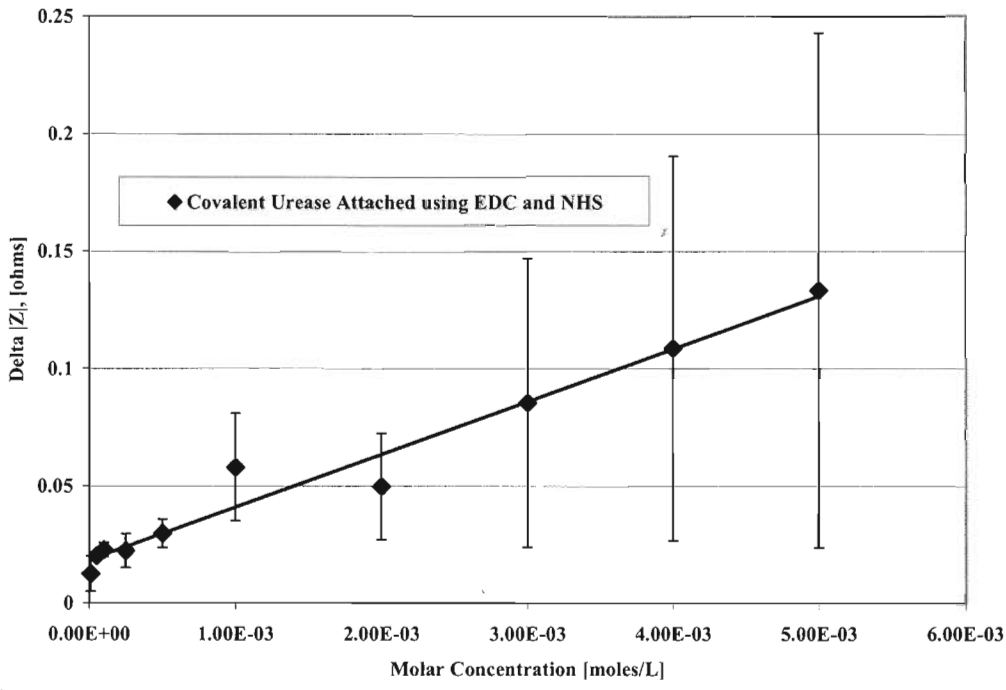

(b)

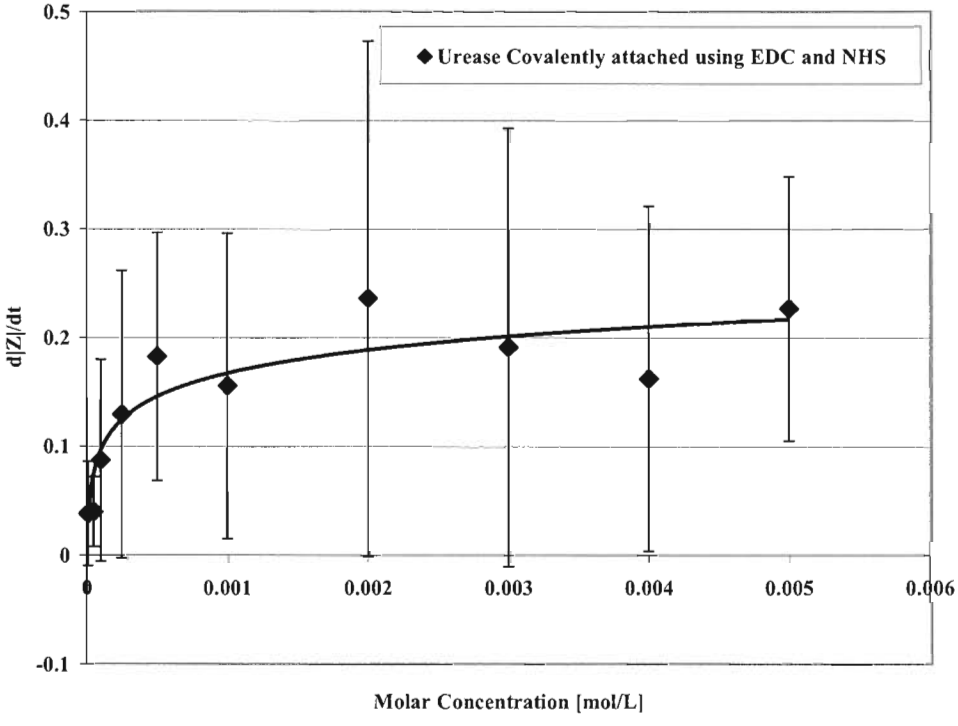

Figure 44: *Calibration plots of (a) Δ|Z| vs. [S] and (b) d|Z|/dt vs. [S] for Covalently Attached Urease.*

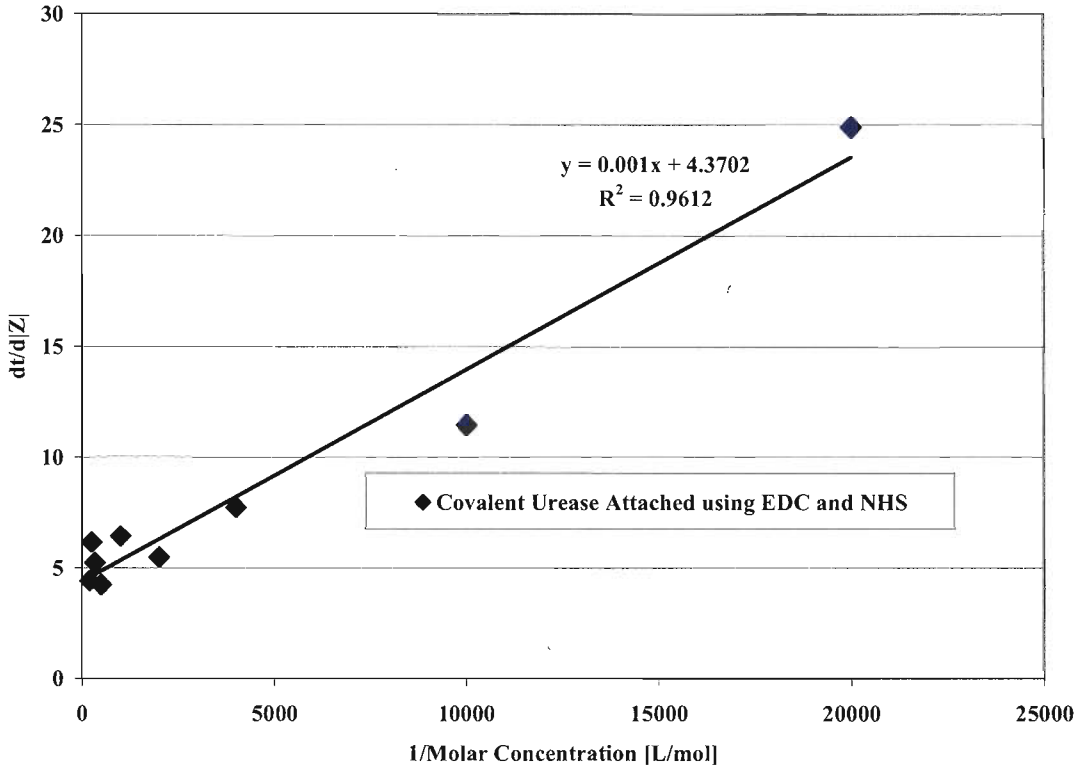

Figure 45: *Lineweaver-Burk plot of the impedimetric response for Covalently Attached Urease.*

Type of Biosensor	K_M Value [mM]	Z_{MAX} Value [Ω/min]	E_o [mol/L] x 10^{-6}	k_{cat} [Ω*L/min*mol] x 10^3	k_{cat}/K_M [Ω*L²/min*mol²] x 10^{-6}
unPEGylated Urease|Gel	0.8 ± 0.4	0.1	1.4	73.0	93.2
PEGylated Urease|Gel	34.2 ± 37.7	0.5	26.0	19.5	0.7
BSA + Glut	0.7 ± 0.3	0.2	62.5	2.5	3.4
Covalent Urease w/ EDC & NHS	0.1 ± 0.01	0.2	4.2	50.3	351.2
Covalent Urease w/ EDC & NHS *(Sheppard et al. 1995)*	4.0	3.6×10^{-10} [mol/cm²*s]			
Free Urease	1.4 ± 0.3	0.2	4.2	53.1	35.7
Free Urease (*Cesareo 1992*)	1.3 ± 0.2	-	-	-	-

Table 3*: Michaelis-Menten kinetic parameters for the various urease biosensor formats.*

5.1.8. Comparison of five urease biosensor formats

The immobilization of urease within the cross-linked p(HEMA) hydrogel (K_M = 0.8) has no appreciable impact on the kinetic performance of the enzyme compared to its performance in solution (K_M = 1.3-1.5). Biosensors formed from immobilized urease within a hydrogel biorecognition layer did not suffer any limitation due to a reduced flux of urea through the hydrogel. In this case, the kinetic curves followed the pattern expected for Michaelis–Menten kinetics and the kinetic parameters obtained were similar to that obtained in solution. Hydrogels of this type are typically 70% hydrated (Abraham et al. 2005) and so provide an immobilization milieu that is quite similar to water. This portends well of the use of hydrogels to serve as the biorecognition layer in enzyme biosensors.

Based upon a comparison of the kinetic plots (*$\Delta|Z|$ vs. [S] and (b) $d|Z|/dt$ vs. [S]*) obtained from the PEGylated-urease (**Figure 36**) and unPEGylated urease (**Figure 33**) biosensors, it is apparent that the unPEGylated-urease biosensor follows the pattern expected for Michaelis–Menten kinetics while the PEGylated-urease biosensor shows a straight line associated with diffusion controlled enzyme kinetics.

When a biosensor is under diffusion controlled enzyme kinetics, a different equation is applied. This equation follows Fick's Law for the formation of product in an enzymatic reaction. It takes into account the coupling of the urease-catalyzed reaction in the enzyme layer with the one-dimensional-in-space diffusion. The equation is shown:

$$\frac{\partial P}{\partial t} = D_P \frac{\partial^2 P}{\partial x^2} - \frac{V_{MAX} P}{K_M + P}$$

$$0 < x < d$$

$$0 < t \leq T$$

where x and t stand for space and time, respectively, and P(x,t) denotes the concentration function of the reaction product, respectively, V_{MAX} is the maximal enzymatic rate attainable with that amount of enzyme, when the enzyme is fully saturated with substrate, K_M the Michaelis constant, d the thickness of the enzyme layer, and D_P is the diffusion coefficient of the product, respectively, T is the full time of biosensor operation to be analyzed (Baronas et al. 2004).

The PEGylated-urease sensor showed a lower affinity for urease binding to urea (K_M = 34.2) than its unPEGylated counterpart (K_M =0.8) within the hydrogel. The difference may be directly attributable to the process of PEGylation and the impact this has on access of urea to the enzyme's active site. The unPEGylated-urease sensor indicated the higher k_{cat}/K_M values than the PEGylated-urease sensor. The kinetic parameters support that unPEGylated-urease had a higher enzyme-substrate binding rate and catalytic rate than PEGylated and would thus provide a faster impedimetric response to various molar concentrations of urea. PEGylation may directly alter the active site via covalent modification and may also lead to a protective PEG layer around the enzyme through which the urea must diffuse.

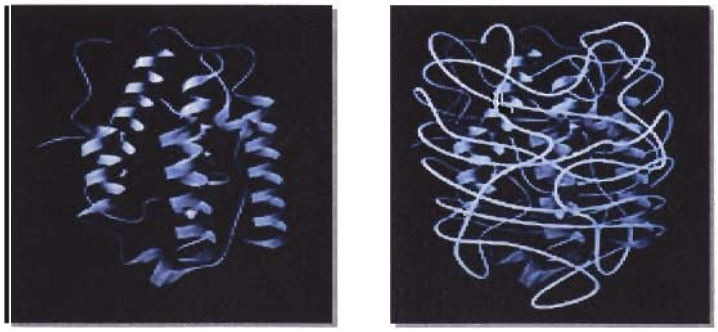

unPEGylated Molecule PEGylated Molecule

***Figure 46**: Diagram of unPEGylated versus PEGylated molecule. (Zhang et al. 2002)*

Figure 40a and b show the kinetic plots for urease immobilized using BSA and Glutaraldehyde. These plots indicate that as the molar concentration of urea increases towards 5mM, the enzyme reached its saturation limit and its impedimetric response would no longer continue to increase. The curvature of the calibration plots indicates that the enzymatic reaction was kinetically driven, rather than controlled by diffusion. The biosensor format of urease immobilized using BSA and Glutaraldehyde showed a K_M value of 0.7 mM. This is somewhat lower than the value obtained in free solution (K_M = 1.3 mM) but similar to that for unPEGylated urease immobilized within the hydrogel (K_M = 0.8 mM). This observation supports the view that whether immobilized within a proteinacious hydrogel (formed form BSA) or a synthetic hydrogel [formed from p(HEMA)] the urease has essentially the same performance.

The Michaelis-Menten kinetic parameters revealed that free urease had higher Z_{MAX}, K_M, k_{cat} and E_o values compared to the unPEGylated-urease and PEGylated-urease sensors. Free urease was not immobilized within any hydrogel, therefore its active sites were freely available for binding with substrate and catalytic conversion of substrate to product. The calibration plot of the free urease format shown in **Figure 42b** indicates that as the urea molar concentration increased towards 5mM, the enzyme attained its saturation limit and its impedimetric response would no longer continues to rise. The curvature of the calibration plot indicated that the enzymatic reaction was kinetically driven, rather than by diffusion. The K_M value of free urease was expected to be the smallest, being unaffected by PEGylation and unconstrained by immobilization.

When comparing the urea biosensors formed by the direct covalent attachment of urease using 1-ethyl-3- (3-dimethylaminopropyl)carbodiimide-HCl (EDC) and N-hydroxysulfosuccinimide (Sulfo-NHS) to the other urea biosensors, it was found that covalent immobilization yielded a lower K_M value compared to hydrogel matrix entrapment. The urea biosensor attached via covalent bonding provided values of $K_M = 0.1$ mM and $Z_{MAX} = 0.2\ \Omega s^{-1}$. This is an order of magnitude smaller K_M than found for any of the other formats investigated. Typically, covalent attachment leads to an increase in the apparent K_M of the immobilized enzyme (Goldstein 1972). A hydrogel matrix favored a better environment for the enzyme to retain its natural enzymatic activity than covalent immobilization and also had a higher volume of enzyme entrapped within the hydrogel. The analyte had a faster binding rate to the enzyme since there was a lower concentration of enzyme.

The calibration plots of all urease biotransducer formats demonstrated a greater variability in the $\Delta|Z|$ vs. [S] plot compared to the $d|Z|/dt$ vs. [S] plot. The significant variability in the $\Delta|Z|$ vs. [S] plot is due to the electrochemical reactions not reaching complete equilibrium. The plots may appear to be at equilibrium, approaching the asymptotic limit after the initial fall, but the reaction itself has not reached completion. Due to this variability between each replicate for one urease biotransducer format, it has resulted in a large range of error for the $\Delta|Z|$ vs. [S] plots.

5.1.9. FTIR Analysis

FTIR was used to obtain spectra for the analysis of covalent coupling of amino acid groups ($-NH_2$) of the urease enzyme to carboxylic acid groups (-COOH) of the Acryl-PEG-

NHS ester used in PEGylation. **Figure 47** illustrates the FTIR spectra for three types of urease samples: free urease, undialyzed PEGylated (2:1) urease in HEPES buffer, and dialyzed PEGylated urease (2:1) in Tris buffer.. Upon PEGylation, it was suggested from the peak, around 3000 cm^{-1}, that there was a depletion of free N-H groups on the urease enzyme. From the peaks ca. 1500 and ca. 2000 cm^{-1}, it was suggested that there was an increase of –CONH– groups due to reaction between A-PEG-NHS and urease enzyme. When comparing undialyzed versus dialyzed PEGylated(2:1) urease, the presence of the primary amine of Tris is shown as a broad band between 3,000 and 3,500 cm^{-1}. Dialyzing a PEG coupled enzyme helped clean up the PEGylated enzyme solution of uncoupled PEG moieties and exchanged the HEPES buffer for Tris buffer.

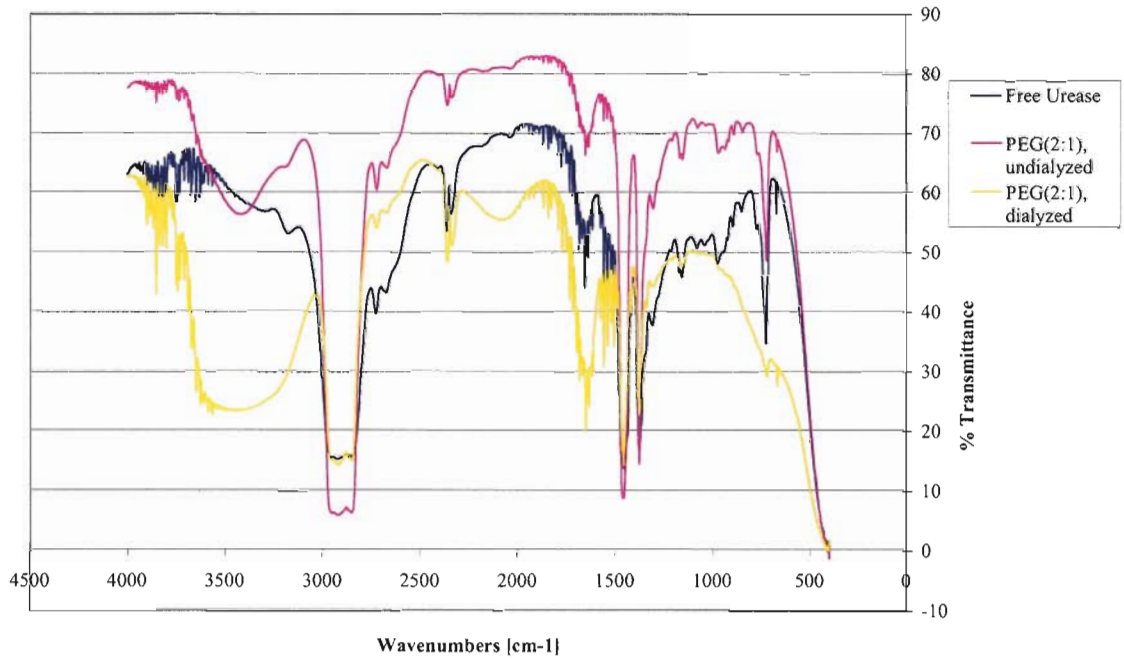

***Figure 47**: FTIR spectra for three types of urease: free urease, PEG(2:1) undialyzed and PEG(2:1) dialyzed.*

5.1.10. Storage Stability of PEGylated Urease Biosensor

After 30 days of storage in 10mM Tris buffer at 4°C, the biosensor containing the covalently immobilized and entrapped PEGylated urease within the hydrogel retained 55% and 37% of its activity when tested with 1mM urea and 5mM urea, respectively. These values are compared to the values from Day 0 of testing.

5.2. Instrumentation and Software Results

The 3EIC is designed to interrogate and capture real-time impedimetric response data from three (3) four-electrode cells that are simultaneously under test. The three cells provide separate test environments to perform tests on a control, a blank and the sample. Several design and operational issues were revealed during the implementation phase that affected the proper performance of the 3EIC instrumentation.

A. The 50 mV_{PP}, 4kHz sine wave output from the operational amplifier (U154, MAX410) was designed to ideally output a sinusoidal wave. The sine wave from the function generator (MAX038) provided approximately a $2V_{PP}$, 4.1 kHz sine wave. This was verified. The output sine wave was clean without any interference or noise. However, when sent through the operational amplifier (U154, MAX410), the sine wave became a noisy 4kHz sine wave. To address this problem, the 38 kΩ input resistor to the operational amplifier was replaced by potentiometer and the potentiometer was adjusted until a clean $750mV_{PP}$, 4kHz sine wave was obtained. The input resistor was accordingly set to 3.9 kΩ. However, it was observed that the bottom half of the $750mV_{PP}$, 4kHz sine wave was clipped. This was implemented

as a temporary change until a proper solution could be found in order to eliminate the noise from the $50mV_{PP}$, 4kHz sine wave.

B. The μDAQ Data Acquisition unit, a USB30 was initially specified as the D/A-A/D interface. During troubleshooting of the software code, it was found that the "Write Digital Line" VIs were being reset to "0" when the "Read Digital Line" and "AD Sample Channel" VI were set to read. The DIO would not hold their states while simultaneously reading digital signals and analog signals. One attempted solution was to place the "Write Digital Line" VIs outside of the WHILE loop and separate from the "Read Digital Line" VI and "AD Sample Channel" VI. A second attempted approach was to place the "Write Digital Line" VIs in a separate WHILE loop in order to have them hold their states while digital and analog signals were being read. Neither of these approaches worked to address the problem. The solution was found in recognizing that the Digital Inputs/Outputs (DIOs) from the μDAQ USB30 were set to be either a "Write Digital Line" or "Read Digital Line" and NOT both. The μDAQ USB30 DIO had only 3 ports containing 8 channel lines each. The 3 ports (as a whole) could be set as "read" or "write" states. The individual channel lines within the port could not be individually set to be both "read" and "write". This was why the "Write Digital Line" VIs became reset when the reading of digital and analog signals occurs (since the ports cannot read and write simultaneously). Therefore, the originally specified μDAQ USB30 unit was found to be incompatible with the needs of this project. Ideally, at least 10 Digital Write channel lines and at least 12 Digital Read channel lines were needed. The

μDAQ USB30 was accordingly replaced with a μDAQ USB-48A-30A16 that contained 48 DIO + 16 ADC + 4 DAC (Eagle Technology).

C. The originally specified electronic switches, ADG 733, were found to be incompatible with the μDAQ USB series. These switches were powered by ± 2.5V voltage supply and could only accept logic inputs (A0, A1, A2) of +2.5V. The μDAQ USB units outputs +5.0V as the logic input. The solution was to specify new electronic switches, the ADG 633 that is powered by ± 5.0V and could accept logic inputs of +5.0V.

D. The purpose of the "power on" latching circuit was to convert the momentary switch (non-latching) of the Antec Minuet chassis into a latching switch by shorting the PS-ON and GND on the ATX12V power connector. However, it was found that within the 3EIC printed circuit board, there appeared to be a short between the PS-ON and GND caused by the SPST switch (ADG721). This meant that the chassis fan and power supply were constantly running, even though it appeared that the condition of the SPST switch (ADG721) was changing between open/closed. To address this problem, the SPST switch (ADG721) was removed from the printed circuit board and a two-pin jumper was placed in the S1 and D1 pin holes on the PCB. The momentary switch of the Antec Minuet chassis was physically replaced with a latching SPST switch. This switch was then connected to the two-pin jumper in the S1 and D1 pin holes. Cuts were made in the lead lines that delivered the +5V input supply voltages to the latching circuit ICs from the PS-

ON lead lines. A wire was connected from one of the jumper pins to the PS-ON pin out position on the printed circuit board.

Table 4 summarizes the above issues and their resolution to date. At this writing, the testing of the re-specified switches and the attenuation of the function generator signal to permit a non-perturbating interrogation of the biosensors remains an outstanding issues.

Component	Problem	Solution
AD/DA and DIO Interface	µDAQ USB 30 inappropriately specified; 3 ports containing 8 channel lines, the individual channel lines could not be individually set to be read or write	Replaced with µDAQ USB-48A-30A16, which contains 48 DIO (6 ports of 8 channel lines), ports as a whole can be set as digital read/write
Function Generator	Noisy 50mV_{PP}, 4kHz sine wave	Changed input resistor at OpAmp to produce output of 750mV_{PP}, 4kHz
Power ON Latching Circuit	Chassis power supply would not stop running regardless of change in state of latching circuit	Hardwired PS-ON and GND to non-latching chassis switch
Electronic switches	Incorrect specification of AGD 733 SPDT switch: ±2.5V supply and +2.5V logic input	Replace with ADG 633 SPDT: accepts ±5V supply and +5V logic input from µDAQ USB-48A-30A16

***Table 4**: Troubleshooting of Urea Impedance BioAnalyzer Hardware.*

Regarding the Urea Impedance Biosensor software program, the digital inputs provided by the µDAQ USB-48A-30A16, the analog outputs read in from the Urea Impedance Biosensor and the signal processing of the analog outputs seem to be in logical order. The problems and troubleshooting for this portion of the Biosensor system would not be able to begin until the hardware issues are resolved.

Chapter 6. Conclusions

Five biosensors consisting of various enzyme immobilization methods were fabricated. Two biosensors consisting of a composite polymer matrix of p(HEMA)/TEGDA using two types of urease: unPEGylated and PEGylated were fabricated. The polymerization process involved UV induced polymerization of the hydrogel component from a monomer cocktail (HEMA:TEGDA) containing either unPEGylated or PEGylated urease. Overall it was concluded that an unPEGylated-urease sensor provided a higher enzyme-substrate binding rate and catalysis rate than PEGylated and would thus provide a faster impedimetric response to various molar concentrations of urea. However, it was the PEGylated-urease sensor which would provide initial long-term stability for the enzyme and reproducibility of impedance responses than the other four biosensors. The primary purpose for characterization of the free urease, urease covalently attached using EDC and NHS and urease immobilized in BSA using Glutaraldehyde biosensors were to serve as comparison points of the Michaelis-Menten kinetic parameters with the unPEGylated and PEGylated-urease biosensors. The urease covalently attached using EDC and NHS showed highest enzyme-substrate binding rate and catalysis rate than the free urease, urease immobilized in BSA using Glutaraldehyde, unPEGylated and PEGylated-urease biosensors. However, the initial long-term stability for the enzyme in the other sensor systems would not be sustained for the same length of time as the PEGylated urease biosensor.

The hardware and software development for the Impedance Analyzer is still under analysis and troubleshooting. Several hardware design errors have been discovered and

addressed (**Table 4**). The complete analysis and troubleshooting for the software program awaits the resolution of all problems with the hardware.

Chapter 7. Recommendations and Further Work

Several recommendations for the PEGylated Urease biosensor could be made to improve its impedimetric performance and linear concentration range. As seen in the impedimetric calibration curves for the PEGylated Urease biosensor, the biosensor had not reached a saturation concentration at 5mM urea as the other three biosensors. This means that the detection range for the PEGylated urease biosensor was higher than what was tested. Further investigation could be conducted to determine the maximum urea concentration at which the PEGylated urease biosensor reaches saturation.

A second recommendation is to add a diffusional layer of p(HEMA) without any urease immobilized within the layer on top of the urease immobilized p(HEMA) layer on the IME. This would help increase the linear range of urea molar concentration since the urea would have to diffuse through a thicker hydrogel layer in order to interact with the urease enzyme. This allowed for an easier extrapolation of the urea molar concentration based on the magnitude impedance drop of the urease biosensor.

The normal physiologic level of urea in the human body was about 8-20 mg/dL (1.3 to ~3.5 mM) (Rajesh et al. 2005). The concentration was much higher for those suffering from renal failure and seeking kidney dialysis treatment. This supported that the PEGylated urease sensor served as the best biosensor for use in a Urea Impedance Biosensor based on its impedimetric response and detection range. The calibration curves for the PEGylated Urease biosensor showed that the biosensor did not indicate an impedimetric response to urea until 1mM and had a higher detection range (beyond 5mM) than the other urease biosensors. This characteristic would be especially useful in a

clinical urea detection system for kidney dialysis patients at hospitals or other health treatment centers.

Literature Cited

Abraham, S., Brahim, S., Ishihara, K. Guiseppi-Elie, A. "Molecularly engineered p(HEMA)-based hydrogels for implant biochip biocompatibility." Biomaterials, vol. 26, pp. 4767-4778, 2005.

Adeloju, S; Shaw, S.; Wallace, G. "Pulsed-amperometric detection of urea in blood samples on a conducting polypyrrole-urease biosensor." Analytica Chimica Acta, vol. 341, pp. 155-160, 1997.

Anonymous. "Bioanalytical Applications of Fiber-Optic Chemical Sensors." Analytical Chemistry, vol. 58, pp. 766A-770A, 1986.

Baronas, R.; Kulys, J.; Ivanauskas, F. "Modelling amperometric enzyme electrode with substrate cyclic conversion." Biosensors and Bioelectronics, vol. 19, pp. 915-922, 2004.

Blanch, Harvey W.; Clark, Douglas S. Biochemical Engineering. New York: M. Dekker. 1997.

Brahim, S., Narinesingh, D. Guiseppi-Elie, A. "Amperometric determination of cholesterol in serum using a biosensor of cholesterol oxidase contained within a polypyrrole-hydrogel membrane." Analytica Chimica Acta. vol. 448, pp. 27-36, 2001.

Brahim, S., Narinesingh, D. Guiseppi-Elie, A. "Polypyrrole-hydrogel composites for the construction of clinically important biosensors." Biosens. Bioelectron. vol. 17, pp. 53-59, 2002.

Brett, C.M.A.; Brett, A.M.O. Electrochemistry, Principles, Methods and Applications. New York: Oxford University Press. 1993.

Byrne, Mark; Park, Kinam; and Peppas, Nicholas A. "Molecular Imprinting within Hydrogels." Advanced Drug Delivery Reviews, vol. 54, pp. 149-161, 2002.

Calvo, E.J.; Danilowicz, C. "Amperometric Enzyme Electrodes." J. Braz. Chem. Soc, vol. 8, no. 6, pp. 563-574, 1997.

Cané, C.; Gràcia, I.; Merlos, A. "Microtechnologies for pH ISFET Chemical Sensors." Microelectronics Journal, vol. 28, no. 4, pp. 389-405, 1997.

Cass, A.E.G. Biosensors: A Practical Approach. New York: Oxford University Press. 1990.

Castillo, J.; Gáspár, S.; Leth, S.; Niculescu, M.; Mortari, A.; Bontidean, I.; Soukharev, V.; Dorneanu, S.A.; Ryabov, A.D.; Csöregi, E. "Biosensors for life quality: Design, development and applications." Sensors and Actuators B: Chemical, vol. 102, pp. 179-184, 2004.

Cesareo, S.D.; Langton, S.R. "Kinetic Properties of Helicobacter pylori urease compared with jack bean urease." FEMS Microbiology Letters, vol. 99, pp. 15-22, 1992.

Chaubey, Asha; Malhotra, B.D. "Mediated biosensors." Biosensors and Bioelectronics, vol. 17, pp. 441-456, 2002.

Cifova, I; Brynda, E; Mandys, V; Stol, M. "Irritation effects of residual products derived from p(HEMA) gels. II. Compounds extracted from hydrogels." Biomaterials, vol. 9, pp. 372-375, 1988.

Cunningham, Alice. Bioanalytical Sensors. New York: John Wiley & Sons, Inc. 1998.

Goldstein, L. "Microenvironmental effects on enzyme catalysis. A kinetic study of polyanionic and polycationic derivatives of chymotrypsin." Biochemistry, vol. 11, pp. 4072-4084, 1972.

Gorchkov, D. V.; Poyard, S.; Soldatkin, A.P.; Jaffrezic-Renault, N.; Martelet, C. "Application of the charged polymeric materials as additional permselective membranes for improvement of the performance characteristics of urea-sensitive ENFETs. 2. Urea determination in blood serum." Materials Science and Engineering: C, vol. 5, pp. 29-34, 1997.

Griffiths, Peter; de Haseth, James A. Fourier transform infrared spectrometry. New York: John Wiley & Sons, Inc. 1986.

Jdanova, A.S.; Poyard, S.; Soldatkin, A.P.; Jaffrezic-Renault, N.; Martelet, C. "Conductometric urea sensor. Use of additional membranes for the improvement of its analytical characteristics." Analytica Chimica Acta, vol. 321, pp. 35-40, 1996.

Jin, J.; Min, N.; Kang, C.; Park, S.; Hong, S. "Characteristics of Urea Sensor Based on Platinum Deposited Porous Silicon." Journal of Korean Physical Society, vol. 39, pp S67-S69, 2001.

Katz, E.; Schlereth, D.D.; Schmidt, H.L. "Electrochemical study of pyrroloquinoline quinone covalently immobilized as monolayer onto a cystamine modified gold electrode," J. Electroanal. Chem., vol. 367, pp. 59-70, 1994.

Kemp, William. Organic Spectroscopy. London: Macmillian Education, Ltd. 1991.

Kovács, Barna; Nagy, Géza; Dombi, Roland; Tóth, Klára. "Optical biosensor for urea with improved response time." Biosensors and Bioelectronics, vol. 18, pp. 111-118, 2003.

Kell, D. B. 1987. The Principles and Potential of Electrical Admittance Spectroscopy: An Introduction. Pages 427-468 in A. Turner, I. Karube, and G. S. Wilson, eds. *Biosensors;Fundamentals and Applications*. Oxford University Press, Oxford.

Lopez-Gallego, F., Betancor, L., Mateo, C., Hidalgo, A., Alonso-Morales, N., Dellamora-Ortiz, G., Guisan, J., Fernandez-Lafuente, R. "Enzyme stabilization by glutaraldehyde crosslinking of absorbed proteins on aminated supports." Journal of Biotechnology, *In Press*, 2005.

Luo, Yung-Chien; Jing-Shan, D. "Urea biosensor based on PANi(urease)-Nafion®/Au composite electrode." Biosensors and Bioelectronics, vol. 20, pp. 15-23, 2004.

Macdonald, J.R. Impedance Spectroscopy: Emphasizing Solid Materials and Systems. New York: John Wiley & Sons, 1987.

de Melo, J.V.; Soldatkin, A.; Martelet, C.; Jaffrezic-Renault, N.; Cosnier, S. "Use of competitive inhibition for driving sensitivity and dynamic range of urea ENFETs." Biosensors and Bioelectronics, vol. 18, pp. 345-351, 2003.

Murray, M.J.; Snowden, M.J. "The preparation, characterization and applications of colloidal microgels." Advances in Colloid and Interface Science, vol. 54, pp. 73, 1995.

Noordwijk, Jacob van. Dialysing for life: the development of the artificial kidney. Boston: Kluwer Academic Publishers, 2001.

O'Neill, M.A.A.; Beezer, A.E.; Mitchell, J.C.; Connor, J.A. "Determination of Michaelis-Menten parameters obtained from isothermal flow calorimetric data." Thermochimica Acta, vol. 417, pp. 187-192, 2004.

Osaka, Tetsuya; Komaba, Shinichi; Seyama, Michiko; Tanabe, Katsuhisa. "High-sensitivity urea sensor based on the composite film of electroinactive polypyrrole with polyion complex." Sensors and Actuators B: Chemical, vol. 36, pp. 463-469, 1996.

Peppas, N.A.; Keys, K.B.; Torres-Lugo, M; Lowman, A.M. "Poly (ethylene glycol)-containing hydrogels in drug delivery." Journal of Controlled Release, vol 62, pp. 81–87, 1999.

Rajesh; Bisht, Vandana; Takashima, Wataru; Kaneto, Keiichi. "An amperometric urea biosensor based on covalent immobilization of urease onto an electrochemically prepared copolymer poly (*N*-3-aminopropyl pyrrole-co-pyrrole) film." Biomaterials, vol. 26, pp. 3683-3690, 2005.

Roberts, M.J.; Bentley, M.D.; Harris, J.M. "Chemistry for peptide and protein PEGylation." Advanced Drug Delivery Reviews, vol. 54, pp. 459-476, 2002.

Sant, W.; Pourciel, M.L.; Launay, J.; Do Conto, T; Martinez, A.; Temple-Boyer, P. "Development of chemical field effect transistors for the detection of urea." Sensors and Actuators B: Chemical, vol. 95, pp. 309-314, 2003.

Scouten, William; Luong, John; Brown, R. "Enzyme or Protein Immobilization Techniques for Applications in Biosensor Design," TIBTECH, vol. 13, pp. 178-185, 1995.

Sheppard, N.F.; Mears, D.J.; Guiseppi-Elie, A. "Model of an immobilized enzyme conductimetric urea biosensor," Biosens. Bioelectron, vol. 11, pp. 967-979, 1995.

Solomans, T.W. Grahams. Organic Chemistry. New York, New York: John Wiley & Sons. 1988.

Suvarna, R. P.; Rao, K. R.; Subbarangaiah, K. "A Simple Technique for A.C. Conductivity Measurements." Bull. Mater. Sci., vol. 25, pp. 647-651, 2002.

Tozeren, Aydin; Byers, Stephen. New Biology for Engineers and Computer Scientists. Upper Saddle River, New Jersey: Pearson Education, Inc. 2004.

Trojanowicz, Marek. "Application of Conducting Polymers in Chemical Analysis." Microchima Acta, vol. 143, pp. 75-91, 2003.

Willner, Itamar; Katz, E. "Integration of Layered Redox Proteins and Conductive Supports for Bioelectronic Applications," Angew. Chem. Int. Ed, vol. 39, pp. 1180-1218, 2000.

Yoneyama, Kenji; Fujino, Yusuke; Osaka, Tetsuya; Satoh, Ikuo. "Amperometric sensing system for the detection of urea by a combination of the pH-stat method and flow injection analysis." Sensors and Actuators B: Chemical, vol. 76, pp. 152-157, 2001.

Zhang M, Li X. H, Gong Y. D, Zhao N. M, Zhang X. F. "Properties and biocompatibility of chitosan films modified by blending with PEG." Biomaterials, vol. 23, pp. 2641-2648, 2002.

APPENDIX A: Conceptual Schematics of Electrochemical Impedance Cells circuit

Each schematic below represents the circuit board layout and cell circuit during each step of the Urea Impedance BioAnalyzer. The Interrogation step contains four different sensor modes.

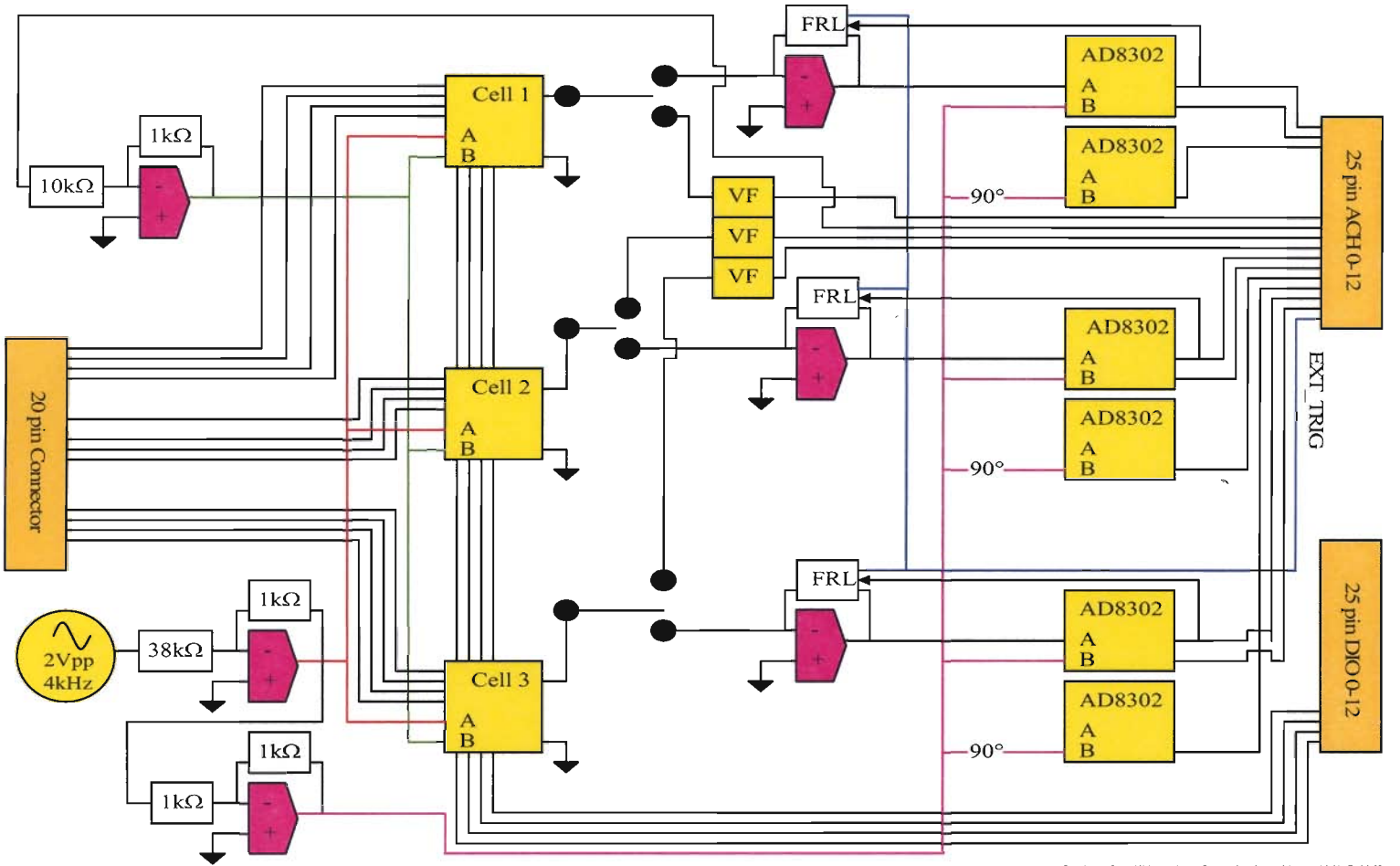

CIRCUIT BOARD LAYOUT

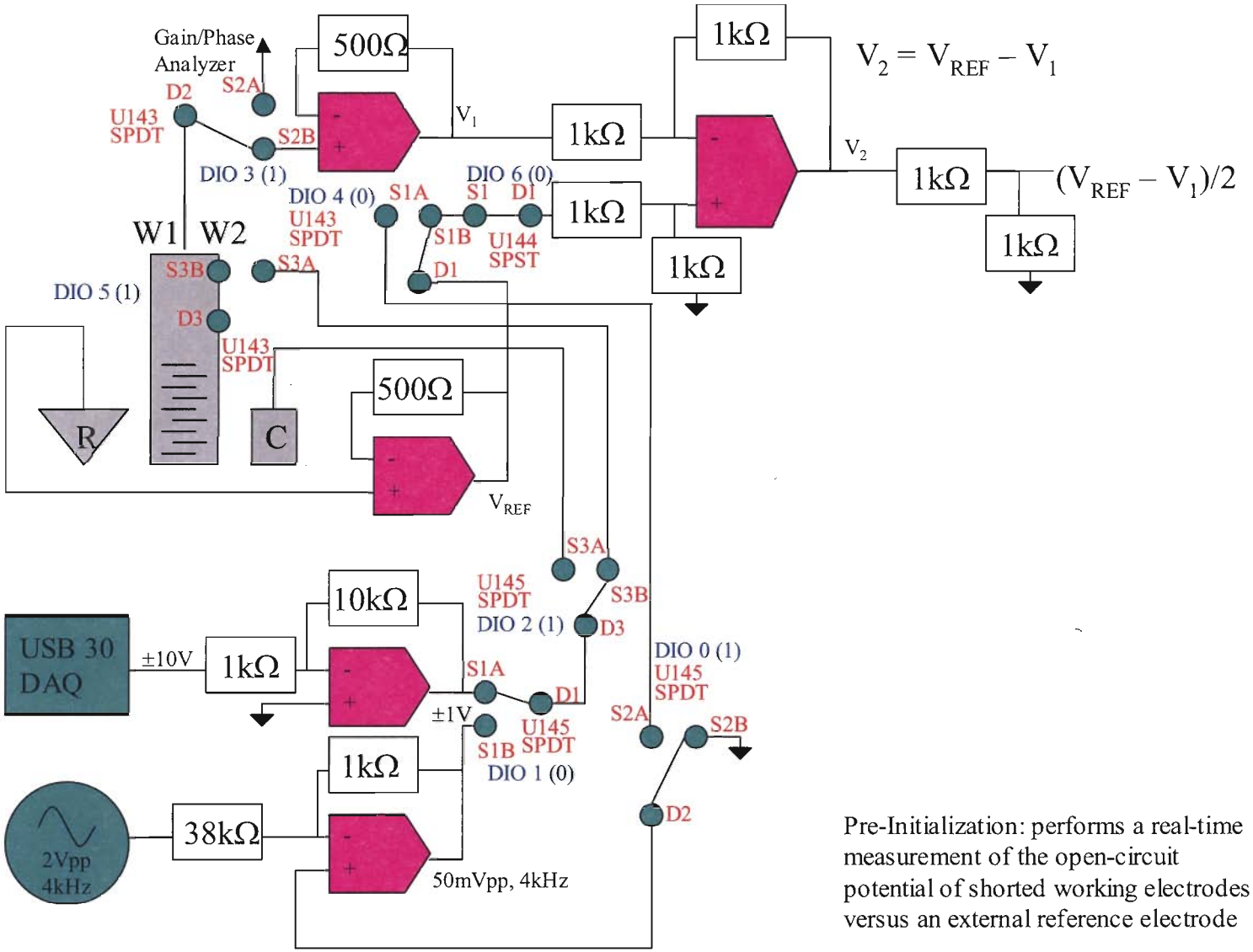

Pre-Initialization: performs a real-time measurement of the open-circuit potential of shorted working electrodes versus an external reference electrode

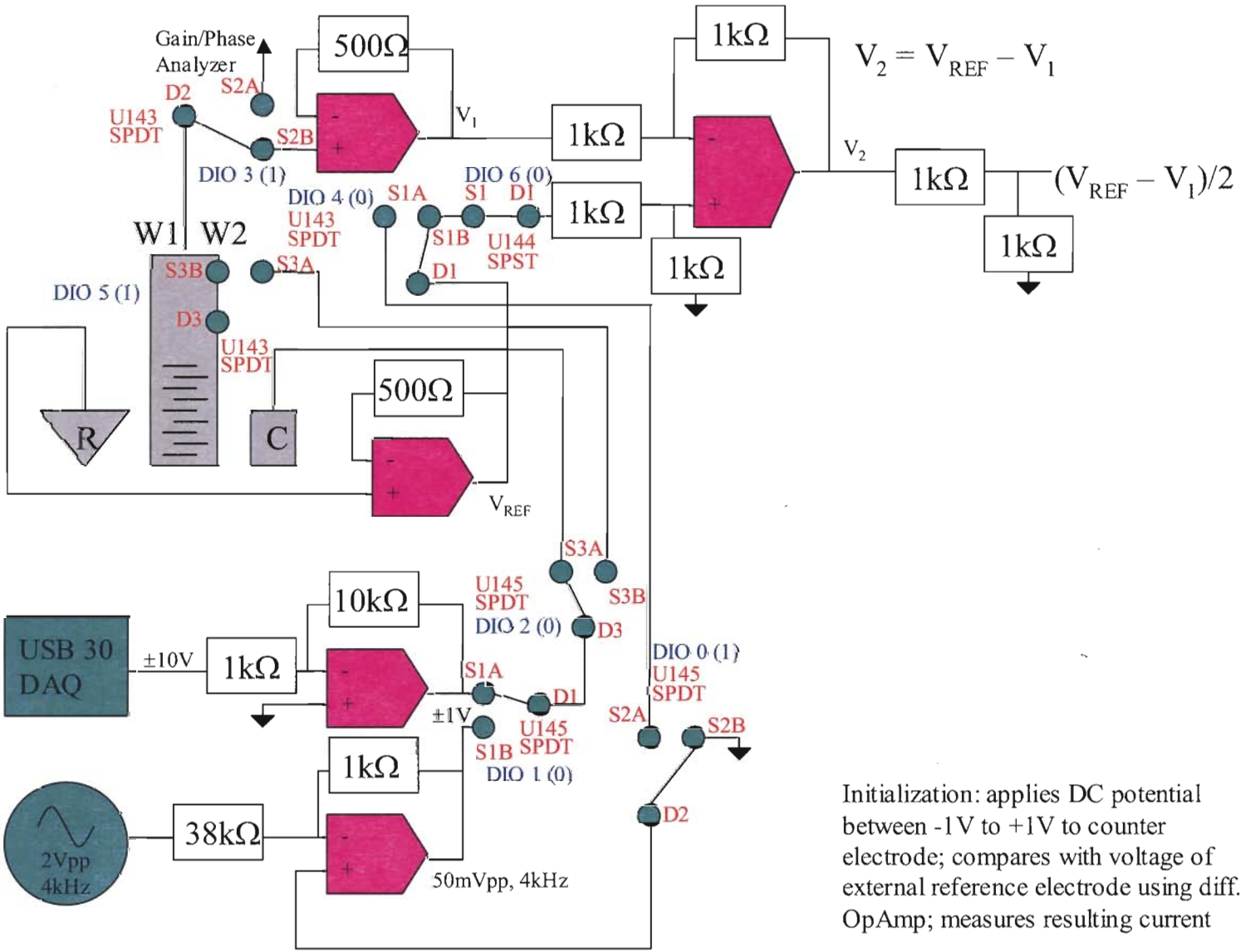

Initialization: applies DC potential between -1V to +1V to counter electrode; compares with voltage of external reference electrode using diff. OpAmp; measures resulting current

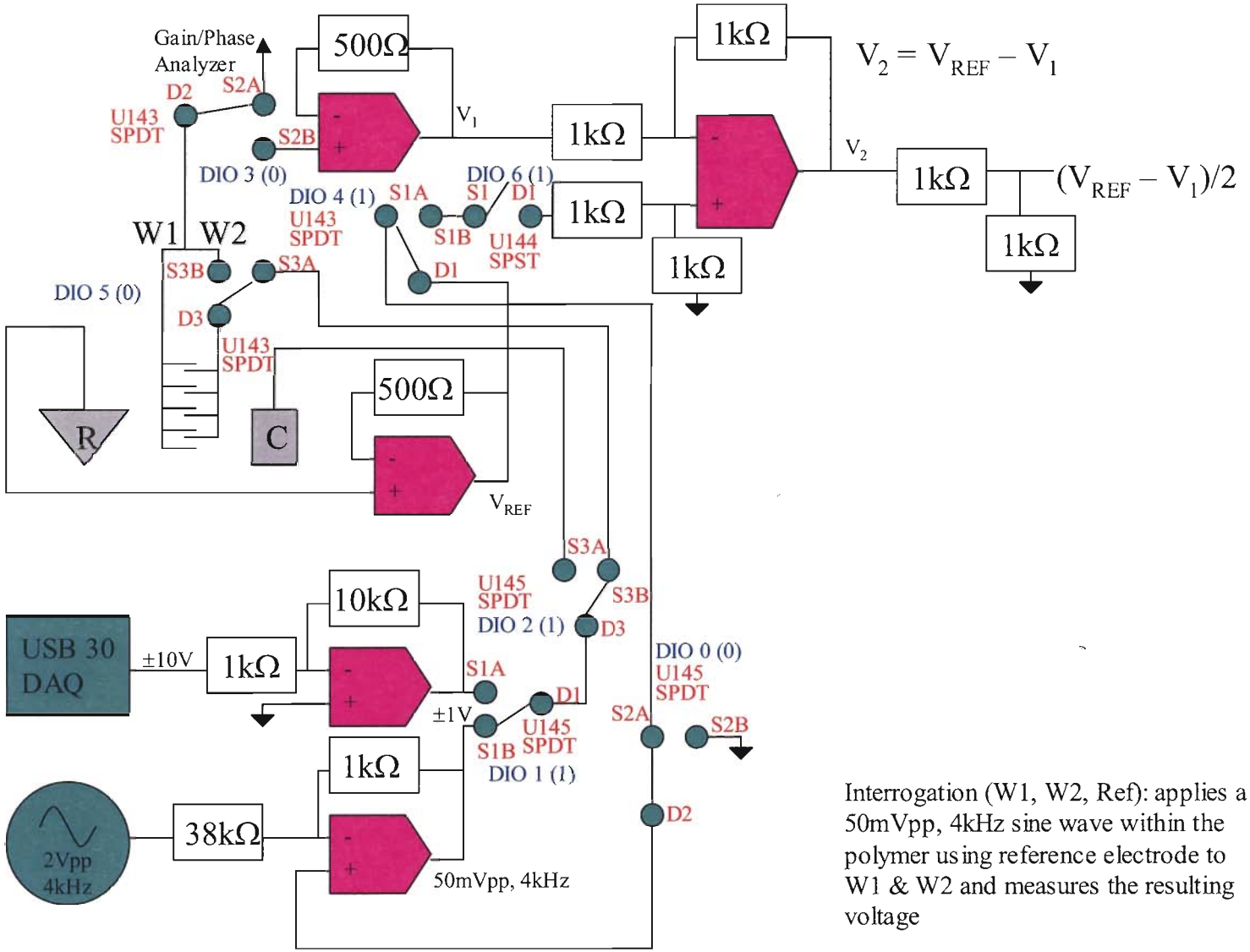

Interrogation (W1, W2, Ref): applies a 50mVpp, 4kHz sine wave within the polymer using reference electrode to W1 & W2 and measures the resulting voltage

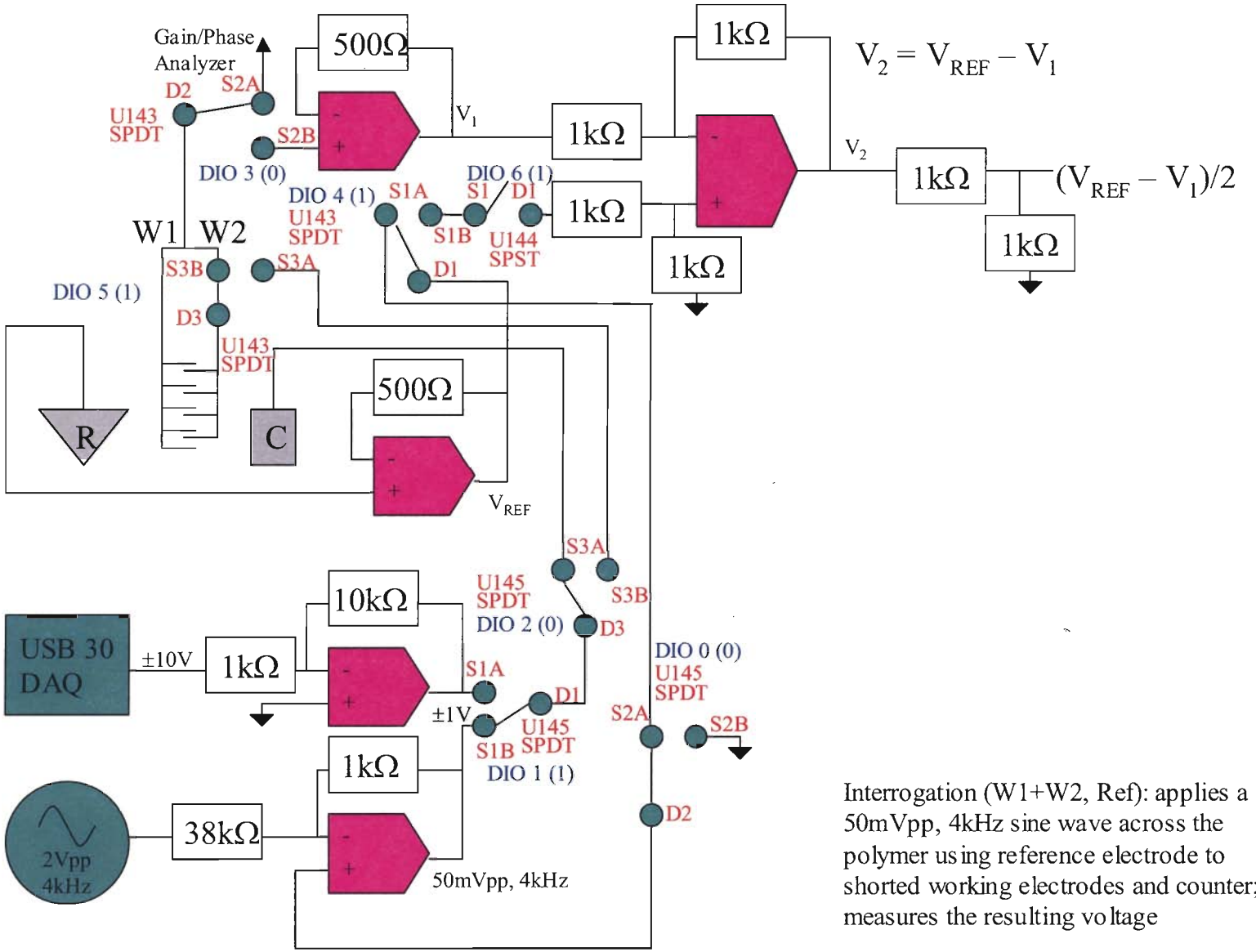

Interrogation (W1+W2, Ref): applies a 50mVpp, 4kHz sine wave across the polymer using reference electrode to shorted working electrodes and counter; measures the resulting voltage

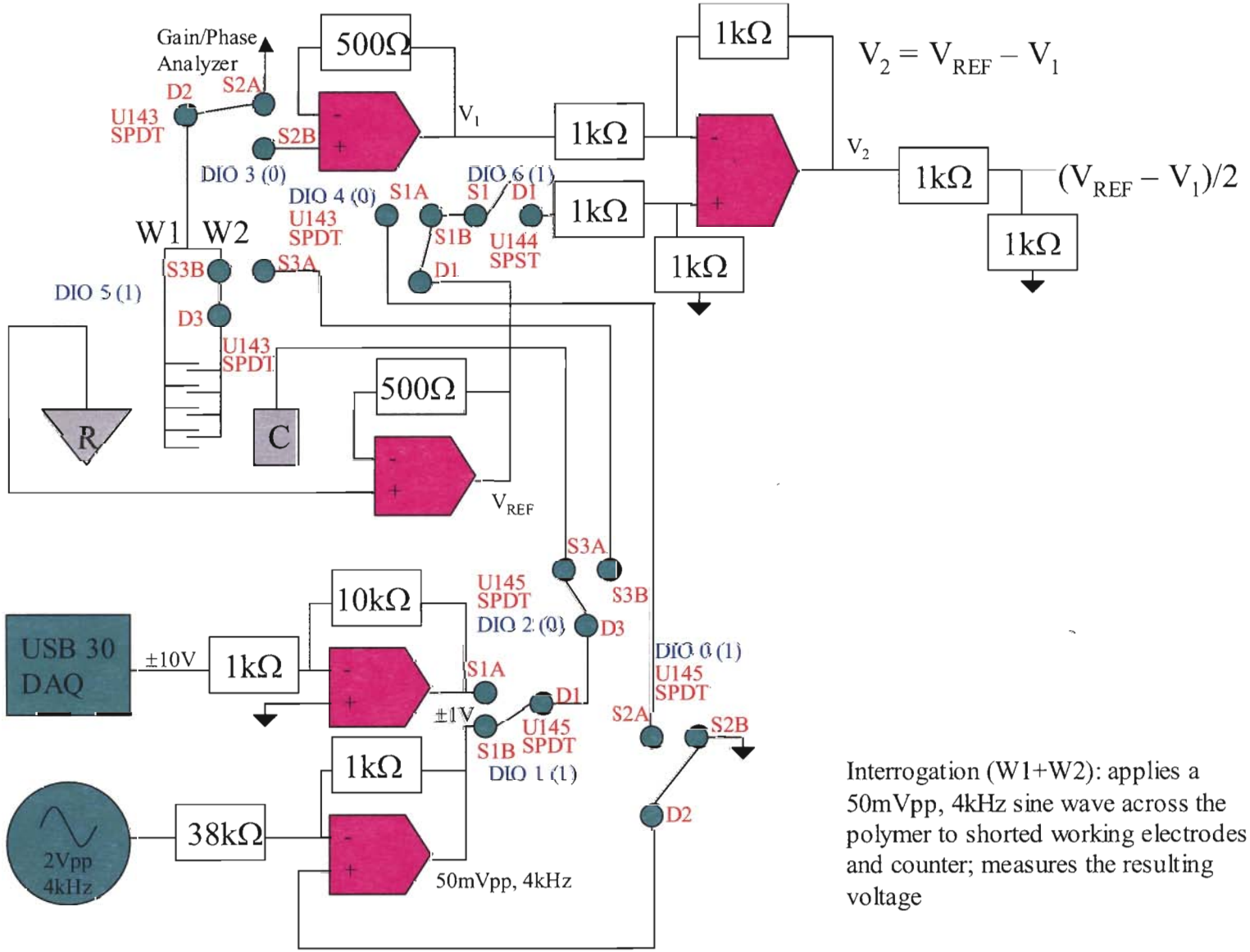

Interrogation (W1+W2): applies a 50mVpp, 4kHz sine wave across the polymer to shorted working electrodes and counter; measures the resulting voltage

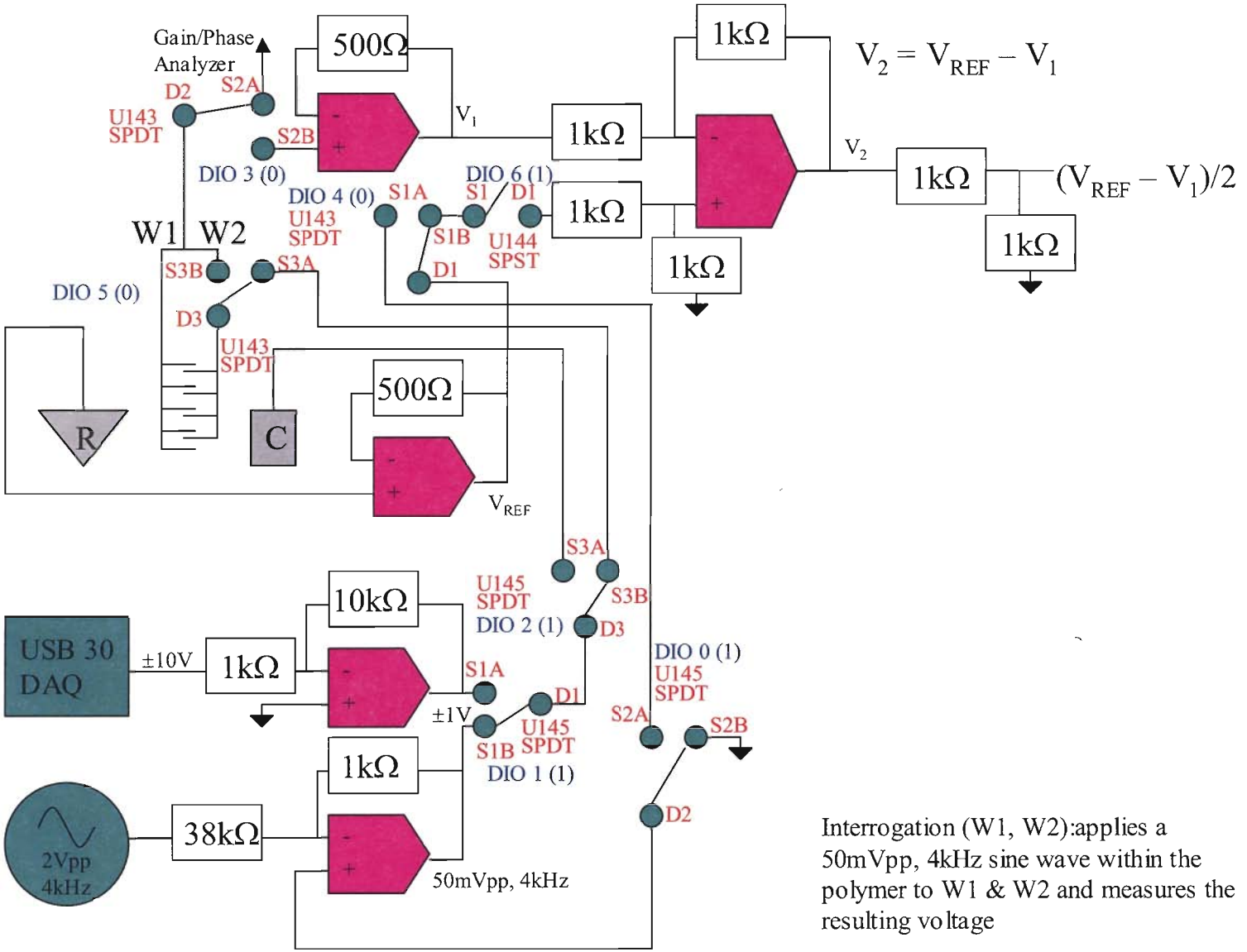

Interrogation (W1, W2):applies a 50mVpp, 4kHz sine wave within the polymer to W1 & W2 and measures the resulting voltage

APPENDIX B: OrCAD Schematics of Electrochemical Impedance BioAnalyzer Hardware

The following OrCAD schematics represent the circuit design for the Urea Impedance BioAnalyzer.

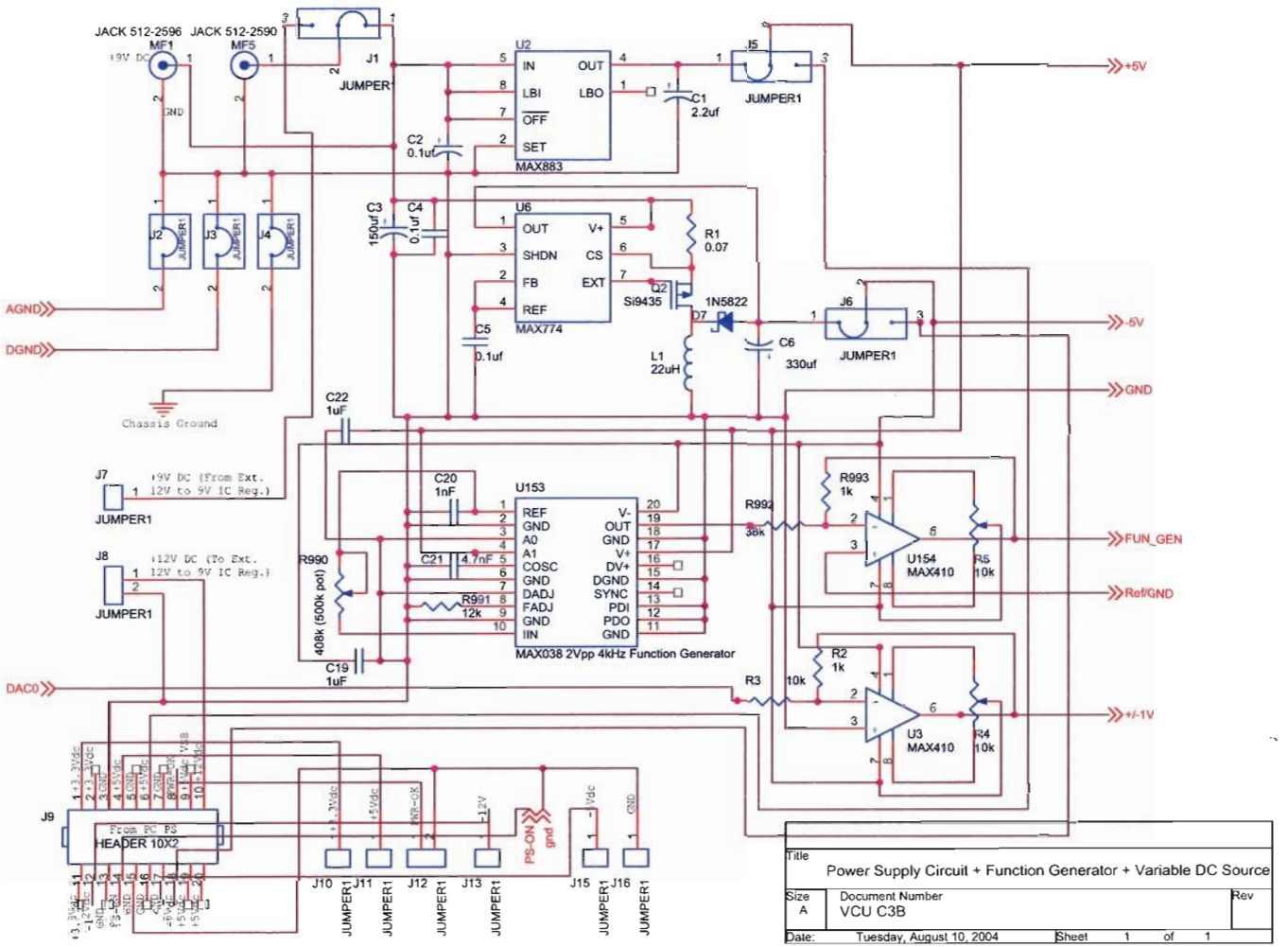
JACK 512-2596
JACK 512-2590
MF1
MF5
+9V DC
GND
J1
JUMPER1
U2
IN
OUT
LBI
LBO
OFF
SET
MAX883
C1
2.2uf
C2
0.1uf
J5
JUMPER1
+5V
C3
150uf
C4
0.1uf
U6
OUT
V+
SHDN
CS
FB
EXT
REF
MAX774
R1
0.07
Q2
Si9435
1N5822
D7
C5
0.1uf
L1
22uH
C6
330uf
J6
JUMPER1
-5V
GND
J2
J3
J4
JUMPER1
AGND
DGND
Chassis Ground
C22
1uF
J7
+9V DC (From Ext. 12V to 9V IC Reg.)
JUMPER1
J8
+12V DC (To Ext. 12V to 9V IC Reg.)
JUMPER1
C20
1nF
U153
REF
GND
A0
A1
COSC
GND
DADJ
FADJ
GND
IIN
V-
OUT
GND
V+
DV+
DGND
SYNC
PDI
PDO
GND
MAX038 2Vpp 4kHz Function Generator
C21
4.7nF
R991
12k
R990
408k (500k pot)
C19
1uF
R992
38k
R993
1k
U154
MAX410
R5
10k
FUN_GEN
Ref/GND
R2
1k
R3
10k
U3
MAX410
R4
10k
+/-1V
DAC0
J9
HEADER 10X2
J10
J11
J12
J13
J15
J16
JUMPER1
PS-ON
gnd
Title
Power Supply Circuit + Function Generator + Variable DC Source
Size
A
Document Number
VCU C3B
Rev
Date:
Tuesday, August 10, 2004
Sheet
1
of
1

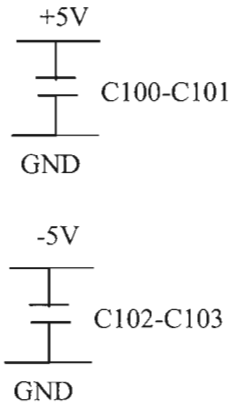
+5V
C100-C101
GND
-5V
C102-C103
GND

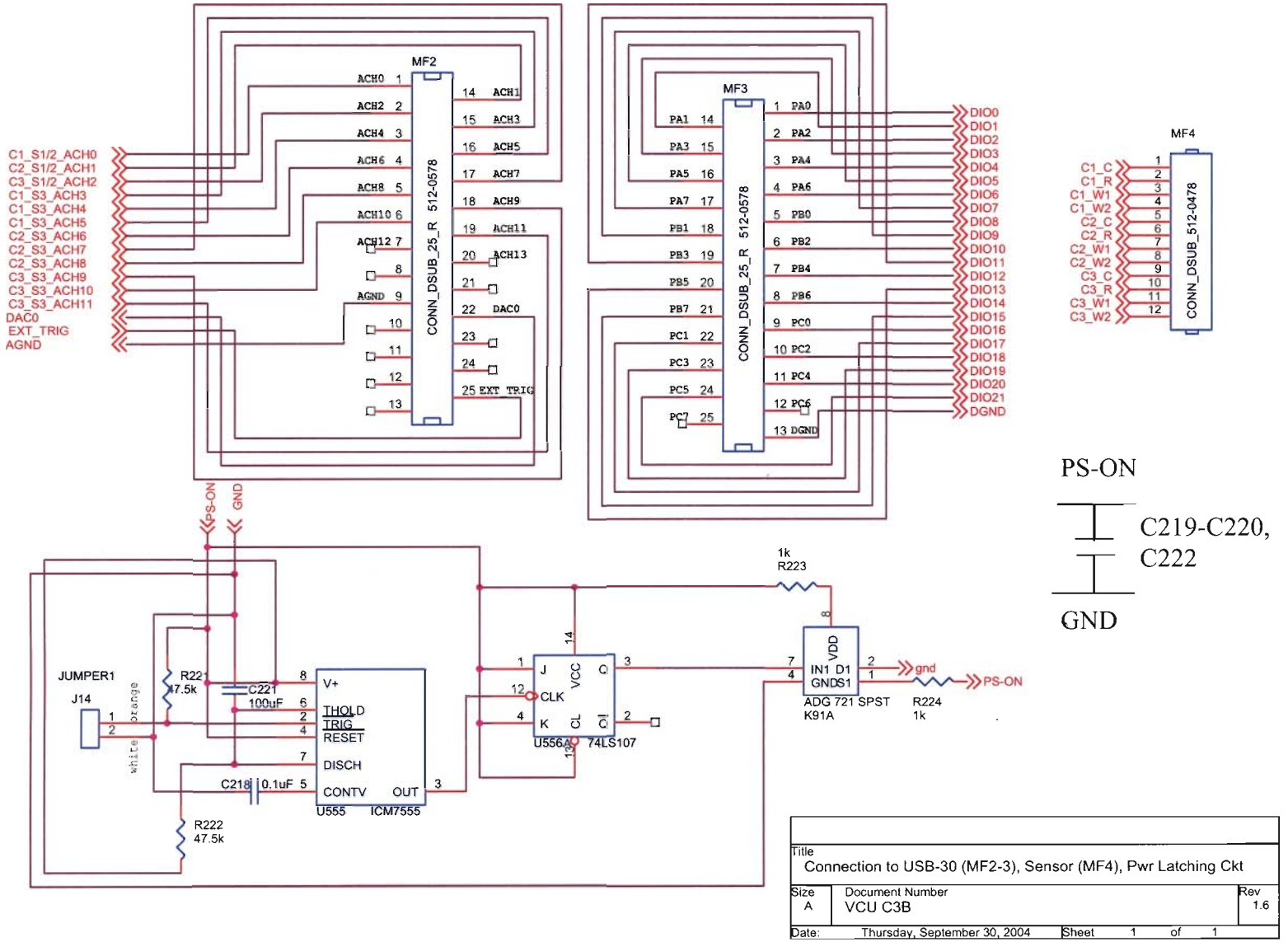

Title	Connection to USB-30 (MF2-3), Sensor (MF4), Pwr Latching Ckt	
Size A	Document Number VCU C3B	Rev 1.6
Date: Thursday, September 30, 2004	Sheet 1 of 1	

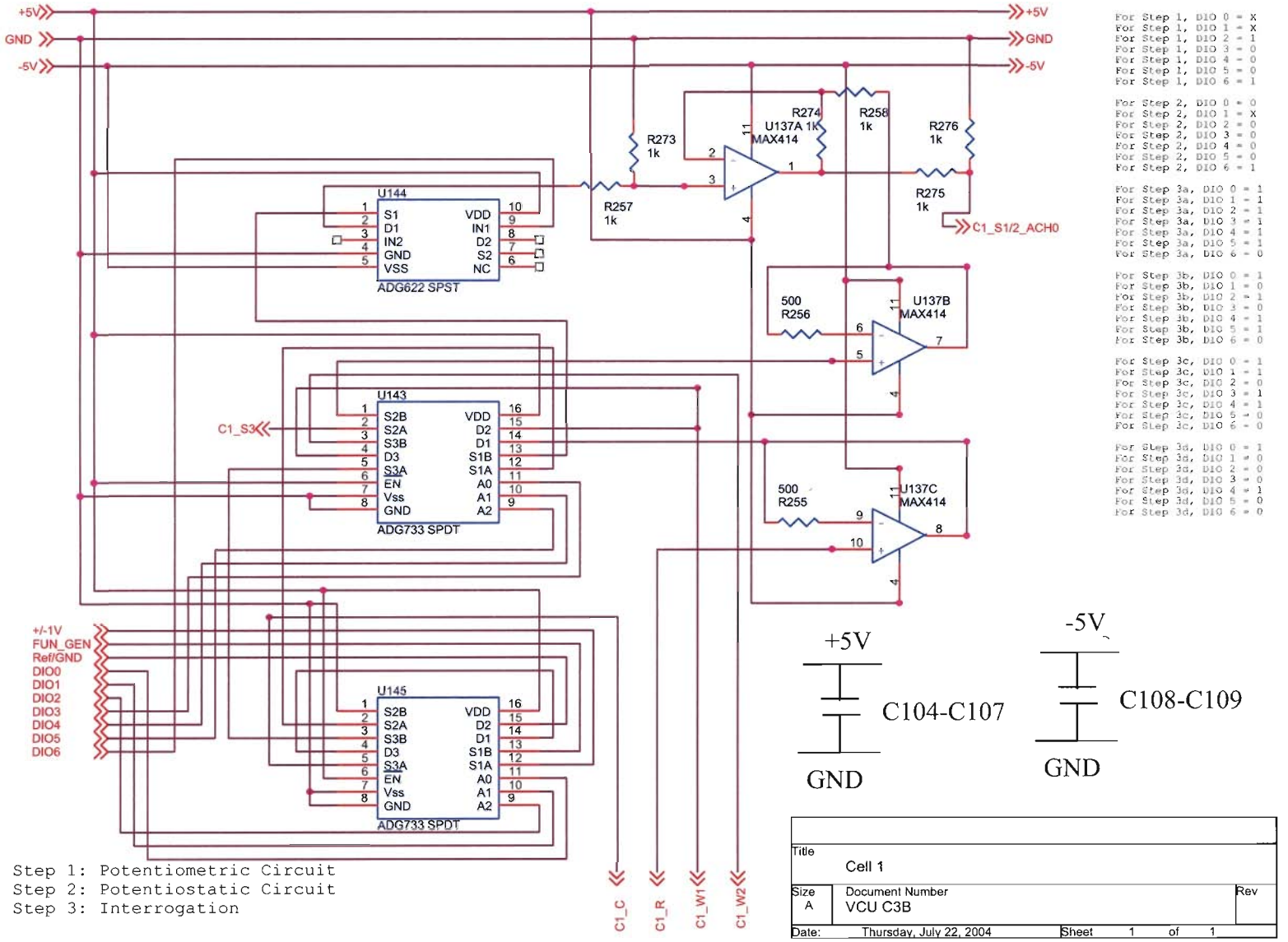


```
For Step 1, DIO 0 = X
For Step 1, DIO 1 = X
For Step 1, DIO 2 = 1
For Step 1, DIO 3 = 0
For Step 1, DIO 4 = 0
For Step 1, DIO 5 = 0
For Step 1, DIO 6 = 1

For Step 2, DIO 0 = 0
For Step 2, DIO 1 = X
For Step 2, DIO 2 = 0
For Step 2, DIO 3 = 0
For Step 2, DIO 4 = 0
For Step 2, DIO 5 = 0
For Step 2, DIO 6 = 1

For Step 3a, DIO 0 = 1
For Step 3a, DIO 1 = 1
For Step 3a, DIO 2 = 1
For Step 3a, DIO 3 = 1
For Step 3a, DIO 4 = 1
For Step 3a, DIO 5 = 1
For Step 3a, DIO 6 = 0

For Step 3b, DIO 0 = 1
For Step 3b, DIO 1 = 0
For Step 3b, DIO 2 = 1
For Step 3b, DIO 3 = 0
For Step 3b, DIO 4 = 1
For Step 3b, DIO 5 = 1
For Step 3b, DIO 6 = 0

For Step 3c, DIO 0 = 1
For Step 3c, DIO 1 = 1
For Step 3c, DIO 2 = 0
For Step 3c, DIO 3 = 1
For Step 3c, DIO 4 = 1
For Step 3c, DIO 5 = 0
For Step 3c, DIO 6 = 0

For Step 3d, DIO 0 = 1
For Step 3d, DIO 1 = 0
For Step 3d, DIO 2 = 0
For Step 3d, DIO 3 = 0
For Step 3d, DIO 4 = 1
For Step 3d, DIO 5 = 0
For Step 3d, DIO 6 = 0
```

Step 1: Potentiometric Circuit
Step 2: Potentiostatic Circuit
Step 3: Interrogation

Title: Cell 1		
Size: A	Document Number: VCU C3B	Rev:
Date: Thursday, July 22, 2004	Sheet 1 of 1	

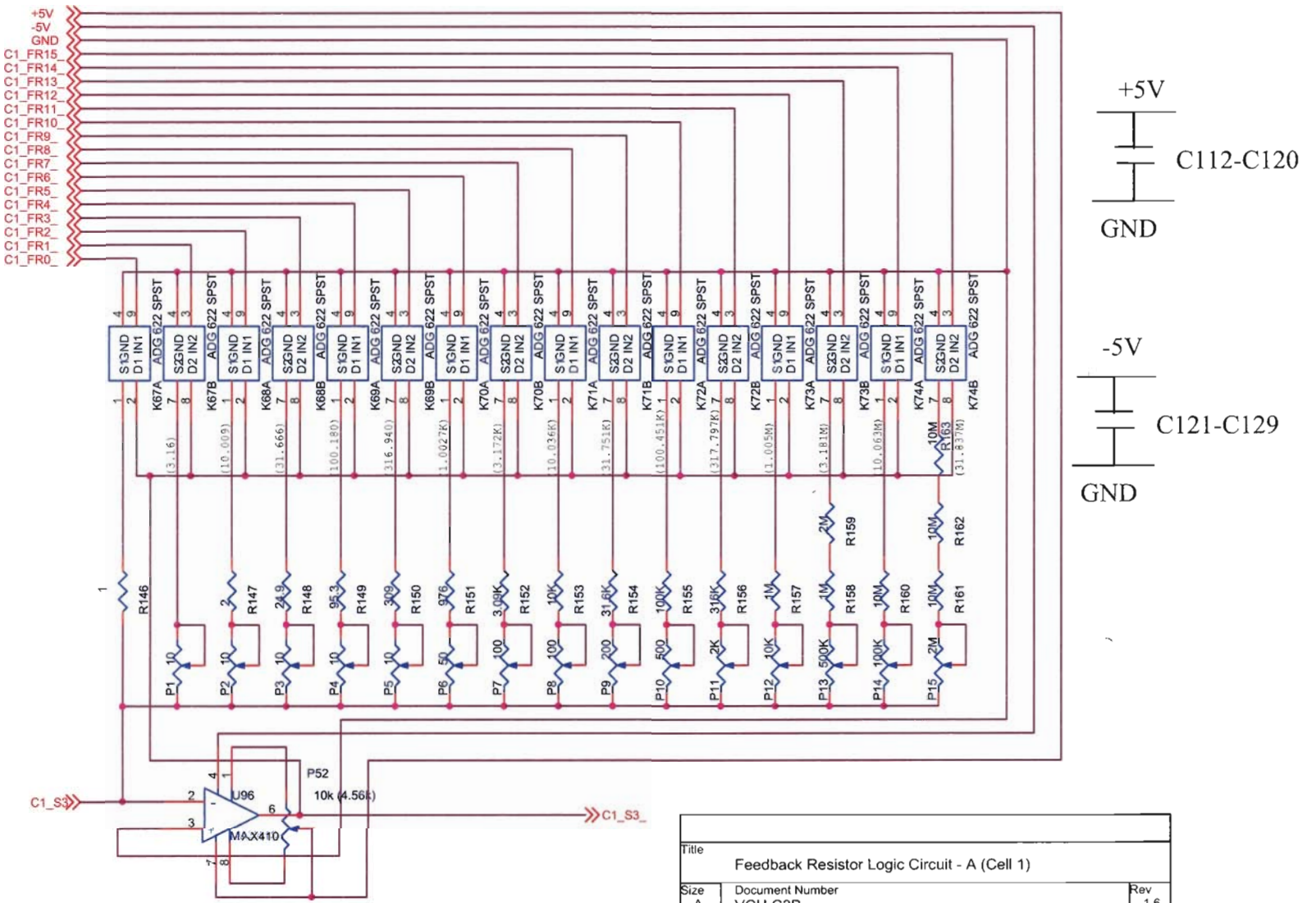

Title	Feedback Resistor Logic Circuit - A (Cell 1)	
Size A	Document Number VCU C3B	Rev 1.6
Date: Thursday, September 30, 2004	Sheet 1 of 26	

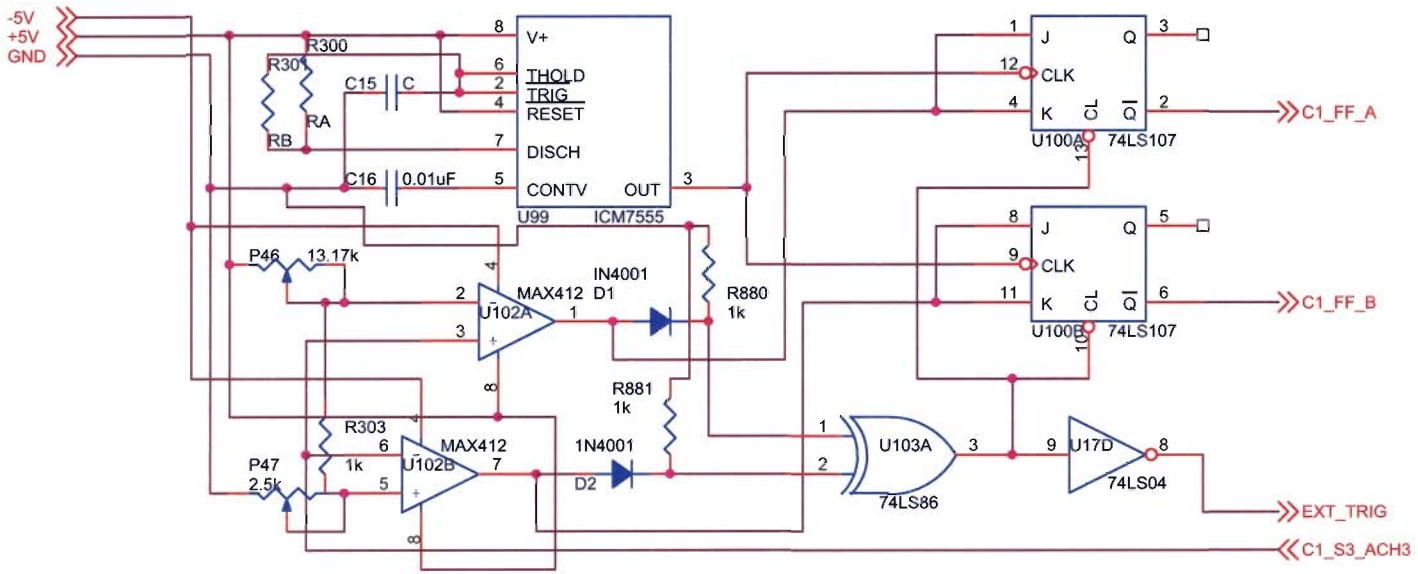

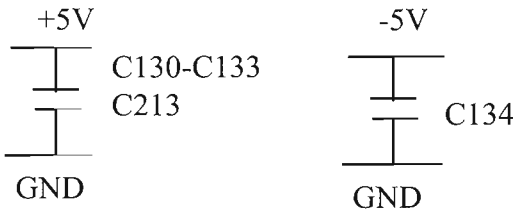

Title: Feedback Resistor Logic Circuit - B (Cell 1)			
Size: A	Document Number: VCU C3B		Rev
Date: Thursday, July 22, 2004	Sheet 25 of 26		

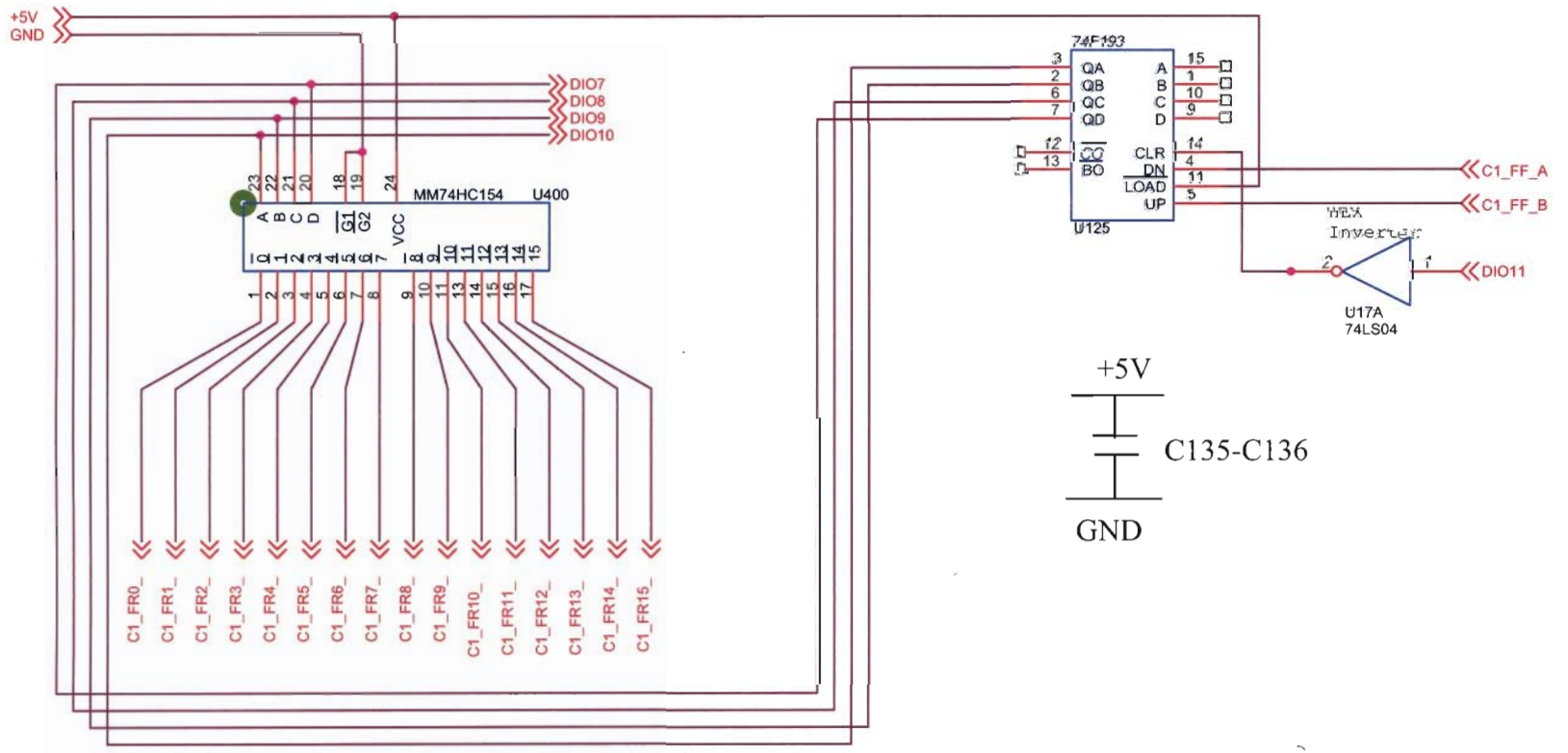

Title	Feedback Resistor Logic Circuit - C (Cell 1)		
Size A	Document Number VCU C3B		Rev
Date: Thursday, July 22, 2004		Sheet 23 of 26	

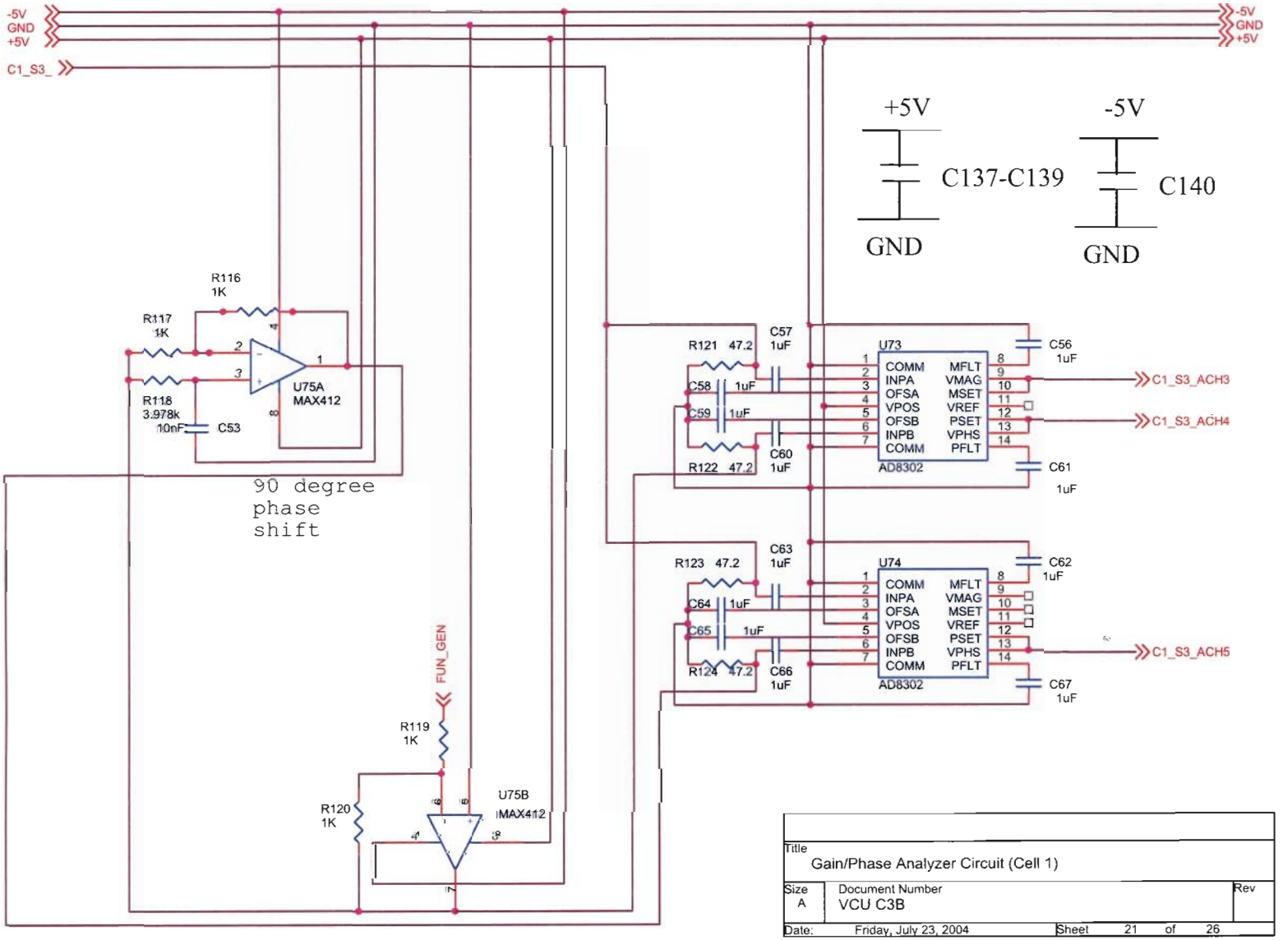

Title: Gain/Phase Analyzer Circuit (Cell 1)		
Size: A	Document Number: VCU C3B	Rev
Date: Friday, July 23, 2004	Sheet 21 of 26	

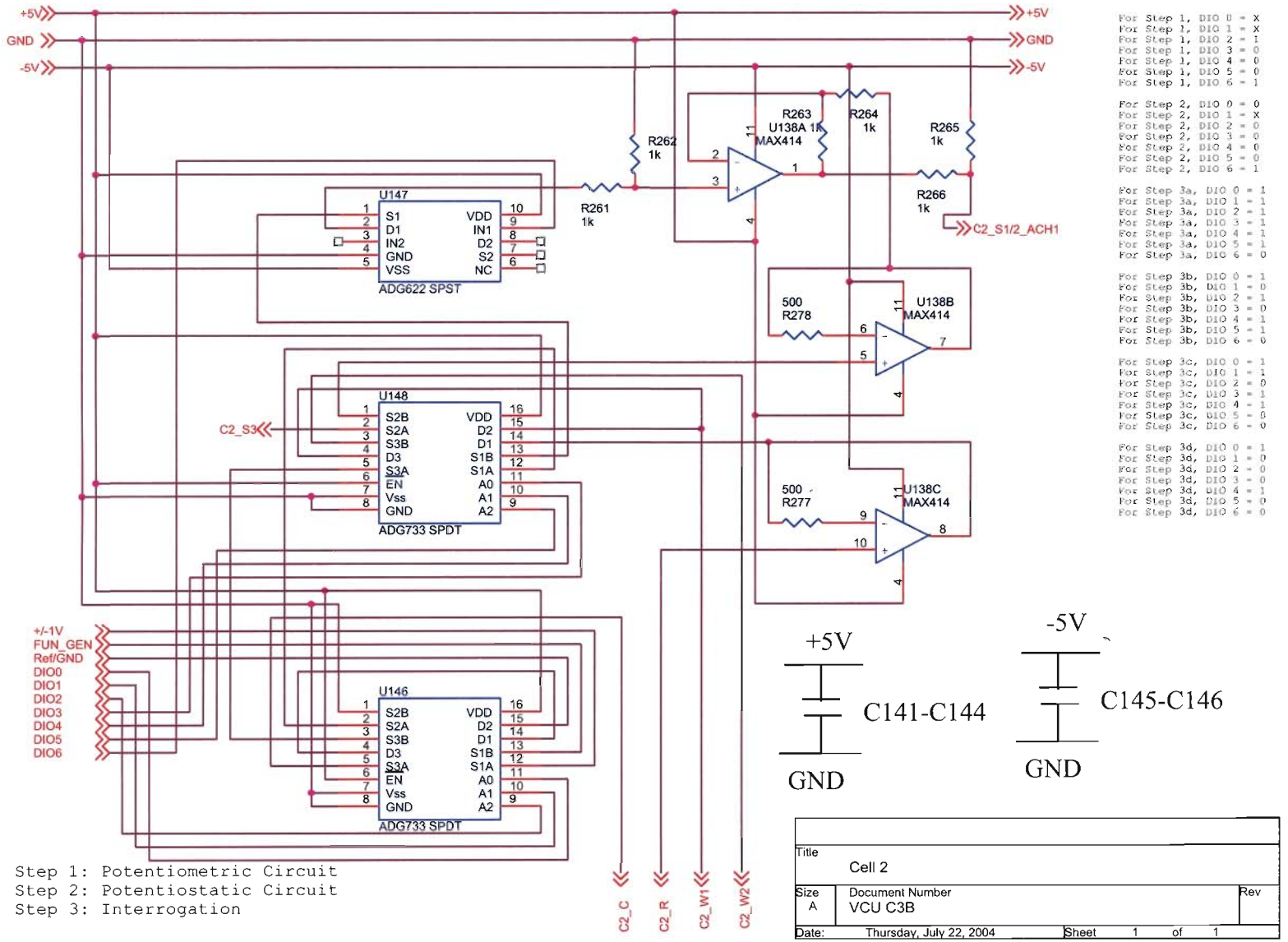


```
For Step 1, DIO 0 = X
For Step 1, DIO 1 = X
For Step 1, DIO 2 = 1
For Step 1, DIO 3 = 0
For Step 1, DIO 4 = 0
For Step 1, DIO 5 = 0
For Step 1, DIO 6 = 1

For Step 2, DIO 0 = 0
For Step 2, DIO 1 = X
For Step 2, DIO 2 = 0
For Step 2, DIO 3 = 0
For Step 2, DIO 4 = 0
For Step 2, DIO 5 = 0
For Step 2, DIO 6 = 1

For Step 3a, DIO 0 = 1
For Step 3a, DIO 1 = 1
For Step 3a, DIO 2 = 1
For Step 3a, DIO 3 = 1
For Step 3a, DIO 4 = 1
For Step 3a, DIO 5 = 1
For Step 3a, DIO 6 = 0

For Step 3b, DIO 0 = 1
For Step 3b, DIO 1 = 0
For Step 3b, DIO 2 = 1
For Step 3b, DIO 3 = 0
For Step 3b, DIO 4 = 1
For Step 3b, DIO 5 = 1
For Step 3b, DIO 6 = 0

For Step 3c, DIO 0 = 1
For Step 3c, DIO 1 = 1
For Step 3c, DIO 2 = 0
For Step 3c, DIO 3 = 1
For Step 3c, DIO 4 = 1
For Step 3c, DIO 5 = 0
For Step 3c, DIO 6 = 0

For Step 3d, DIO 0 = 1
For Step 3d, DIO 1 = 0
For Step 3d, DIO 2 = 0
For Step 3d, DIO 3 = 0
For Step 3d, DIO 4 = 1
For Step 3d, DIO 5 = 0
For Step 3d, DIO 6 = 0
```

Step 1: Potentiometric Circuit
Step 2: Potentiostatic Circuit
Step 3: Interrogation

Title: Cell 2		
Size: A	Document Number: VCU C3B	Rev
Date: Thursday, July 22, 2004	Sheet 1 of 1	

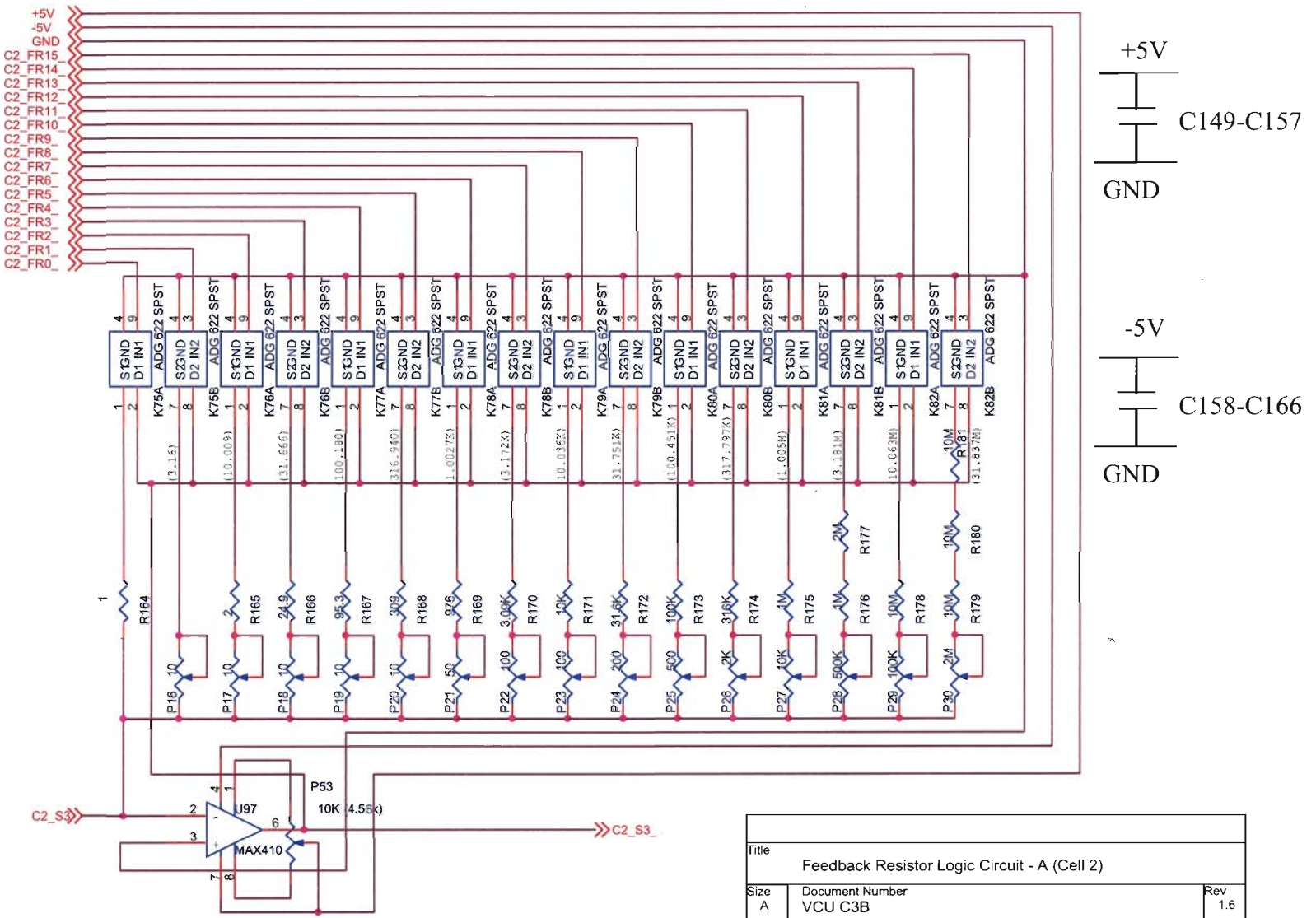

Title	Feedback Resistor Logic Circuit - A (Cell 2)	
Size A	Document Number VCU C3B	Rev 1.6
Date: Thursday, September 30, 2004	Sheet 1 of 26	

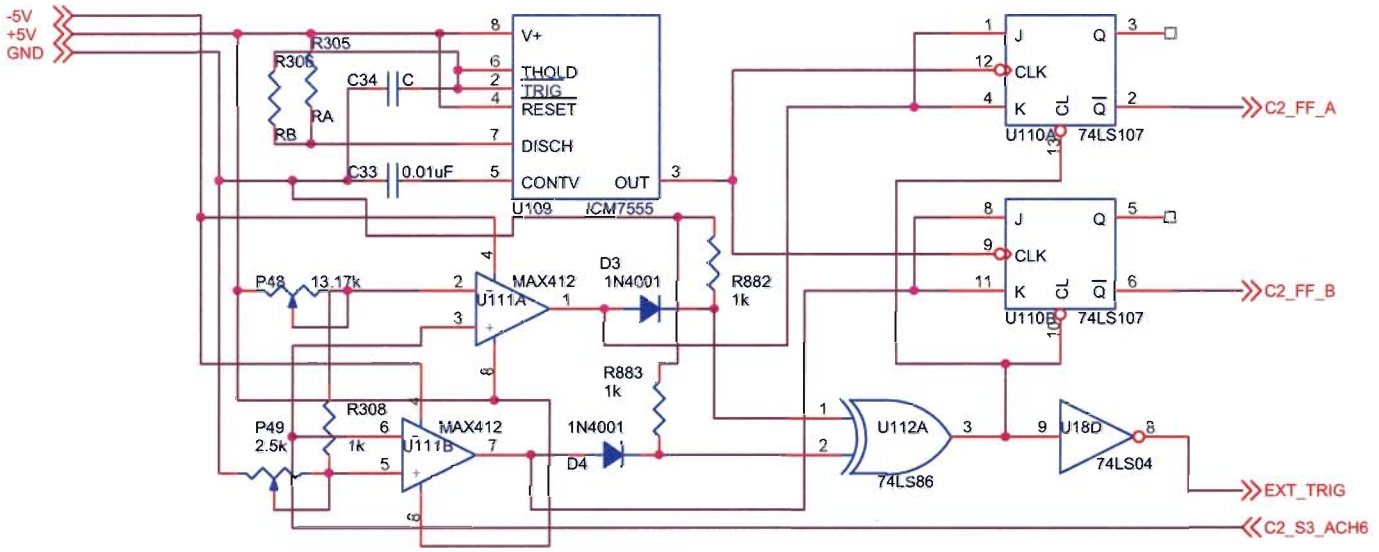

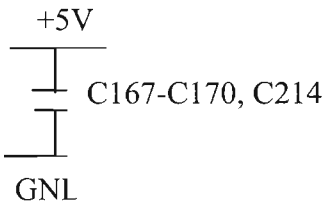

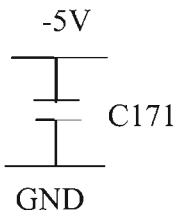

Title: Feedback Resistor Logic Circuit - B (Cell 2)		
Size: A	Document Number: VCU C3B	Rev
Date: Thursday, July 22, 2004	Sheet 25 of 26	

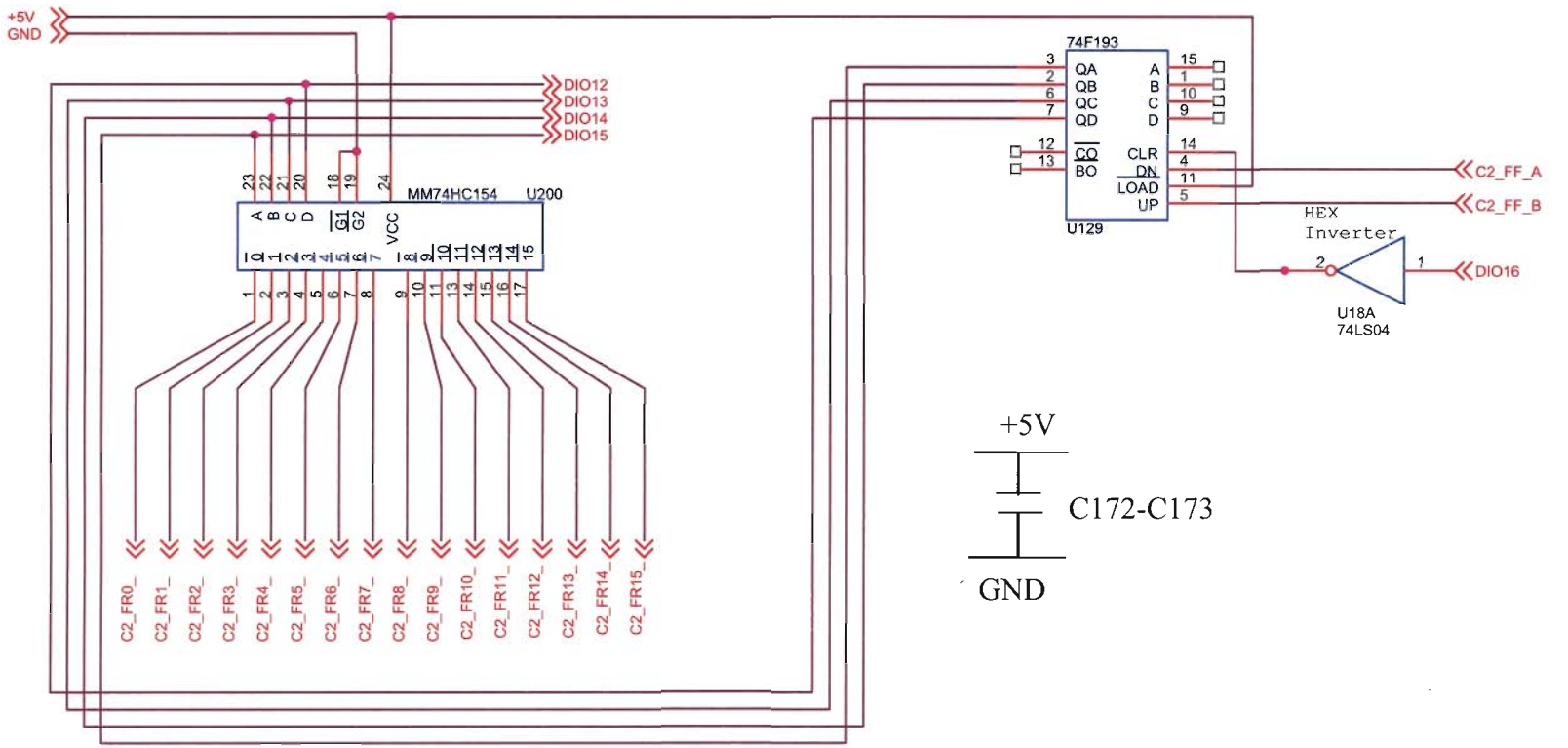

Title	Feedback Resistor Logic Circuit - C (Cell 2)		
Size A	Document Number VCU C3B		Rev
Date: Thursday, July 22, 2004		Sheet 23 of 26	

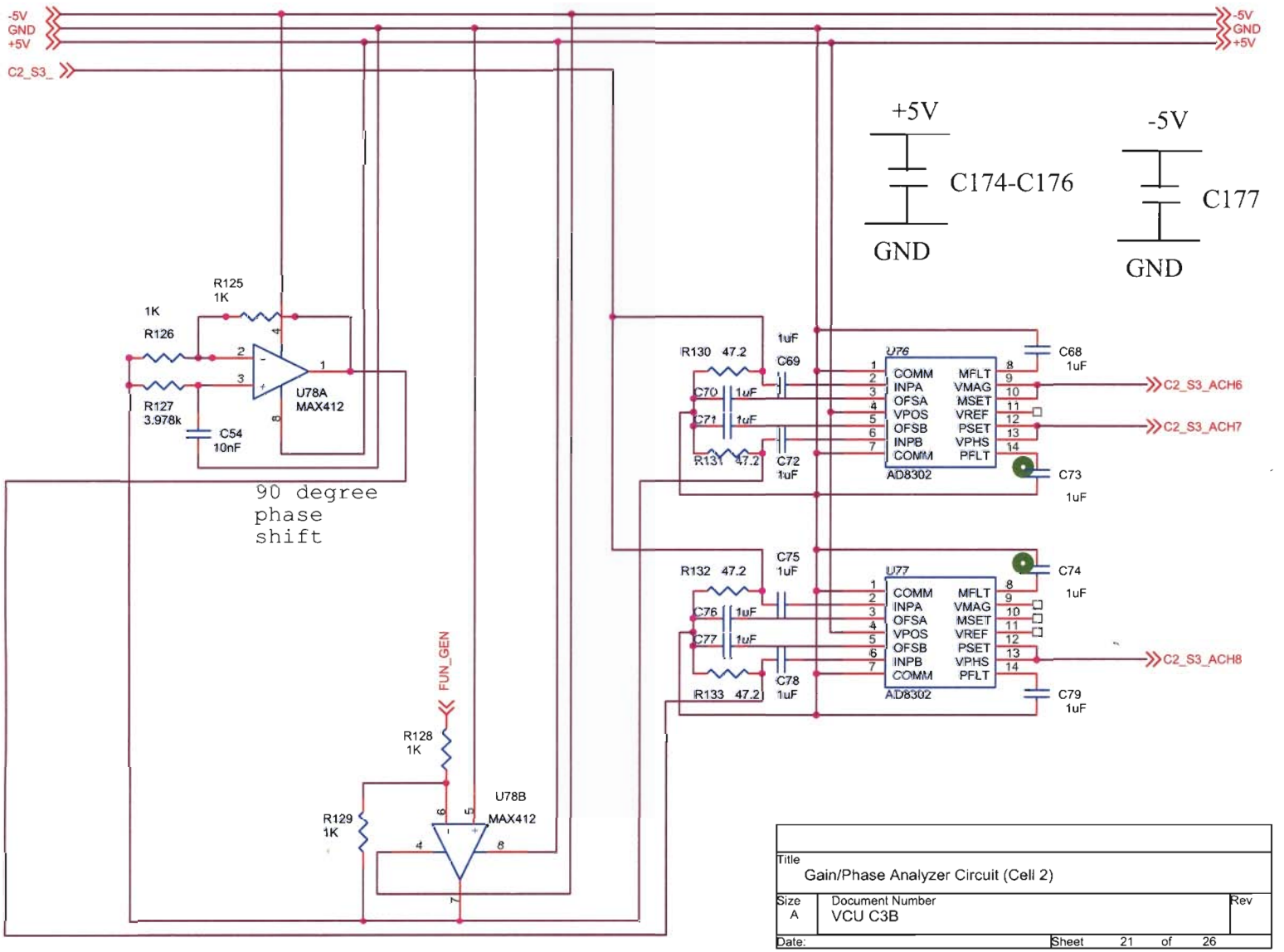
-5V
GND
+5V
C2_S3_
+5V
C174-C176
GND
-5V
C177
GND
R125
1K
1K
R126
R127
3.978k
C54
10nF
U78A
MAX412
90 degree
phase
shift
R130 47.2
C69
1uF
C70 1uF
C71 1uF
R131 47.2
C72
1uF
U76
COMM
INPA
OFSA
VPOS
OFSB
INPB
COMM
MFLT
VMAG
MSET
VREF
PSET
VPHS
PFLT
AD8302
C68
1uF
C73
1uF
C2_S3_ACH6
C2_S3_ACH7
R132 47.2
C75
1uF
C76 1uF
C77 1uF
R133 47.2
C78
1uF
U77
AD8302
C74
1uF
C79
1uF
C2_S3_ACH8
FUN_GEN
R128
1K
R129
1K
U78B
MAX412
Title
Gain/Phase Analyzer Circuit (Cell 2)
Size
A
Document Number
VCU C3B
Rev
Date:
Sheet 21 of 26

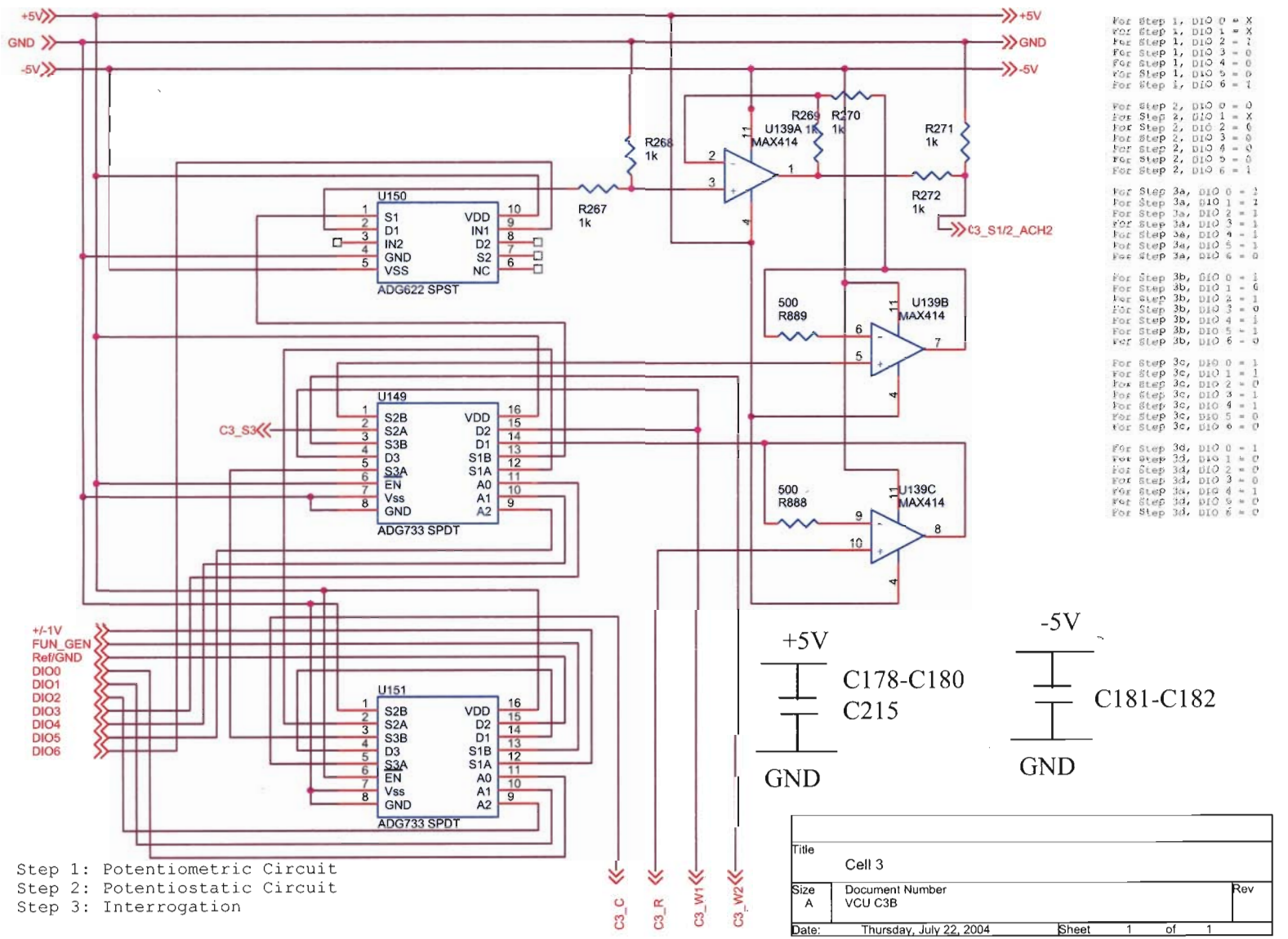


```
For Step 1, DIO 0 = X
For Step 1, DIO 1 = X
For Step 1, DIO 2 = 1
For Step 1, DIO 3 = 0
For Step 1, DIO 4 = 0
For Step 1, DIO 5 = 0
For Step 1, DIO 6 = 1

For Step 2, DIO 0 = 0
For Step 2, DIO 1 = X
For Step 2, DIO 2 = 0
For Step 2, DIO 3 = 0
For Step 2, DIO 4 = 0
For Step 2, DIO 5 = 0
For Step 2, DIO 6 = 1

For Step 3a, DIO 0 = 1
For Step 3a, DIO 1 = 1
For Step 3a, DIO 2 = 1
For Step 3a, DIO 3 = 1
For Step 3a, DIO 4 = 1
For Step 3a, DIO 5 = 1
For Step 3a, DIO 6 = 0

For Step 3b, DIO 0 = 1
For Step 3b, DIO 1 = 0
For Step 3b, DIO 2 = 1
For Step 3b, DIO 3 = 0
For Step 3b, DIO 4 = 1
For Step 3b, DIO 5 = 1
For Step 3b, DIO 6 = 0

For Step 3c, DIO 0 = 1
For Step 3c, DIO 1 = 1
For Step 3c, DIO 2 = 0
For Step 3c, DIO 3 = 1
For Step 3c, DIO 4 = 1
For Step 3c, DIO 5 = 0
For Step 3c, DIO 6 = 0

For Step 3d, DIO 0 = 1
For Step 3d, DIO 1 = 0
For Step 3d, DIO 2 = 0
For Step 3d, DIO 3 = 0
For Step 3d, DIO 4 = 1
For Step 3d, DIO 5 = 0
For Step 3d, DIO 6 = 0
```

Step 1: Potentiometric Circuit
Step 2: Potentiostatic Circuit
Step 3: Interrogation

Title	Cell 3	
Size A	Document Number VCU C3B	Rev
Date: Thursday, July 22, 2004	Sheet 1 of 1	

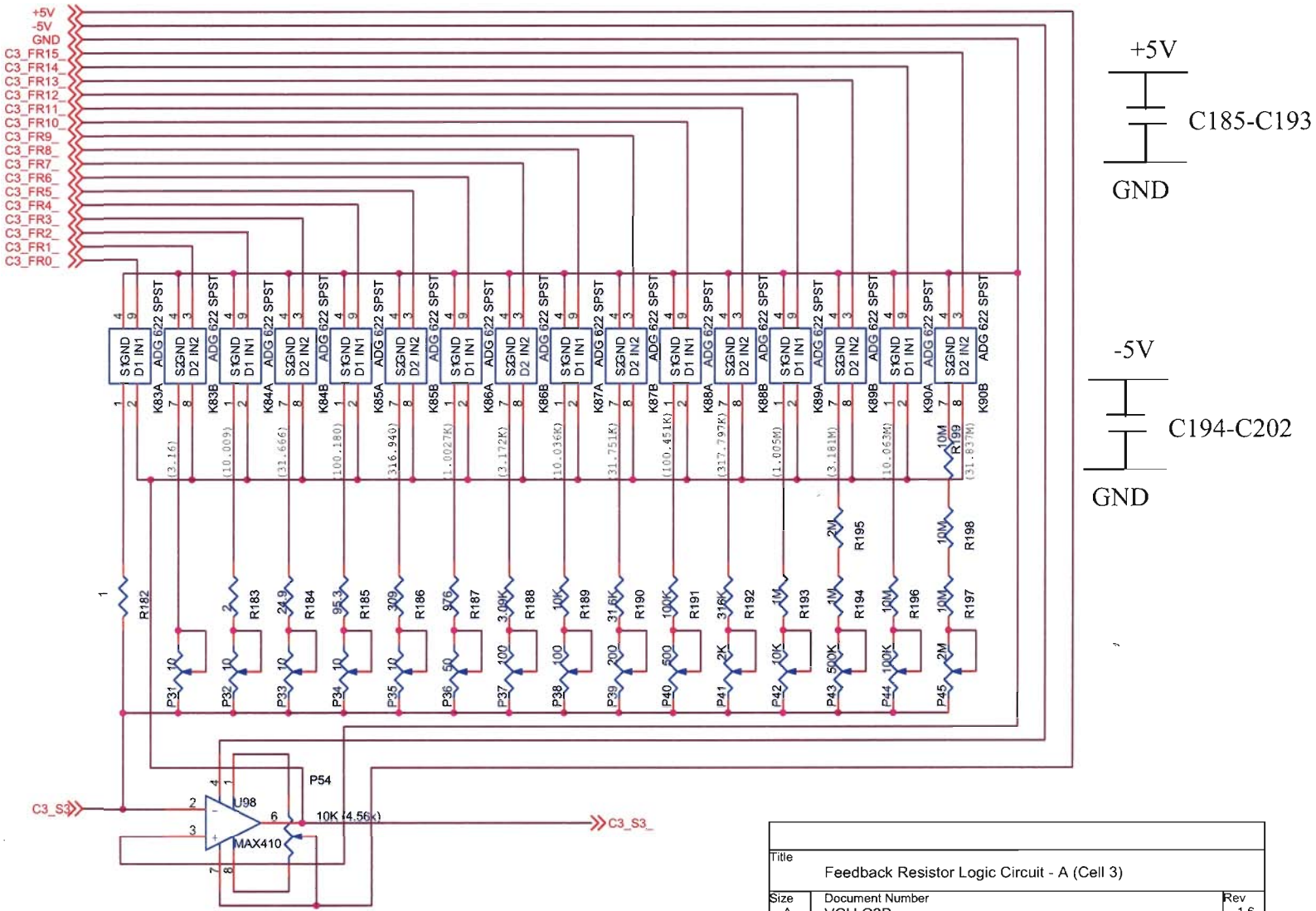
+5V
-5V
GND
C3_FR15_
C3_FR14_
C3_FR13_
C3_FR12_
C3_FR11_
C3_FR10_
C3_FR9_
C3_FR8_
C3_FR7_
C3_FR6_
C3_FR5_
C3_FR4_
C3_FR3_
C3_FR2_
C3_FR1_
C3_FR0_
S1GND D1 IN1 ADG 622 SPST S2GND D2 IN2
K83A K83B K84A K84B K85A K85B K86A K86B K87A K87B K88A K88B K89A K89B K90A K90B
R182 R183 R184 R185 R186 R187 R188 R189 R190 R191 R192 R193 R194 R195 R196 R197 R198 R199
P31 P32 P33 P34 P35 P36 P37 P38 P39 P40 P41 P42 P43 P44 P45
P54
U98
MAX410
C3_S3
C3_S3_
+5V
C185-C193
GND
-5V
C194-C202
GND
Title
Feedback Resistor Logic Circuit - A (Cell 3)
Size A
Document Number VCU C3B
Rev 1.6
Date: Thursday, September 30, 2004
Sheet 1 of 26

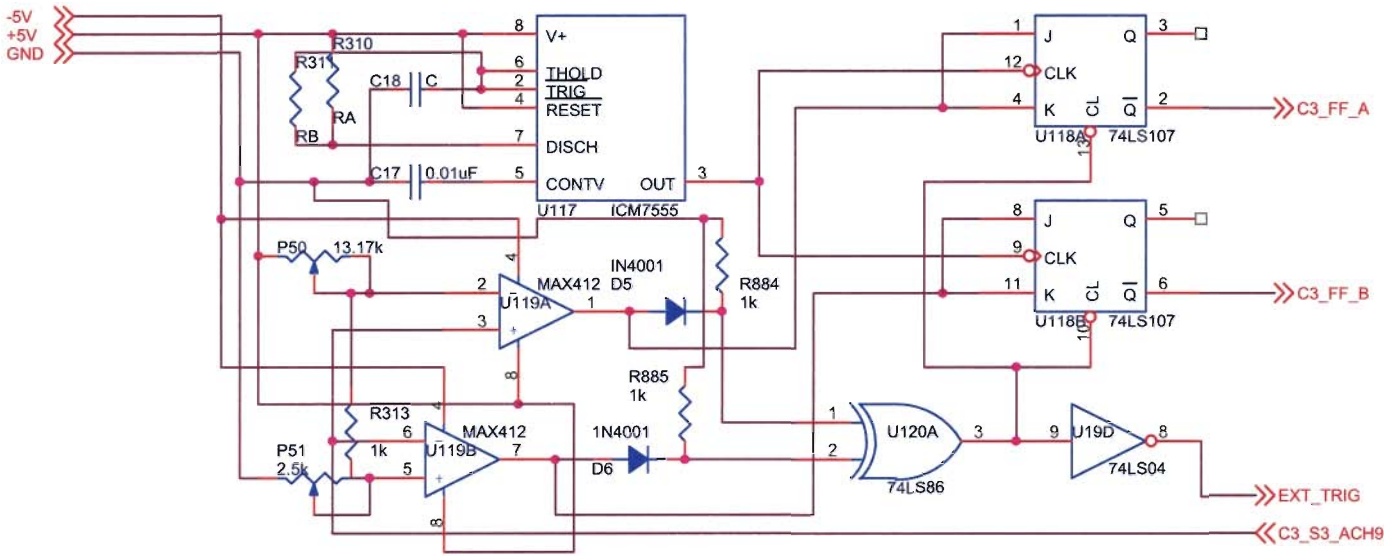

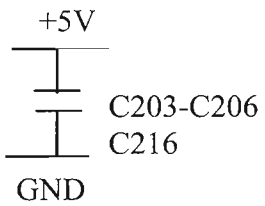

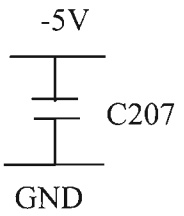

Title: Feedback Resistor Logic Circuit - B (Cell 3)		
Size: A	Document Number: VCU C3B	Rev:
Date: Thursday, July 22, 2004	Sheet 25 of 26	

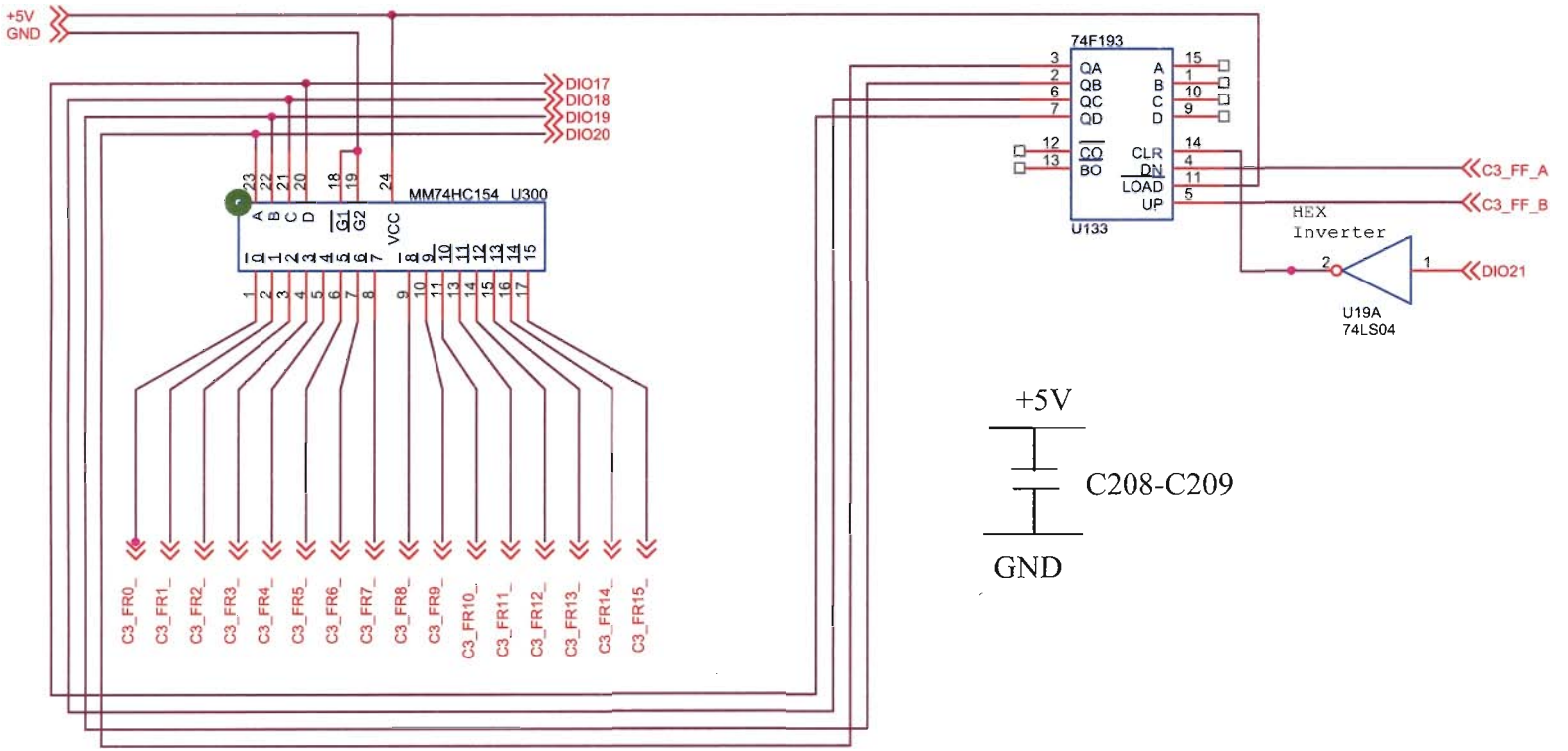

Title: Feedback Resistor Logic Circuit - C (Cell 3)		
Size: A	Document Number: VCU C3B	Rev:
Date: Thursday, July 22, 2004	Sheet 23 of 26	

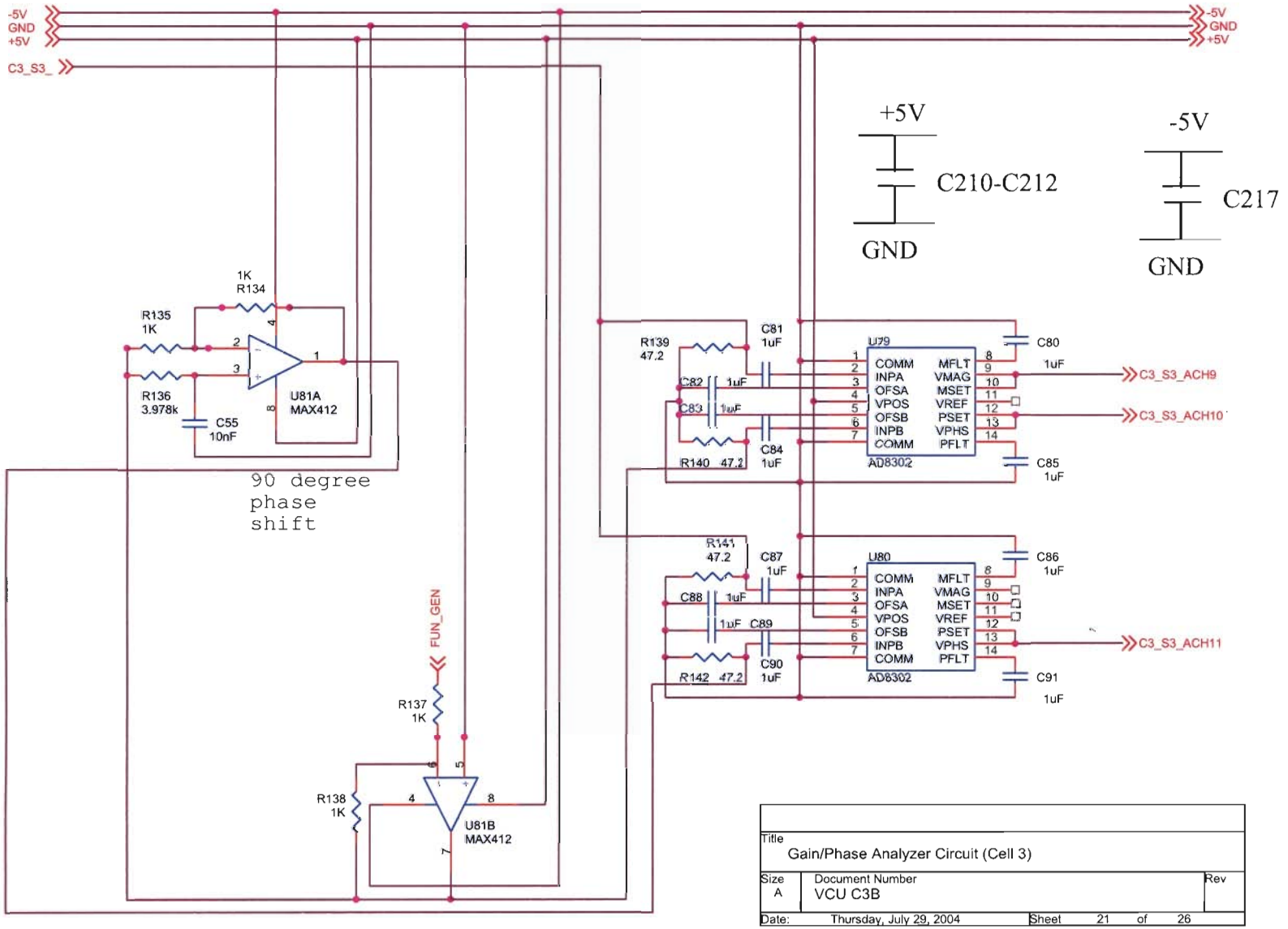
-5V
GND
+5V
C3_S3_
+5V
C210-C212
GND
-5V
C217
GND
1K
R134
R135
1K
R136
3.978k
C55
10nF
U81A
MAX412
90 degree
phase
shift
FUN_GEN
R137
1K
R138
1K
U81B
MAX412
R139
47.2
C81
1uF
C82
1uF
C83
1uF
R140
47.2
C84
1uF
U79
COMM
INPA
OFSA
VPOS
OFSB
INPB
COMM
MFLT
VMAG
MSET
VREF
PSET
VPHS
PFLT
AD8302
C80
1uF
C85
1uF
C3_S3_ACH9
C3_S3_ACH10
R141
47.2
C87
1uF
C88
1uF
C89
1uF
R142
47.2
C90
1uF
U80
C86
1uF
C91
1uF
C3_S3_ACH11
Title
Gain/Phase Analyzer Circuit (Cell 3)
Size
A
Document Number
VCU C3B
Rev
Date:
Thursday, July 29, 2004
Sheet
21
of
26

APPENDIX C: 3EIC Parts List

3 EIC Components List

Model	Manufacturer	Supplier	Supplier Cat#	Description	Qty.	Orcad Reference							
Power Supply Circuit + Function Generator Circuit + Variable DC Source													
MAX038CPP	Maxim-IC	Digikey	MAX038CPP-ND	Waveform Generator	1	U153							
MAX410	Maxim-IC	Digi-Key	MAX410CPA	28Mhz Precision OpAmp	2	U154	U3						
RN55E3802BB14	Vishay	Mouser	71-RN 55E3802B	38k ohm resistor	1	R992							
MFR-25FBF-1K00	Yageo	Digi-Key	1.00KXBK-ND	1k ohm resistor	2	R993	R2						
043P504	Vishay/spectrol	Mouser	594-43P504	500K ohm potentiometer (408k)	1	R990							
CFR-12JB-12K	Yageo	Digi-Key	12KEBK-ND	12k ohm resistor	1	R991							
MY.001	Mylar	Jameco	26833CF	1nF Capacitor	1	C20							
C062C105K5R5CA	KEMET	Newark	08B3926	1uF Ceramic Capacitor	2	C19	C22						
DC.0047		Jameco	15211	4.7 nF Capacitor	1	C21							
R2.2/50		Jameco	93729	2.2uF Capacitor electroliytic	1	C1							
TM.1		Jameco	33486	0.1uF Electrolytic Capacitor	1	C2							
C317C104M5U5CA	KEMET	Digi-Key	399-2143-ND	0.1uF Bypass Capacitor	6	C4	C5	C100	C101	C102	C103		
KMG35VB151M8X11LL	United Chemi=Con	Newark	03B1217	150uF Capacitor electroliytic	1	C3							
EC33016H811		Jameco	93796	330uF Capacitor electroliytic	1	C6							
12FR070	Ohmite Mfg. Co.	Digi-Key	12FR070-ND	0.07 ohm resistor	1	R1							
MFR-25FBF-10K0	Yageo	Digi-Key	10.0KXBK-ND	10k ohm resistor	1	R3							
043P103	Vishay/spectrol	Mouser	594-43P103	10K ohm potentiometer	2	R4	R5						
1N5822	Fairchild	Newark	38C7703	IN5822 Diode	1	D7							
Si9435DY	Vishay	Newark	95B6825	Si9435 MOSFET	1	Q2							
E8-0003	e-P Board Design	e-P Board Design	E8-0003	SOIC-8 to DIP-8 IC Adapter (Adapter for Si9435 MOSFET)	1	-do-							
Max883CPA	Maxim	Maxim	MAX883	Linear Regulator	1	U2							
Max774CPA	Maxim	Maxim	MAX774	Inverting DC-DC Controllers	1	U6							
414026-2	Amp/Tyco Electronics	ALLIED	5122596	SMB Connectors, 50 ohm PC Board Jacks, Mil-Type	1	MF1							
413990-2	Amp/Tyco Electronics	ALLIED	5122590	SMB Connectors, 50 ohm PC Board Jacks, Mil-Type	1	MF5							
4-103186-0	Amp/Tyco Electronics	Digi-Key	A26529-ND	Jumper	15	J2	J3	J4	J1	J5	J6	J7	J8
						J10	J11	J12	J13	J15	J16		
39-29-9206	Molex	Molex	39-29-9206	4.20mm (.165") Pitch Mini-Fit, Jr.™ Header, Vertical, Dual Row with PCB Snap-In Peg Locks	1	J9							
542-5900-220	J.W. Miller Magnetics	Mouser	542-5900-220	22uH Inductor	1	L1							
Connectors and Pwr Latching Ckt													
747846-3		ALLIED	5120578	25 pins Straight Up Posted D-Sub Connector for USB 30	2	MF2	MF3						
747841-4		ALLIED	5120446	15 pins Right Angle Posted D-Sub Connector for 3EIC (male)	1	MF4							
4-103186-0	Amp/Tyco Electronics	Digi-Key	A26529-ND	Jumper	1	J14							
C317C104M5U5CA	KEMET	Digi-Key	399-2143-ND	0.1uF Bypass Capacitor	3	C218	C219	C220					
		Jameco	25962	100 uF Electrolytic Capacitor	1	C221							
47.5KXTR-ND	Yageo	Digi-Key	47.5KXTR-ND	47.5 k ohm resistor	2	R221	R222						
MFR-25FBF-1K00	Yageo	Digi-Key	1.00KXBK-ND	1k ohm resistor	2	R223	R224						
ICM7555IPA-ND	Maxim-IC	Digi-Key	ICM7555IPA-ND	Timer	1	U555							
SN74LS107AN	Texas Instruments	Newark	06F5657	Dual J-K flip-flops	1	U556							
ADG721BRM	Analog Devices	Digi-Key	ADG721BRM	CMOS, 4ohm, Low Voltage, Dual SPST Switches	1	K91							
E8-0045	e-P Board Design	e-P Board Design	E8-0045	PCB Adaptor uSOP to DIP for ADG721	1	-do-							

Cell 1														
Cell 1 Circuit														
ADG733BRU	Analog Devices	Digi-Key	ADG733BRU	CMOS, 2.5ohm, Low Voltage, Triple SPDT Switches	2	U143	U145							
E16-0015	e-P Board Design	e-P Board Design	E16-0015	PCB Adaptor TSSOP to DIP for ADG733	2	-do-	-do-							
ADG622BRM	Analog Devices	Digi-Key	ADG622BRM	CMOS, +/- 5V, 4 ohm Dual SPST Switches	1	U144								
E10-0046	e-P Board Design	e-P Board Design	E10-0046	PCB Adaptor uSOP to DIP for ADG622	1	-do-								
MFR-25FBF-1K00	Yageo	Digi-Key	1.00KXBK-ND	1k ohm resistor	6	R273	R274	R275	R276	R257	R258			
MAX414CPD	Maxim-IC	Digi-Key	MAX414CPD	28Mhz Precision OpAmps	1	U137A	U137B	U137C						
FA8325500R0JR	INT RESISTIVE CO	Newark	95B5976	500 ohm resistor	2	R255	R256							
C317C104M5U5CA	KEMET	Digi-Key	399-2143-ND	0.1uF Bypass Capacitor	6	C104	C105	C106	C107	C108	C109			
Feedback Resistor Logic Circuit - A (Cell 1)														
ADG622BRM	Analog Devices	Digi-Key	ADG622BRM	CMOS, +/- 5V, 4 ohm Dual SPST Switches	8	K67	K68	K69	K70	K71	K72	K73	K74	
E10-0046	e-P Board Design	e-P Board Design	E10-0046	PCB Adaptor uSOP to DIP for ADG622	8	-do-	-do-	-do-	-do-	-do-	-do-	-do-	-do-	
043P103	Vishay/spectrol	Mouser	594-43P103	10K ohm potentiometer (4.56k)	1	P52								
MAX410	Maxim-IC	Digi-Key	MAX410CPA	28Mhz Precision OpAmp	1	U96								
CMF601R0000FLRE	Vishay/Dale	Mouser	71-CMF60-1.0	1 ohm resitor	1	R146								
				**3.164 ohm resistance-> 10 ohm pot.										
043P100	Vishay/spectrol	Mouser	594-43P100	10 ohm potentiometer	1	P1								
				**10.009 ohm resistance->2ohm in series with 10 ohm pot.										
MF1/4DLT52R2R00F	KOA Speer	Mouser	660-MF1/4DLT52R2R00F	2 ohm resitor	1	R147								
043P100	Vishay/spectrol	Mouser	594-43P100	10 ohm potentiometer	1	P2								
				**31.66 ohm resistance-> 24.9 ohm in series with 10 ohm pot.										
MFR-25FBF-24R9	Yageo	Digikey	24.9XBK-ND	24.9 ohm resistor	1	R148								
043P100	Vishay/spectrol	Mouser	594-43P100	10 ohm potentiometer	1	P3								
				**100.180 ohm resistance->95.3 ohm in series with 10 ohm pot.										
MFR-25FRF-95R3	Yageo	Digikey	95.3XTR-ND	95.3 ohm resitor	1	R149								
043P100	Vishay/spectrol	Mouser	594-43P100	10 ohm potentiometer	1	P4								
				**316.940 ohm resistance->309 ohm in series with a 10 ohm pot.										
MFR-25FBF-309R	Yageo	Digikey	309XBK-ND	309 ohm resistor	1	R150								
043P100	Vishay/spectrol	Mouser	594-43P100	10 ohm potentiometer	1	P5								
				**1.0027k ohm resistance->976 ohm in series with 50 ohm pot.										
5063JD976R0F12AF5BC	BC Components	Digikey	BC976XCT-ND	976 ohm resistor	1	R151								
043P500	Vishay/spectrol	Mouser	594-43P500	50 ohm potentiometer	1	P6								
				**3.172K ohm resistance->3.09 ohm in series with 100 ohm pot										
5043ED3K090F12AF5BC	BC Components	Digikey	BC3.09KYCT-ND	3.09k ohm resistor	1	R152								
043P101	Vishay/spectrol	Mouser	594-43P101	100 ohm potentiometer	1	P7								
				**10.038K ohm resistance->10K ohm in series with 100 ohm pot										
MFR-25FBF-10K0	Yageo	Digikey	10.0KXBK-ND	10K ohm resistor	1	R153								
043P101	Vishay/spectrol	Mouser	594-43P101	100 ohm potentiometer	1	P8								
				**31.751K ohm resistance->31.6K ohm in series with 200ohm pot										
MFR-25FBF-31K6	Yageo	Digikey	31.6KXBK-ND	31.6K ohm resistor	1	R154								
043P201	Vishay/spectrol	Mouser	594-43P201	200 ohm potentiometer	1	P9								
				**100.451kohm resistance->100kohm in series with 500ohm pot										
MFR-25FBF-100K	Yageo	Digikey	100KXBK-ND	100k ohm resistor	1	R155								
043P501	Vishay/spectrol	Mouser	594-43P501	500 ohm potentiometer	1	P10								
				**317.797kohm resistace->316kohm in series with 2kohm pot										
MFR-25FBF-316K	Yageo	Digikey	316KXBK-ND	316k ohm resistor	1	R156								
043P202	Vishay/spectrol	Mouser	594-43P202	2k Ohm potentiometer	1	P11								
				**1.005M ohm resistance->1M ohm in series with 10k ohm pot										
MFR-25FBF-1M00	Yageo	Digikey	1.00MXBK-ND	1M ohm resistor	1	R157								
043P103	Vishay/spectrol	Mouser	594-43P103	10K ohm potentiometer	1	P12								
				**3.181M ohm resistance->1+2M ohm in series with 500K ohm pot										
MFR-25FBF-1M00	Yageo	Digikey	1.00MXBK-ND	1.0M ohm resistor	1	R158								
5043ED2M000F12AF5BC	BC Components	Digikey	BC2.00MYCT-ND	2.0M ohm resistor	1	R159								
043P504	Vishay/spectrol	Mouser	594-43P504	500K ohm potentiometer	1	P13								
				**10.063M ohm resistance->10M ohm in series with 100k ohm pot										
CMF5510M000FKBF	Vishay/Dale	Mouser	71-CMF55-10M	10M ohm resistor	1	R160								
043P104	Vishay/spectrol	Mouser	594-43P104	100k ohm potentiometer	1	P14								
				**31.837M ohm resistance->3x10M ohm in series with 2M ohm pot										
CMF5510M000FKBF	Vishay/Dale	Mouser	71-CMF55-10M	10M ohm resistor	3	R161	R162	R163						
043P205	Vishay/spectrol	Mouser	594-43P205	2M ohm potentiometer	1	P15								
C317C104M5U5CA	KEMET	Digi-Key	399-2143-ND	0.1uF Bypass Capacitor	18	C112	C113	C114	C115	C116	C117	C118	C119	
						C120	C121	C122	C123	C124	C125	C126	C127	
						C128	C129							

Feedback Resistor Logic Circuit - B (Cell 1)													
ICM7555IPA-ND	Maxim-IC	Digi-Key	ICMAX7555IPA-ND	Timer	1	U99							
MAX412CPA	Maxim-IC	Digi-Key	MAX412	28Mhz Precision OpAmp	1	U102							
SN74LS86AN	Texas Instruments	Newark	08F7642	2 input X-OR	1	U103A							
SN74LS04N	Texas Instruments	Digi-Key	296-1629-5-ND	Hex Inverter	1	U17							
SN74LS107AN	Texas Instruments	Newark	08F6657	Dual J-K flip-flops	1	U100							
MY.01		Jameco	26884CP	.01uF Ceramic Capacitor	1	C16							
043P203	Vishay/spectrol	Mouser	594-43P203	13.17K ohm resistor (20K pot)	1	P46							
043P502	Vishay/spectrol	Mouser	594-43P502	2.5K ohm resistor (5K pot)	1	P47							
MFR-25FBF-1K00	Yageo	Digi-Key	1.00KXBK-ND	1k ohm resistor	3	R303	R880	R881					
MFR-25FBF-100	Yageo	digikey	100XBK-ND	RA (100 OHM 1/4W 1% METAL FILM)	1	R300							
MFR-25FBF-100	Yageo	digikey	100KXBK-ND	RB (100K OHM 1/4W 1% METAL FILM)	1	R301							
DO NOT ORDER, GET FROM LAB (green capacitor)				3.7 nF Capacitor	1	C15							
1N4001	ON SEMICONDUCTOR	Newark	09F3576	1N4001 Diode	2	D1	D2						
C317C104M5U5CA	KEMET	Digi-Key	399-2143-ND	0.1uF Bypass Capacitor	2	C135	C136						
Feedback Resistor Logic Circuit - C (Cell 1)													
MM74HC154	Fairchild Semiconductor	Digikey	MM74HC154N-ND	4-16 Decoder	1	U400							
74F193N	Fairchild	Newark	34C8086	Up/down Binary Counter	1	U125							
C317C104M5U5CA	KEMET	Digi-Key	399-2143-ND	0.1uF Bypass Capacitor	6	C130	C131	C132	C133	C134	C213		
Gain/Phase Analyzer Circuit (Cell 1)													
MAX412CPA	Maxim-IC	Digi-Key	MAX412	28Mhz Precision OpAmp	1	U75							
AD8302	Analog Devices	Analog Devices	AD8302	Gain and Phase Detector IC AD8302	2	U73	U74						
E14-0015	e-P Board Design	e-P Board Design	E14-0015	PCB Adaptor TSSOP to DIP for AD8302	2	-do-	-do-						
MFR-25FBF-1K00	Yageo	Digi-Key	1.00KXBK-ND	1k ohm resistor	4	R116	R117	R119	R120				
CFR-50JB-3K9	Yageo	Digi-Key	3.9KH-ND	3.978k ohm resistor	1	R118							
MY.01		Jameco	26884CP	.01uF Ceramic Capacitor	1	C53							
C062C105K5R5CA	KEMET	Newark	08B3926	1uF Ceramic Capacitor	12	C57	C58	C59	C60	C63	C64	C65	C66
						C56	C61	C62	C67				
ERO-S2PHF47R0	Panasonic ECG	Digi-Key	P47.0CACT-ND	47.2 ohm resistor	4	R121	R122	R123	R124				
C317C104M5U5CA	KEMET	Digi-Key	399-2143-ND	0.1uF Bypass Capacitor	4	C137	C138	C139	C140				

Cell 2														
Cell 2 Circuit														
ADG733BRU	Analog Devices	Digi-Key	ADG733BRU	CMOS, 2.5ohm, Low Voltage, Triple SPDT Switches	2	U146	U148							
E16-0015	e-P Board Design	e-P Board Design	E16-0015	PCB Adaptor TSSOP to DIP for ADG733	2	-do-	-do-							
ADG622BRM	Analog Devices	Digi-Key	ADG622BRM	CMOS, +/- 5V, 4 ohm Dual SPST Switches	1	U147								
E10-0046	e-P Board Design	e-P Board Design	E10-0046	PCB Adaptor uSOP to DIP for ADG622	1	-do-								
MFR-25FBF-1K00	Yageo	Digi-Key	1.00KXBK-ND	1k ohm resistor	8	R261	R262	R263	R264	R265	R266			
MAX414CPD	Maxim-IC	Digi-Key	MAX414CPD	28Mhz Precision OpAmps	1	U138A	U138B	U138C						
FA8325500R0JR	INT RESISTIVE CO	Newark	95B5976	500 ohm resistor	2	R277	R278							
C317C104M5U5CA	KEMET	Digi-Key	399-2143-ND	0.1uF Bypass Capacitor	8	C141	C142	C143	C144	C145	C146			
Feedback Resistor Logic Circuit - A (Cell 2)														
ADG622BRM	Analog Devices	Digi-Key	ADG622BRM	CMOS, +/- 5V, 4 ohm Dual SPST Switches	8	K75	K76	K77	K78	K79	K80	K81	K82	
E10-0046	e-P Board Design	e-P Board Design	E10-0046	PCB Adaptor uSOP to DIP for ADG622	8	-do-	-do-	-do-	-do-	-do-	-do-	-do-	-do-	
043P103	Vishay/spectrol	Mouser	594-43P103	10K ohm potentiometer (4.56k)	1	P53								
MAX410	Maxim-IC	Digi-Key	MAX410CPA	28Mhz Precision OpAmp	1	U97								
CMF601R0000FLRE	Vishay/Dale	Mouser	71-CMF60-1.0	1 ohm resitor	1	R164								
				**3.164 ohm resistance-> 10 ohm pot.										
043P100	Vishay/spectrol	Mouser	594-43P100	10 ohm potentiometer	1	P16								
				**10.009 ohm resistance->2ohm in series with 10 ohm pot.										
MF1/4DLT52R2R00F	KOA Speer	Mouser	660-MF1/4DLT52R2R00F	2 ohm resitor	1	R165								
043P100	Vishay/spectrol	Mouser	594-43P100	10 ohm potentiometer	1	P17								
				**31.66 ohm resistance-> 24.9 ohm in series with 10 ohm pot.										
MFR-25FBF-24R9	Yageo	Digikey	24.9XBK-ND	24.9 ohm resistor	1	R166								
043P100	Vishay/spectrol	Mouser	594-43P100	10 ohm potentiometer	1	P18								
				**100.180 ohm resistance->95.3 ohm in series with 10 ohm pot.										
MFR-25FRF-95R3	Yageo	Digikey	95.3XTR-ND	95.3 ohm resitor	1	R167								
043P100	Vishay/spectrol	Mouser	594-43P100	10 ohm potentiometer	1	P19								
				**316.940 ohm resistance->309 ohm in series with a 10 ohm pot.										
MFR-25FBF-309R	Yageo	Digikey	309XBK-ND	309 ohm resistor	1	R168								
043P100	Vishay/spectrol	Mouser	594-43P100	10 ohm potentiometer	1	P20								
				**1.0027k ohm resistance->976 ohm in series with 50 ohm pot.										
5063JD976R0F12AF5BC	BC Components	Digikey	BC976XCT-ND	976 ohm resistor	1	R169								
043P500	Vishay/spectrol	Mouser	594-43P500	50 ohm potentiometer	1	P21								
				**3.172K ohm resistance->3.09 ohm in series with 100 ohm pot										
5043ED3K090F12AF5BC	BC Components	Digikey	BC3.09KYCT-ND	3.09k ohm resistor	1	R170								
043P101	Vishay/spectrol	Mouser	594-43P101	100 ohm potentiometer	1	P22								
				**10.038K ohm resistance->10K ohm in series with 100 ohm pot										
MFR-25FBF-10K0	Yageo	Digikey	10.0KXBK-ND	10K ohm resistor	1	R171								
043P101	Vishay/spectrol	Mouser	594-43P101	100 ohm potentiometer	1	P23								
				**31.751K ohm resistance->31.6K ohm in series with 200ohm pot										
MFR-25FBF-31K6	Yageo	Digikey	31.6KXBK-ND	31.6K ohm resistor	1	R172								
043P201	Vishay/spectrol	Mouser	594-43P201	200 ohm potentiometer	1	P24								
				**100.451kohm resistance->100kohm in series with 500ohm pot										
MFR-25FBF-100K	Yageo	Digikey	100KXBK-ND	100k ohm resistor	1	R173								
043P501	Vishay/spectrol	Mouser	594-43P501	500 ohm potentiometer	1	P25								
				**317.797kohm resistace->316kohm in series with 2kohm pot										
MFR-25FBF-316K	Yageo	Digikey	316KXBK-ND	316k ohm resistor	1	R174								
043P202	Vishay/spectrol	Mouser	594-43P202	2k 0hm potentiometer	1	P26								
				**1.005M ohm resistance->1M ohm in series with 10k ohm pot										
MFR-25FBF-1M00	Yageo	Digikey	1.00MXBK-ND	1M ohm resistor	1	R175								
043P103	Vishay/spectrol	Mouser	594-43P103	10K ohm potentiometer	1	P27								
				**3.181M ohm resistance->1+2M ohm in series with 500K ohm pot										
MFR-25FBF-1M00	Yageo	Digikey	1.00MXBK-ND	1.0M ohm resistor	1	R176								
5043ED2M000F12AF5BC	BC Components	Digikey	BC2.00MYCT-ND	2.0M ohm resistor	1	R177								
043P504	Vishay/spectrol	Mouser	594-43P504	500K ohm potentiometer	1	P28								
				**10.063M ohm resistance->10M ohm in series with 100k ohm pot										
CMF5510M000FKBF	Vishay/Dale	Mouser	71-CMF55-10M	10M ohm resistor	1	R178								
043P104	Vishay/spectrol	Mouser	594-43P104	100k ohm potentiometer	1	P29								
				**31.837M ohm resistance->3x10M ohm in series with 2M ohm pot										
CMF5510M000FKBF	Vishay/Dale	Mouser	71-CMF55-10M	10M ohm resistor	3	R179	R180	R181						
043P205	Vishay/spectrol	Mouser	594-43P205	2M ohm potentiometer	1	P30								
C317C104M5U5CA	KEMET	Digi-Key	399-2143-ND	0.1uF Bypass Capacitor	18	C149	C150	C151	C152	C153	C154	C155	C156	
						C157	C158	C159	C160	C161	C162	C163	C164	
						C165	C166							

Feedback Resistor Logic Circuit - B (Cell 2)													
ICM7555IPA-ND	Maxim-IC	Digi-Key	ICMAX7555IPA-ND	Timer	1	U109							
MAX412CPA	Maxim-IC	Digi-Key	MAX412	28Mhz Precision OpAmp	1	U111							
SN74LS86AN	Texas Instruments	Newark	08F7642	2 input X-OR	1	U112A							
SN74LS04N	Texas Instruments	Digi-Key	296-1629-5-ND	Hex Inverter	1	U18D							
SN74LS107AN	Texas Instruments	Newark	08F6657	Dual J-K flip-flops	1	U110							
MY.01		Jameco	26884CP	.01uF Ceramic Capacitor	1	C33							
043P203	Vishay/spectrol	Mouser	594-43P203	13.17K ohm resistor (20K pot)	1	P48							
043P502	Vishay/spectrol	Mouser	594-43P502	2.5K ohm resistor (5K pot)	1	P49							
MFR-25FBF-1K00	Yageo	Digi-Key	11.00KXBK-ND	1k ohm resistor	3	R308	R882	R883					
MFR-25FBF-100	Yageo	digikey	100XBK-ND	RA (100 OHM 1/4W 1% METAL FILM)	1	R305							
MFR-25FBF-100	Yageo	digikey	100KXBK-ND	RB (100K OHM 1/4W 1% METAL FILM)	1	R306							
DO NOT ORDER, GET FROM LAB (green capacitor)				3.7 nF Capacitor	1	C34							
1N4001	ON SEMICONDUCTOR	Newark	09F3576	1N4001 Diode	2	D3	D4						
C317C104M5U5CA	KEMET	Digi-Key	399-2143-ND	0.1uF Bypass Capacitor	6	C167	C168	C169	C170	C171	C214		
Feedback Resistor Logic Circuit - C (Cell 2)													
MM74HC154	Fairchild Semiconductor	Digikey	MM74HC154N-ND	4-16 Decoder	1	U200							
74F193N	Fairchild	Newark	34C8086	Up/down Binary Counter	1	U129							
C317C104M5U5CA	KEMET	Digi-Key	399-2143-ND	0.1uF Bypass Capacitor	2	C172	C173						
Gain/Phase Analyzer Circuit (Cell 2)													
MAX412CPA	Maxim-IC	Digi-Key	MAX412	28Mhz Precision OpAmp	1	U78							
AD8302	Analog Devices	Analog Devices	AD8302	Gain and Phase Detector IC AD8302	2	U76	U77						
E14-0015	e-P Board Design	e-P Board Design	E14-0015	PCB Adaptor TSSOP to DIP for AD8302	2	-do-	-do-						
MFR-25FBF-1K00	Yageo	Digi-Key	11.00KXBK-ND	1k ohm resistor	4	R125	R126	R128	R129				
CFR-50JB-3K9	Yageo	Digi-Key	3.9KH-ND	3.978k ohm resistor	1	R127							
MY.01		Jameco	26884CP	.01uF Ceramic Capacitor	1	C54							
C062C105K5R5CA	KEMET	Newark	08B3926	1uF Ceramic Capacitor	12	C69	C70	C71	C72	C75	C76	C77	C78
						C68	C73	C74	C79				
ERO-S2PHF47R0	Panasonic ECG	Digi-Key	P47.0CACT-ND	47.2 ohm resistor	4	R130	R131	R132	R133				
C317C104M5U5CA	KEMET	Digi-Key	399-2143-ND	0.1uF Bypass Capacitor	4	C174	C175	C176	C177				

Cell 3														
Cell 3 Circuit														
ADG733BRU	Analog Devices	Digi-Key	ADG733BRU	CMOS, 2.5ohm, Low Voltage, Triple SPDT Switches	2	U149	U151							
E16-0015	e-P Board Design	e-P Board Design	E16-0015	PCB Adaptor TSSOP to DIP for ADG733	2	-do-	-do-							
ADG622BRM	Analog Devices	Digi-Key	ADG622BRM	CMOS, +/- 5V, 4 ohm Dual SPST Switches	1	U150								
E10-0046	e-P Board Design	e-P Board Design	E10-0046	PCB Adaptor uSOP to DIP for ADG622	1	-do-								
MFR-25FBF-1K00	Yageo	Digi-Key	1.00KXBK-ND	1k ohm resistor	6	R267	R268	R269	R270	R271	R272			
MAX414CPD	Maxim-IC	Digi-Key	MAX414CPD	28Mhz Precision OpAmps	1	U139A	U139B	U139C						
FA8325500R0JR	INT RESISTIVE CO	Newark	95B5976	500 ohm resistor	2	R888	R889							
C317C104M5U5CA	KEMET	Digi-Key	399-2143-ND	0.1uF Bypass Capacitor	6	C178	C179	C180	C181	C182	C215			
Feedback Resistor Logic Circuit - A (Cell 3)														
ADG622BRM	Analog Devices	Digi-Key	ADG622BRM	CMOS, +/- 5V, 4 ohm Dual SPST Switches	8	K83	K84	K85	K86	K87	K88	K89	K90	
E10-0046	e-P Board Design	e-P Board Design	E10-0046	PCB Adaptor uSOP to DIP for ADG622	8	-do-	-do-	-do-	-do-	-do-	-do-	-do-	-do-	
043P103	Vishay/spectrol	Mouser	594-43P103	10K ohm potentiometer (4.56k)	1	P54								
MAX410	Maxim-IC	Digi-Key	MAX410CPA	28Mhz Precision OpAmp	1	U98								
CMF601R0000FLRE	Vishay/Dale	Mouser	71-CMF60-1.0	1 ohm resitor	1	R182								
				**3.164 ohm resistance-> 10 ohm pot.										
043P100	Vishay/spectrol	Mouser	594-43P100	10 ohm potentiometer	1	P31								
				**10.009 ohm resistance->2ohm in series with 10 ohm pot.										
MF1/4DLT52R2R00F	KOA Speer	Mouser	660-MF1/4DLT52R2R00F	2 ohm resitor	1	R183								
043P100	Vishay/spectrol	Mouser	594-43P100	10 ohm potentiometer	1	P32								
				**31.66 ohm resistance-> 24.9 ohm in series with 10 ohm pot.										
MFR-25FBF-24R9	Yageo	Digikey	24.9XBK-ND	24.9 ohm resistor	1	R184								
043P100	Vishay/spectrol	Mouser	594-43P100	10 ohm potentiometer	1	P33								
				**100.180 ohm resistance->95.3 ohm in series with 10 ohm pot.										
MFR-25FRF-95R3	Yageo	Digikey	95.3XTR-ND	95.3 ohm resitor	1	R185								
043P100	Vishay/spectrol	Mouser	594-43P100	10 ohm potentiometer	1	P34								
				**316.940 ohm resistance->309 ohm in series with a 10 ohm pot.										
MFR-25FBF-309R	Yageo	Digikey	309XBK-ND	309 ohm resistor	1	R186								
043P100	Vishay/spectrol	Mouser	594-43P100	10 ohm potentiometer	1	P35								
				**1.0027k ohm resistance->976 ohm in series with 50 ohm pot.										
5063JD976R0F12AF5BC	BC Components	Digikey	BC976XCT-ND	976 ohm resistor	1	R187								
043P500	Vishay/spectrol	Mouser	594-43P500	50 ohm potentiometer	1	P36								
				**3.172K ohm resistance->3.09 ohm in series with 100 ohm pot										
5043ED3K090F12AF5BC	BC Components	Digikey	BC3.09KYCT-ND	3.09k ohm resistor	1	R188								
043P101	Vishay/spectrol	Mouser	594-43P101	100 ohm potentiometer	1	P37								
				**10.038K ohm resistance->10K ohm in series with 100 ohm pot										
MFR-25FBF-10K0	Yageo	Digikey	10.0KXBK-ND	10K ohm resistor	1	R189								
043P101	Vishay/spectrol	Mouser	594-43P101	100 ohm potentiometer	1	P38								
				**31.751K ohm resistance->31.6K ohm in series with 200ohm pot										
MFR-25FBF-31K6	Yageo	Digikey	31.6KXBK-ND	31.6K ohm resistor	1	R190								
043P201	Vishay/spectrol	Mouser	594-43P201	200 ohm potentiometer	1	P39								
				**100.451kohm resistance->100kohm in series with 500ohm pot										
MFR-25FBF-100K	Yageo	Digikey	100KXBK-ND	100k ohm resistor	1	R191								
043P501	Vishay/spectrol	Mouser	594-43P501	500 ohm potentiometer	1	P40								
				**317.797kohm resistace->316kohm in series with 2kohm pot										
MFR-25FBF-316K	Yageo	Digikey	316KXBK-ND	316k ohm resistor	1	R192								
043P202	Vishay/spectrol	Mouser	594-43P202	2k 0hm potentiometer	1	P41								
				**1.005M ohm resistance->1M ohm in series with 10k ohm pot										
MFR-25FBF-1M00	Yageo	Digikey	1.00MXBK-ND	1M ohm resistor	1	R193								
043P103	Vishay/spectrol	Mouser	594-43P103	10K ohm potentiometer	1	P42								
				**3.181M ohm resistance->1+2M ohm in series with 500K ohm pot										
MFR-25FBF-1M00	Yageo	Digikey	1.00MXBK-ND	1.0M ohm resistor	1	R194								
5043ED2M000F12AF5BC	BC Components	Digikey	BC2.00MYCT-ND	2.0M ohm resistor	1	R195								
043P504	Vishay/spectrol	Mouser	594-43P504	500K ohm potentiometer	1	P43								
				**10.063M ohm resistance->10M ohm in series with 100k ohm pot										
CMF5510M000FKBF	Vishay/Dale	Mouser	71-CMF55-10M	10M ohm resistor	1	R196								
043P104	Vishay/spectrol	Mouser	594-43P104	100k ohm potentiometer	1	P44								
				**31.837M ohm resistance->3x10M ohm in series with 2M ohm pot										
CMF5510M000FKBF	Vishay/Dale	Mouser	71-CMF55-10M	10M ohm resistor	3	R197	R198	R199						
043P205	Vishay/spectrol	Mouser	594-43P205	2M ohm potentiometer	1	P45								
C317C104M5U5CA	KEMET	Digi-Key	399-2143-ND	0.1uF Bypass Capacitor	18	C185	C186	C187	C188	C189	C190	C191	C192	
						C193	C194	C195	C196	C197	C198	C199	C200	
						C201	C202							

Feedback Resistor Logic Circuit - B (Cell 3)				
ICM7555IPA-ND	Maxim-IC	Digi-Key	ICMAX7555IPA-ND	Timer
MAX412CPA	Maxim-IC	Digi-Key	MAX412	28Mhz Precision OpAmp
SN74LS86AN	Texas Instruments	Newark	08F7642	2 input X-OR
SN74LS04N	Texas Instruments	Digi-Key	296-1629-5-ND	Hex Inverter
SN74LS107AN	Texas Instruments	Newark	08F6657	Dual J-K flip-flops
MY.01		Jameco	26884CP	.01uF Ceramic Capacitor
043P203	Vishay/spectrol	Mouser	594-43P203	13.17K ohm resistor (20K pot)
043P502	Vishay/spectrol	Mouser	594-43P502	2.5K ohm resistor (5K pot)
MFR-25FBF-1K00	Yageo	Digi-Key	1.00KXBK-ND	1k ohm resistor
MFR-25FBF-100	Yageo	digikey	100XBK-ND	RA (100 OHM 1/4W 1% METAL FILM)
MFR-25FBF-100	Yageo	digikey	100KXBK-ND	RB (100K OHM 1/4W 1% METAL FILM)
DO NOT ORDER, GET FROM LAB (green capacitor)				3.7 nF Capacitor
1N4001	ON SEMICONDUCTOR	Newark	09F3576	1N4001 Diode
C317C104M5U5CA	KEMET	Digi-Key	399-2143-ND	0.1uF Bypass Capacitor
Feedback Resistor Logic Circuit - C (Cell 3)				
MM74HC154	Fairchild Semiconductor	Digikey	MM74HC154N-ND	4-16 Decoder
74F193N	Fairchild	Newark	34C8086	Up/down Binary Counter
C317C104M5U5CA	KEMET	Digi-Key	399-2143-ND	0.1uF Bypass Capacitor
Gain/Phase Analyzer Circuit (Cell 3)				
MAX412CPA	Maxim-IC	Digi-Key	MAX412	28Mhz Precision OpAmp
AD8302	Analog Devices	Analog Devices	AD8302	Gain and Phase Detector IC AD8302
E14-0015	e-P Board Design	e-P Board Design	E14-0015	PCB Adaptor TSSOP to DIP for AD8302
MFR-25FBF-1K00	Yageo	Digi-Key	1.00KXBK-ND	1k ohm resistor
CFR-50JB-3K9	Yageo	Digi-Key	3.9KH-ND	3.978k ohm resistor
MY.01		Jameco	26884CP	.01uF Ceramic Capacitor
C062C105K5R5CA	KEMET	Newark	08B3926	1uF Ceramic Capacitor
ERO-S2PHF47R0	Panasonic ECG	Digi-Key	P47.0CACT-ND	47.2 ohm resistor
C317C104M5U5CA	KEMET	Digi-Key	399-2143-ND	0.1uF Bypass Capacitor
3EIC Chip Holder				
747845-4		ALLIED	5120478	15 pins Right Angle Posted D-Sub Connector for 3EIC (female)
MISC				
USB-48A-30A16	Eagle Technology	EMJ Electronics		USB48A-30A16/48 DIO/16 ADC/4 DAC uDAQ Device
ADPT-25-S	Eage Technology	EMJ Electronics	1EAD25S	Short Mini Screw Adapter for USB30 (optional)
DB25M/F	Eagle Technology	EMJ Electronics	1DB25MF	25 Pin Cable for USB 30 (optional)
MINUET	Antec	Page Computer	B1214291	Antec Minuet Chassis
324S	GRUBER	ALLIED	324S	Cable, 15 D-SUB M/F, Shielded, 2'

APPENDIX D: Layout of Circuit on Printed Circuit Board from Mass Design

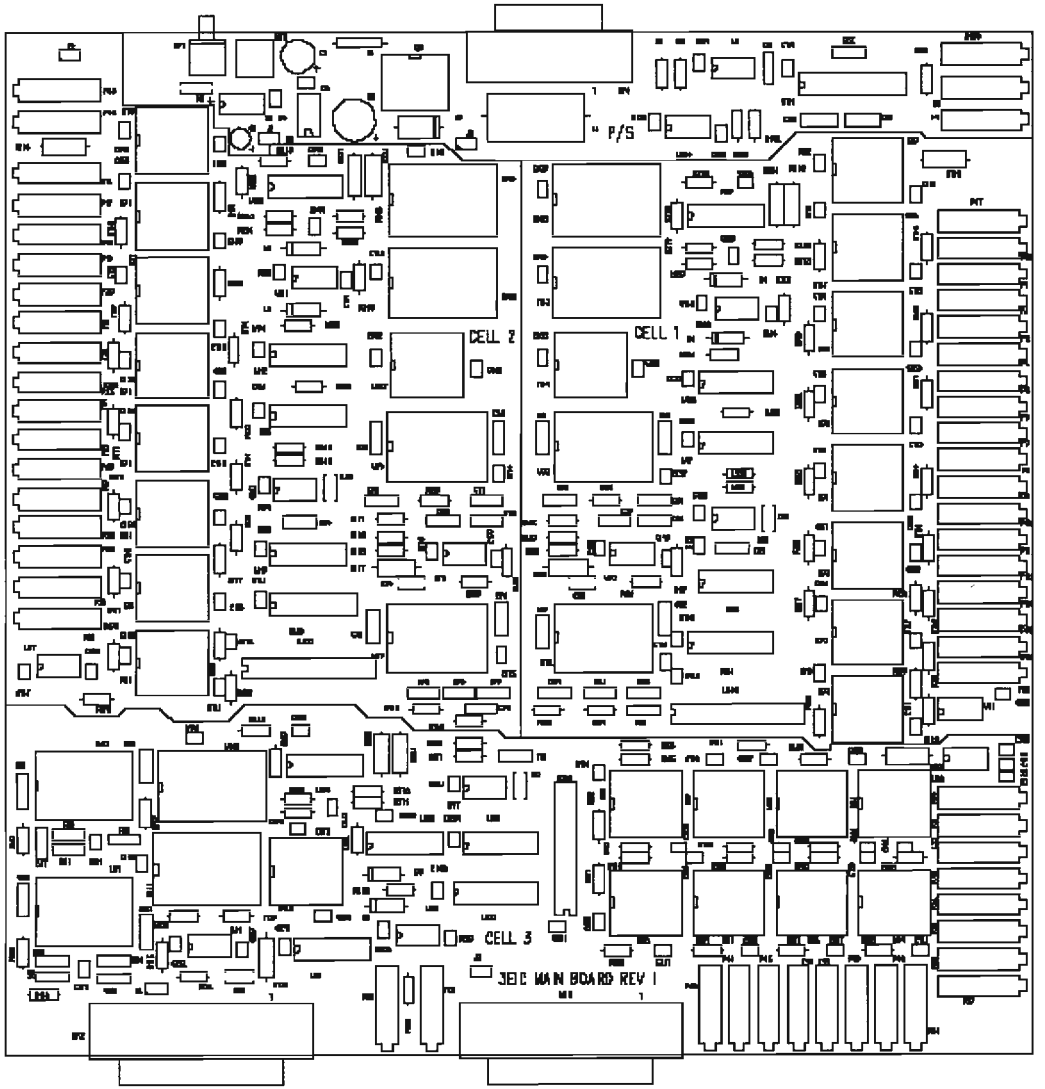

COMP SIDE SILKSCREEN
3EIC MAIN BOARD REV 1

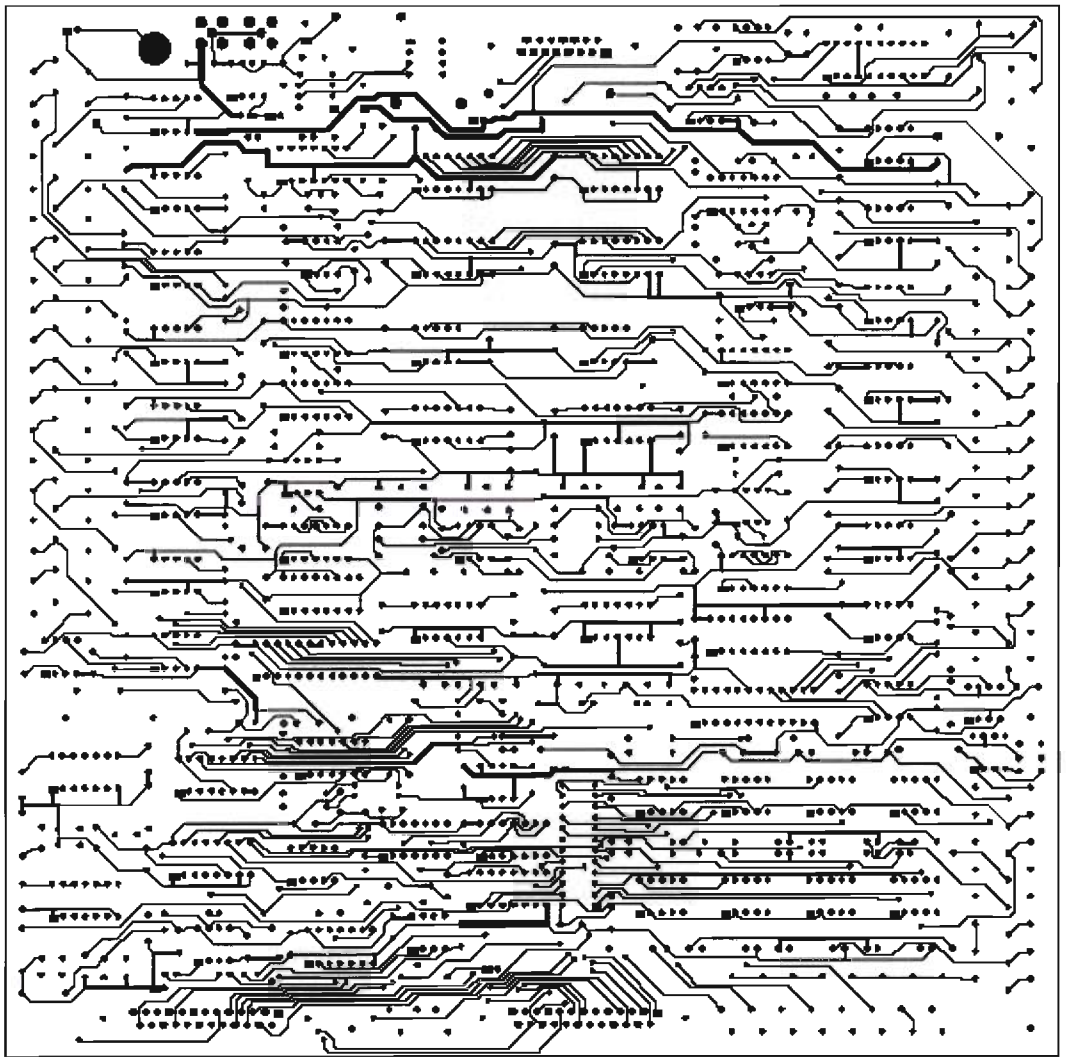

COMP SIDE
3EIC MAIN BOARD REV 1

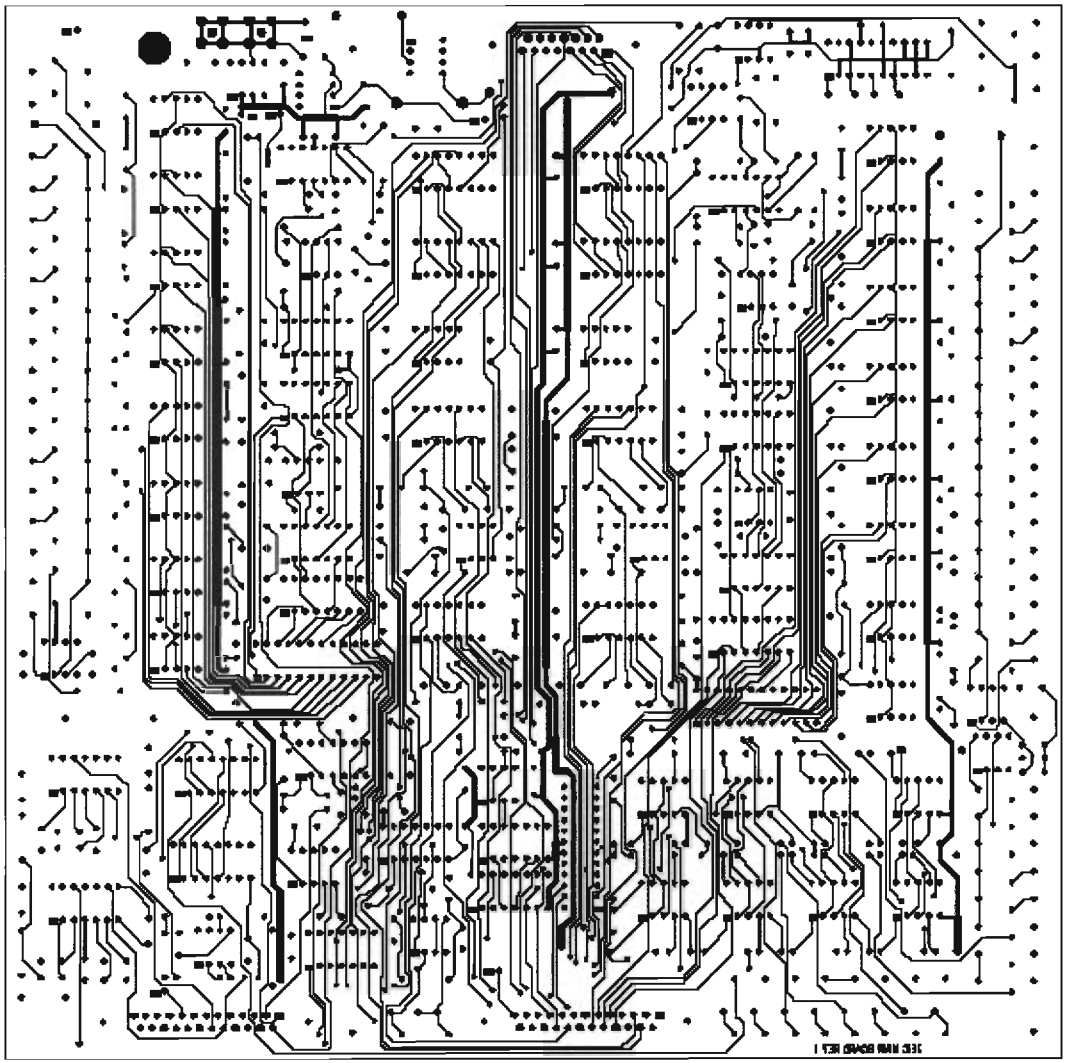

SOLDER SIDE
SEC MAIN BOARD REV 1

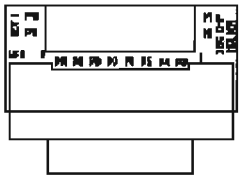

COMP SIDE SILKSCREEN
3EIC CHIP HOLDER REV 1

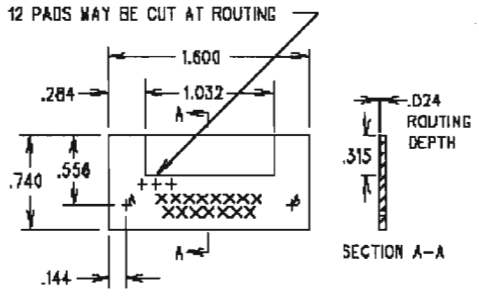

DRILL DRAWING

3EIC CHIP HOLDER REV 1

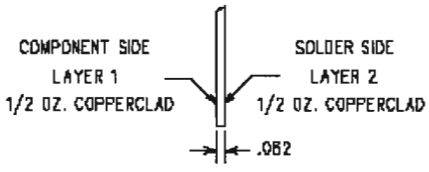

NOTES:

1. MAT'L: .062 THK. FR4 GREEN COPPERCLAD LAMINATE.
2. ALL HOLES TO BE PLATED THRU WITH A MINIMUM WALL THICKNESS OF .001 AND A SOLDER COATING OF .0003.
3. BOARDS TO BE LPIOBC ON BOTH SIDES.
4. BOARDS TO BE HOT AIR LEVELED SOLDER AFTER SOLDERMASK.
5. BOARDS TO BE SILKSCREENED ON COMPONENT SIDE WITH PERMANENT, WHITE EPOXY (CHEMICAL AND SCRATCH RESISTANT).
6. BOARDS SHALL BE MADE FROM UNDERWRITER LABORATORY RECOGNIZED MATERIAL AND THE FINISHED BOARD MUST CARRY THE VENDOR'S U.L. LOGO.
7. ALL DRAWINGS AND FILMS VIEWED FROM COMPONENT SIDE.
8. VENDOR TO INSURE THAT ALL COMPONENT PADS AND HOLES ARE FREE OF SILKSCREEN MATERIAL.

DRILL CHART			
SYMBOL	SIZE	QTY	PLATED TYPE
+	.020	3	PLATED
X	.041	15	PLATED
A	.125	2	NON-PLATED

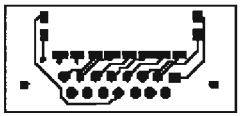

COMP SIDE
3EIC CHIP HOLDER REV 1

SOLDER SIDE
SEIC CHIP HOLDER REV 1

APPENDIX E: Electrochemical Impedance Cells BioAnalyzer Data Acquisition and Instrumentation Control Software

In order to properly explain the coding of this software program for the Urea Impedance BioAnalyzer, only one sensor mode was addressed in the following explanation. The four sensor modes (W1,W2, Ref; W1,W2; W1+W2; W1+W2, Ref) only had variations in DIO configuration, but followed the same signal processing and analysis.

This entire program was within a "While loop" using a shift register. Shift registers are a type of sequential logic circuit, mainly for storage of digital data. They are a group of flip-flops connected in a chain so that the output from one flip-flop became the input of the next flip-flop. Most of the registers possessed no characteristic internal sequence of states. All the flip-flops were driven by a common clock, and all were set or reset simultaneously. The While loop allowed for the program to continuously run for the specified time and created an array of data values.

Pre-Initialization, Initialization, Interrogation and Urea BioAnalyzer buttons

The purpose of these buttons were to set the μDAQ USB-48A-30A16 DIO channels to either 0V or +5V, the DAC to either 0V or +10V, depending on which step the user wanted to analyze the sensor. The user had the option of choosing each step independently or running all three steps (Pre-Initialization, Initialization and Interrogation) as one sequential step.

Figure E1 showed the LabVIEW block diagram of how the four buttons were wired. The four buttons were Boolean buttons, which were sent to a Sub VI. Within this

Sub VI, called "Pgrm Control", each button is inputted to four Boolean Case Structures. The Case Structures were embedded within each other in the False case. When one of the four buttons was pressed, it was assigned a numeric value (0-3). The numeric value was outputted from the Sub VI and sent to another Case Structure (shown above the buttons). This numeric output was summed with a value of "0" and then summed with the value of "+1". The Case Structure was unable to output a value of "0", therefore the "+1" was added in. The output of that Case Structure was sent to another Case Structure (shown below the buttons), which addressed the "Urea BioAnalyzer" button. This Case Structure allowed for when the "Urea BioAnalyzer" button was pressed (True state), then the three steps were run as one sequential step.

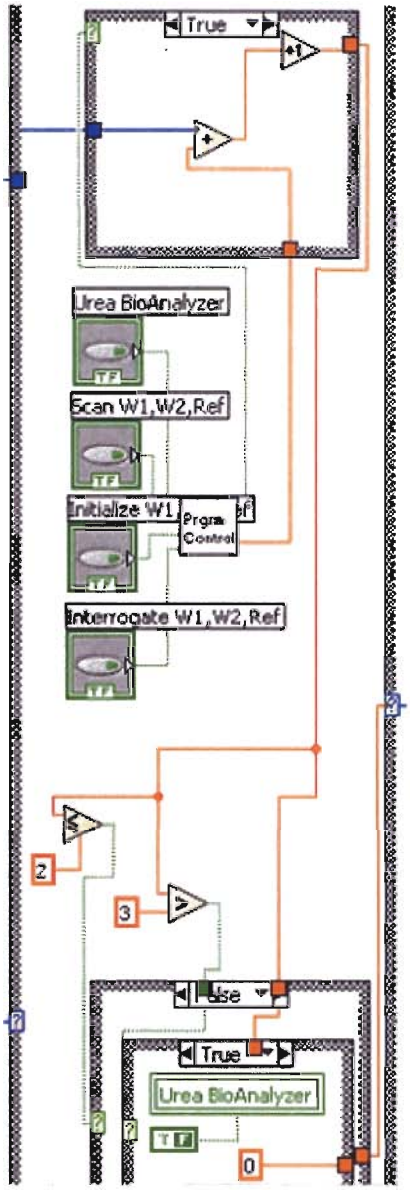

Figure E1: *Four Boolean buttons and Case Structures*

HELP files

HELP files had been incorporated into the software to allow the user to know how the uDAQ USB-48A-30A16 DIO channels were set during each step for each sensor

mode. The HELP buttons, Case Structure and HELP files were within a separate While loop. This allowed for the user to be able to access the HELP files and also be able to run a step during one of the sensor modes. The three HELP buttons were Boolean buttons, which were sent to a Sub VI. Within this Sub VI, called "Help Control", each button was sent to three Boolean Case Structures. The Boolean Case Structures were embedded within each other in the False case. When one of the three buttons was pressed, it was assigned a numeric value (1-3). The numeric value was outputted from the Sub VI and sent to a Numeric Case structure. The "Help Control" output value corresponded to the numeric case and the appropriate HELP file. This was repeated four times for each sensor mode.

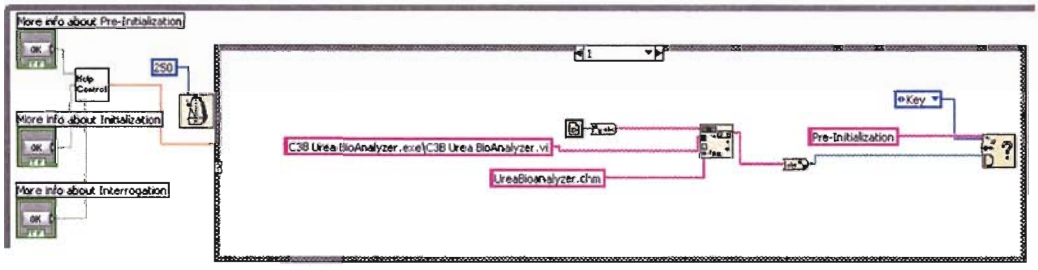

Figure E2: *HELP files block diagram.*

Save button

The Save button was a Boolean button which wrote the |Z|, Phase Angle and time values from the Interrogation step into a MS Excel spreadsheet.

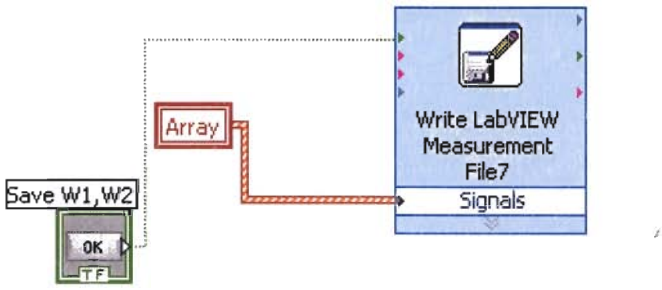

Figure E3*: *Save button block diagram.

Cell 1, Cell 2, Cell 3 option buttons

Three Boolean buttons were placed for each step within each sensor mode. These buttons allowed for the user to have the option of choosing which cell to run, rather than running all three cells at once for the chosen step. For example, if the user chose Cell 1, then Cell 2 and Cell 3 would remain unaffected and thus no data would be collected from those cells.

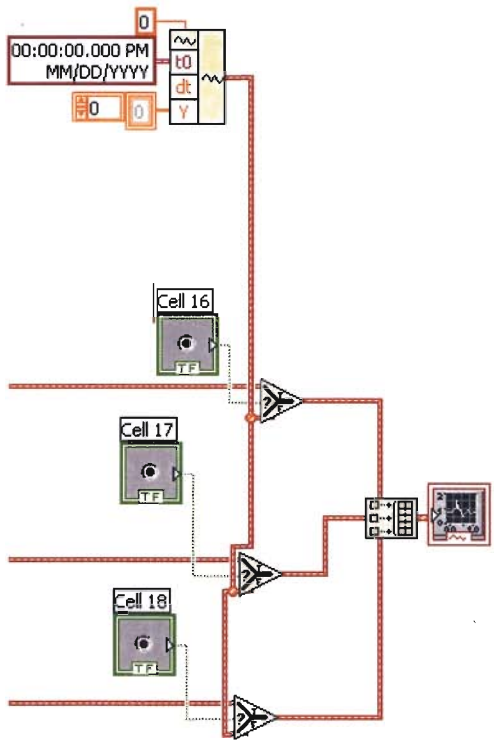

Figure E4: *Boolean buttons to choose which cell to run, rather than running all three cells at once.*

Pre-Initialization

The Pre-Initialization step allowed for the user to make a real-time read of the open circuit or rest potential of the shorted working electrodes versus a suitable reference electrode in the analyte environment.

This step was controlled using a Numeric Stacked Sequence Structure, which ran through the sequence to write to the DIO and DAC channels and also read the analog voltage from the cells. The USB-48A-30A16 µDAQ channels were programmed to provide either a 0V or +5V output during this step using a "Write Digital Line" Sub VI. The DAC 0 channel sent a 0V signal using a "DA Update Channel" Sub VI. The analog

voltages from the cells were read using the "AD Sample Channel" Sub VI and outputted to the indicators. The time period of this step was controlled by the user.

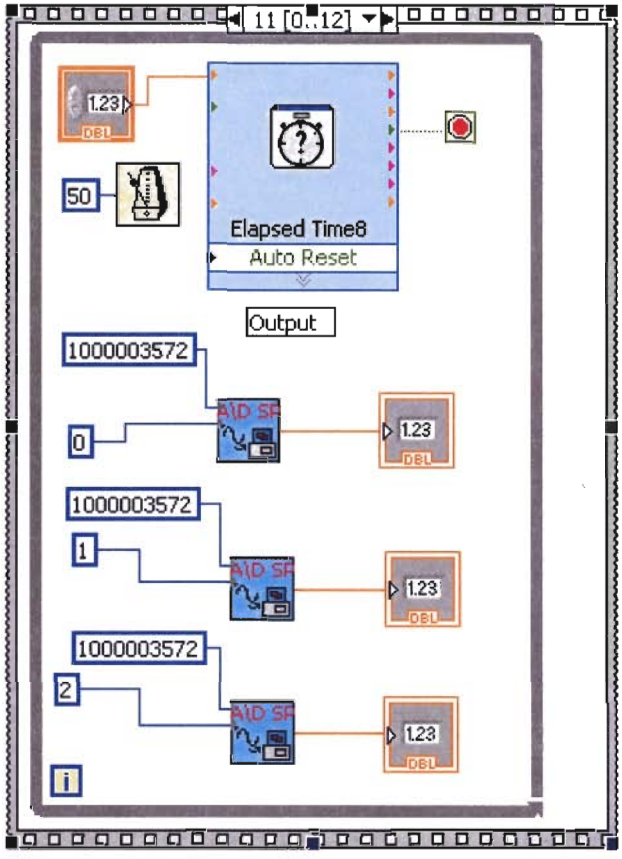

Figure E5: *Numeric Stacked Sequence Structure for Pre-Initialization*

Initialization

A DC potential between –1V to +1V was applied to the counter electrode. It was then compared with the voltage of external reference electrode using a differential OpAmp and measured the resulting current.

This step was controlled using a Numeric Stacked Sequence Structure, which ran through the sequence to write to the DIO and DAC channels and also read the analog voltage from the cells. The USB-48A-30A16 μDAQ channels were programmed to

provide either a 0V or +5V output during this step using a "Write Digital Line" Sub VI. The DAC 0 channel sent a +10V signal using a "DA Update Channel" Sub VI. The analog voltages from the cells were read using the "AD Sample Channel" Sub VI.

These analog voltages were converted into current values by dividing with 1000 ohms. The current values from all 3 cells were outputted to a "Build Waveform" VI. The "Build Waveform" VI also set "t0" at "0" and "dt" at 50ms sampling rates. The three waveforms from each cell were sent into a "Build Array" VI in order to group them onto one waveform graph. The output of the "Build Array" VI was then inputted into the "Waveform Graph" VI, as shown in **Figure E6**. The waveform graph was plotted versus time. These current values were also sent to a Boolean Case Structure (in the middle) shown in **Figure E7**. Since the Initialization step was within a While loop using shift registers (on the left side of the While loop), the current value from the previous iteration and the present iteration could be divided by the sampling time (50ms) to output a slope value during each looping iteration. This slope value was sent to the shift registers (on the right side of the While loop) to be used as the previous current value for the next looping iteration.

The second Boolean Case Structure (top right) used the slope value calculated from the other Boolean Case Structure, both previous and present values, subtracted them, calculated the percent difference and compared with the Initialization threshold, which was defined by the user. The three values were inputted into AND gates. When the calculated percent difference became less than or equal to the Initialization threshold for all three cells, its output was sent into an OR gate along with the user defined

Initialization time period. Depending on which reached to a completion first, user defined time period or Initialization Threshold, the Initialization While loop would stop.

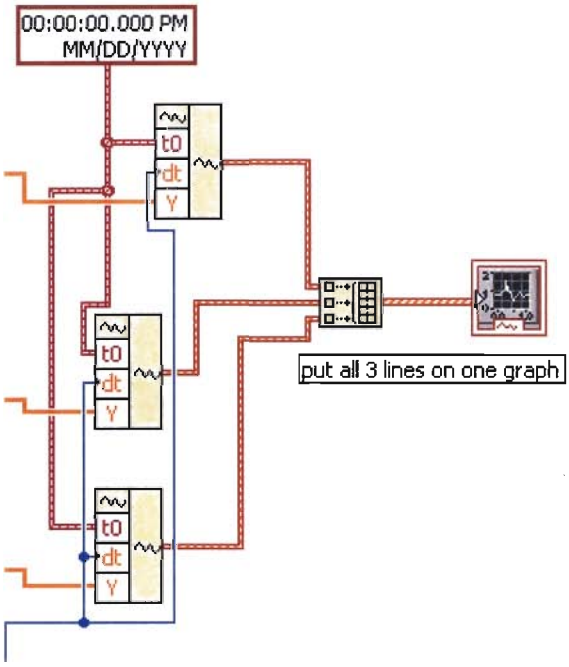

Figure E6: Initialization Waveform graph

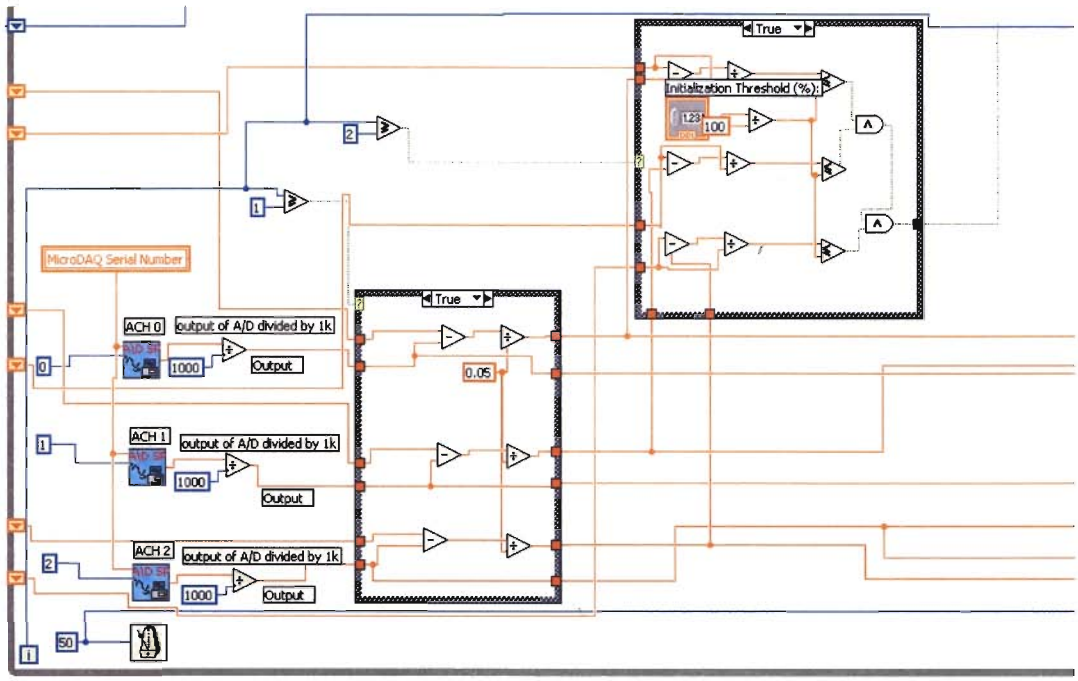

Figure E7: Initialization Numeric Stacked Sequence Structure

Interrogation

A non-perturbating 50mVpp, 4 kHz sine wave was applied to the sensor device to reveal chemically or biologically conferred changes in electrical resistance of the chemically sensitive and chemoresistive film.

This step was controlled using a Numeric Stacked Sequence Structure (**Figure E8**), which ran through the sequence to write to the DIO and DAC channels and also read the analog voltage from the cells. The USB-48A-30A16 µDAQ channels were programmed to provide either a 0V or +5V output during this step using a "Write Digital Line" Sub VI. The DAC 0 channel sent a 0V signal using a "DA Update Channel" Sub VI.

Four digital bits (0/1) (Up/Down Binary Counter IC, 74F193), from each cell, were read from the "Read from Digital Line" Sub VI and outputted into a four bit input

array. The output of the array was inputted into a "Boolean Array to Number" icon. This converted the four bits into an integer, which was inputted into a formula node. The integer corresponded with the Feedback Resistance value defined in the formula node. A magnitude voltage was also measured from the "AD Sample Channel" Sub VI and inputted into the formula node, which corresponded with the voltage measured in the Feedback Resistance circuit on the circuit board. Using the Feedback Resistance value and magnitude voltage, the appropriate gain and magnitude impedance was calculated.

"AD Sample Channel" Sub VI was also used in calculating the Phase angle and direction during the Interrogation step as shown in the formula node. The magnitude impedance and phase angle from all 3 cells were outputted to a "Build Waveform" VI. The "Build Waveform" VI also set "t0" at "0" and "dt" at 50ms sampling rate. The six waveforms from each cell (2 from each cell) were sent into a "Build Array" VI in order to group them onto two waveform graphs (|Z| and Phase Angle). The output of the "Build Array" VI was then inputted into the "Waveform Graph" VI, as shown in **Figure E9**. The waveform graphs were plotted versus time.

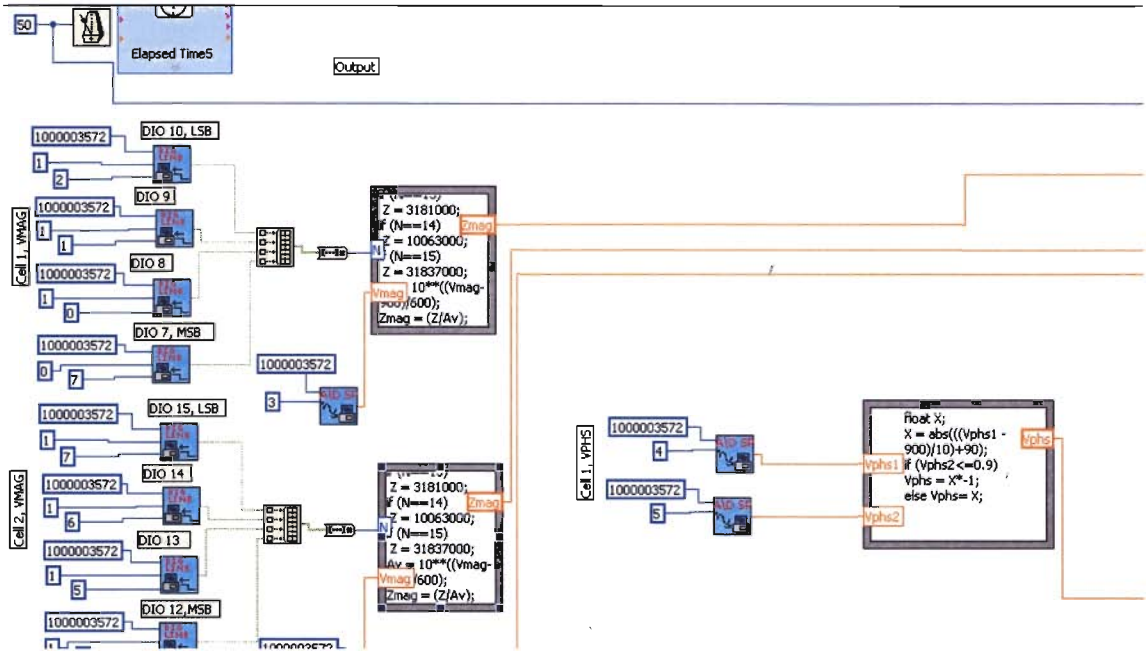

Figure E8: Interrogation Numeric Stacked Sequence Structure

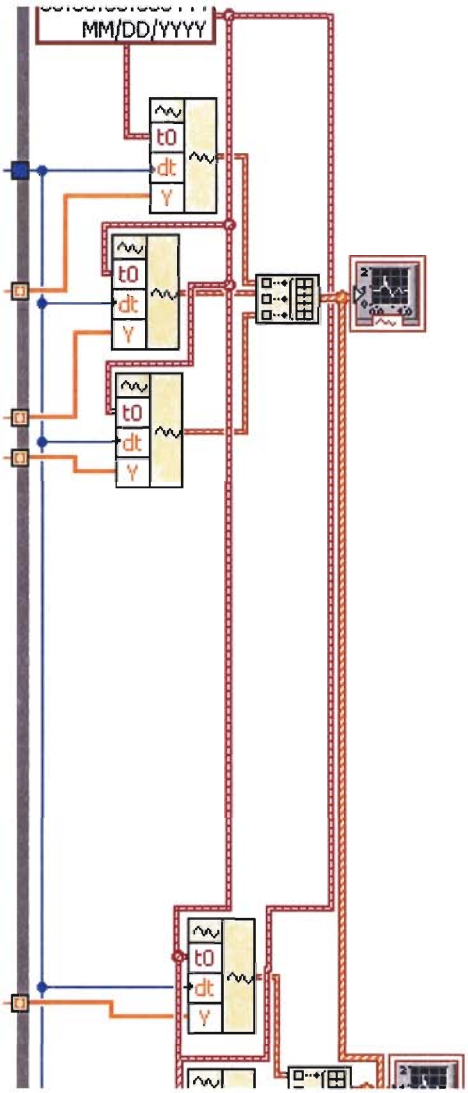

***Figure E9**: Magnitude impedance and phase angle Waveform graphs for Interrogation*

W1, W2, Ref

This sensor mode had only variations in DIO configuration, but followed the same signal processing and analysis as the other three modes. A $50mV_{PP}$, 4kHz sine wave was applied from the function generator that was also superimposed with the reference electrode potential to both working electrodes (W1 and W2). The resulting voltage was measured with respect to the Reference (Ref) electrode. Appendix A

provides a conceptual schematic of the DIO configuration at each switch within the cell circuit.

W1, W2

This sensor mode had only variations in DIO configuration, but followed the same signal processing and analysis as the other three modes. A 50mVpp, 4kHz sine wave was applied to W1 & W2 and the resulting voltage was measured. Appendix A provides a conceptual schematic of the DIO configuration at each switch within the cell circuit.

W1+W2, Ref

This sensor mode had only variations in DIO configuration, but followed the same signal processing and analysis as the other three modes. A 50mVpp, 4kHz sine wave was applied that was also superimposed with reference electrode potential to shorted working electrodes (W1 and W2) and the counter electrode. The resulting voltage was measured with respect to the Reference (Ref) electrode. Appendix A provides a conceptual schematic of the DIO configuration at each switch within the cell circuit.

W1+W2

This sensor mode had only variations in DIO configuration, but followed the same signal processing and analysis as the other three modes. A 50mVpp, 4kHz sine wave was applied across the shorted working electrodes (W1 and W2) and the counter electrode. The resulting voltage was measured at these two points. Appendix A provides a conceptual schematic of the DIO configuration at each switch within the cell circuit.

Glossary of Symbols and Abbreviations

(in order of appearance)

PVP	Polyvinylpyrrolidone
HCl	Hydrochloric acid
FIA	Flow Injection Analysis
FET	Field Effect Transistor
ISFET	Ion-Sensitive Field Effect Transistor
PVC	poly(vinylchloride)
rpm	revolutions per minute
HeNe	helium-neon gas
μM	micro-molar
mM	milli-molar
ENFETs	Enzyme FETs
PANi	polyaniline
PPy	polypyrrole
GA	glutaraldehyde
uA	microamps
mg	milligrams
dl	deciliter
cm	centimeter
Urs	urease
CMOS	Complementary Metal Oxide Semiconductor
SiO_2	silicon dioxide
Si_3N_4	silicon nitride
V	Output DC voltage [Volts]
I	DC current response [Amperes]
Z	Impedance [ohms]
R	Resistance [ohms]

θ	Phase shift in radians
j	Imaginary number
X	Reactance
C	Capacitance [Farads]
L	Inductance [Henries]
X_L	Inductive reactance
X_L	Capacitative reactance
Ω	ohms
I(t)	instantaneous current
A	maximum amplitude
ω	frequency in radians per second = $2\Pi f$
f	frequency [Hertz]
t	time
Z"	Imaginary component of impedance
Z'	Real component of impedance
Z_S	vector sum of circuit components in series
Z_1	impedance of individual circuit component
Z_2	impedance of individual circuit component
Z_S'	vector sum of real component of impedance
Z_S"	vector sum of imaginary component of impedance
Z_1'	impedance of real component of individual circuit component
Z_2'	impedance of real component of individual circuit component
Z_1"	impedance of imaginary component of individual circuit component
Z_2"	impedance of imaginary component of individual circuit component
Z_P	vector sum of circuit components in parallel
WE	Working electrode
RE	Reference electrode
ω	Angular frequency

R_Ω	uncompensated resistance
R_P	polarization resistance
C_{DL}	double layer capacitance
R_{CR}	chemical reaction resistance
C_{CR}	chemical reaction capacitance
R_W	Warburg impedance effect
C_W	Warburg impedance effect
E	enzyme
S	substrate
K_S	dissociation constant for the enzyme-substrate complex
ES	enzyme-substrate complex
k_2	first order constant for rate of product formation
P	product
ν	rate of product formation
E_O	total amount of enzyme initially in the reaction mixture
ν_{MAX}	maximum rate of reaction
K_M	Michaelis constant
S	substrate concentration
S_O	substrate concentration initially in the reaction mixture
k_{CAT}	turnover rate constant
IME	Interdigitated microsensor electrode
EIS	Electrochemical impedance spectroscopy
Z_{DUT}	input impedance
$Z_{Feedback}$	feedback resistor
FTIR	Fourier transform infrared spectroscopy
Hz	Hertz
V_{PP}	voltage peak-to-peak
°C	degrees Celsius
V_{OUT}	output of logarithmic amplifiers

V_{IN}	input voltage
V_Z	intercept (voltage)
V_{SPL}	slope (voltage)
V_{MAG}	difference in the output of two identical logarithmic amplifiers
V_{INA}	input voltage into gain/phase analyzer
V_{INB}	input voltage into gain/phase analyzer
V_{PHS}	phase output of gain/phase analyzer
V_ϕ	phase slope in mV/degree
ϕ	each signal's relative phase
GUI	graphical user interface
DUT	Device Under Test
PC	personal computer
LL	Low-Low logic output
LH	Low-High logic output
HL	High-Low logic output
W1	Working electrode 1
W2	Working electrode 2
Ref	Reference electrode

VITA

Vandana Gupta was born in New Delhi, India on February 17, 1981 to Shashi and Veena Gupta. She lived in Newport News, VA for 18 years. She attended Virginia Commonwealth University in Richmond, VA and obtained a Bachelor of Science in Biomedical Engineering in May 2003. She has continued on to obtain a Master of Science degree in Engineering from Virginia Commonwealth University in Richmond, VA in August 2005.